THERMO-HYDRO-MECHANICAL EFFECTS ON THE BEHAVIOUR OF UNSATURATED SOIL-STRUCTURE INTERFACES AND THE NUMERICAL ANALYSIS OF ENERGY PILES

Zhu Fu

Ph.D. Thesis

Supervisors: Dr. Jules-Ange Infante Sedano and Dr. Erman Evgin

Department of Civil Engineering
Faculty of Engineering
University of Ottawa

August 2017

The Doctor of Philosophy in Civil Engineering is a joint program between Carleton University and the University of Ottawa, which is administered by the Ottawa-Carleton Institute for Civil Engineering

ABSTRACT

The shear strength of soil-structure interfaces is relevant to the stability of energy piles. The thermo-hydro-mechanical processes can have a strong effect on the behaviour of interfaces between unsaturated soils and piles. Temperature changes lead to water movement in the soil. The moisture loss or gain in the soil causes drying or wetting. In addition, water movement influences the heat transfer properties of the soil. Temperature and moisture content changes affect the magnitude of soil suction in unsaturated soils. Changes in soil suction alter the strength and deformation characteristics of the soil mass and soil-structure interfaces. Similar to the effects of temperature changes, the mechanical loading and the changes in hydraulic conditions in the ground would cause changes in the void ratio, degree of saturation, suction, strength and deformation characteristics of soil. The interface behaviour under varying thermo-hydro-mechanical (THM) conditions is classified as a coupled problem and this is the subject of the present research.

In the present investigation, laboratory studies and numerical analyses are carried out to evaluate the THM effect on the behaviour of interfaces between an energy pile material and an unsaturated soil. A 3D interface apparatus (Fakharian and Evgin 1996) has been modified (Fu et al. 2013) to allow the behaviour of an interface to be studied under thermo-mechanical loading conditions.

In the present study, the experiments are conducted on soil samples with low degree of saturation and high degree of saturation. It is found that in interface tests using soil samples with low degree of saturation, the adhesion increased due to a positive effect of suction on strength than the negative effect of increasing temperatures. However, in interface tests on soil samples with high degree of saturation, the adhesion decreased with increasing temperatures while the positive effect of suction was not large enough to overcome the negative effect of increasing temperatures. This is a new finding that has not been reported anywhere in the literature. The friction angle for both soil samples (with different degrees of saturation) changed slightly with temperature change.

Coupled finite element analyses conducted in the present study provide the following geotechnical information that would be useful for the design of energy piles: (a) Bearing capacity of the pile with and without the effect of temperature, (b) The effect of degree of saturation (or suction) on the strength and deformation characteristics of both the soil and the soil-structure interface, (c) Temperature effects on the amount of pile head movements (up or down), (d) Temperature induced stresses in the pile, (f) Amount of heat that can be stored or extracted from the ground as a function of time.

At the initial stages of this study, THM effects on the behaviour of energy piles under saturated and unsaturated conditions are analyzed by using SIGMA/W and VADOSE/W finite element codes of GeoStudio 2012. Although these codes are not multi-physics FE codes, it is possible to use them sequentially to obtain results that will show the trends in pile behaviour. This numerical approach is used first to analyze the behaviour of an energy pile installed partially in unsaturated soil. The moisture content and temperature distributions around a 10 m long, bored pile are calculated using transient analyses. Changes taking place in the stress state along the pile shaft and the bearing capacity of the pile at different temperatures are calculated.

In the second part of the numerical analysis of the present study, THM effects on the behaviour of energy piles under saturated and unsaturated conditions are analyzed by using PLAXIS 2D finite element code. PLAXIS is a fully couples finite element code. In order to enhance present understanding of the behaviour of energy piles and do the analysis correctly, a fully coupled analysis involving thermo-hydro-mechanical processes was carried out. Three simulations (mechanical loading only**,** thermo-mechanical coupling and thermo-hydro-mechanical coupling) are conducted using case studies that are available in the literature. In addition, the behaviour of a generic energy pile, which is installed in a kaolin-sand mixture, is studied by taking into consideration of thermo–hydro-mechanical processes. The coupled analysis provided the distributions of temperature, degree of saturation, suction and heat flux in the analysis domain. Numerical results of the fully-coupled method are compared with the results of sequential method of analysis.

ACKNOWLEDGEMENTS

The author would like to express his sincere thanks to his thesis supervisors, Dr. Jules-Ange Infante Sedano and Dr. Erman Evgin, for their continuous encouragement, generous advice, and financial support throughout their NSERC research grants. The author also wishes to thank Dr. John S. McCartney, Dr. Mohammad Rayhani, and Dr. Mamadou Fall for serving as members of the examination committee. The comments provided by the external examiner Dr. J. McCartney helped me to improve my thesis significantly; therefore, I am grateful to him. I would also like to thank Dr. Vanapalli for letting me to use GeoStudio and PLAXIS finite element codes.

I would like to thank the support staff of the Department of Civil Engineering and the geotechnical laboratory technician Mr. Jean Claude Celestin for their help.

The author would like to thank his parents and sisters, for their encouragement and financial support. Finally, it is the author's wife, Xin Lu, whose encouragement and patience made this Ph.D. study possible.

TABLE OF CONTENTS

ABSTRACT .... **II**

ACKNOWLEDGEMENTS .... **IV**

TABLE OF CONTENTS .... **V**

LIST OF TABLES .... **X**

LIST OF FIGURES .... **XII**

LIST OF APPENDICES .... **XXI**

CHAPTER 1. INTRODUCTION **1**

1.1 Statement of problem 1

1.2 Study objectives 4

1.3 Scope of study 5

1.4 Outline of study 6

CHAPTER 2. LITERATURE REVIEW ON ENERGY PILE 7

2.1 Energy piles 7

2.2 Types of energy piles 8

2.3 Benefits of energy piles 8

2.4 Problems related to energy piles 8

2.4.1 Field tests on energy piles 9

2.4.2 Laboratory tests 14

2.4.3 Numerical analysis of energy piles 18

2.4.4 Effect of temperature change on the behaviour of soil 20

2.4.5 Thermal effects on the behaviour of soil-pile interfaces 24

2.4.6 Coupled analysis of thermal-hydro-mechanical model for energy pile……………………………………………………………..………..………25
2.5 Analysis of pile capacity 34
2.6 Conclusions of literature review 39
CHAPTER 3. COUPLING OF THERMO-HYDRO-MECHANICAL PROCESSES TAKING PLACE AT THE SOIL STRUCTURE INTERFACES............................ 40
3.1 Mathematical formulation.. 41
3.1.1 Static equilibrium (Momentum conservation) 41
3.1.2 Fluid flow (Mass conservation)……………………………………..43
3.1.3 Heat flow (Energy conservation)………………………………………43
3.2 Material constitutive models... 45
3.3 Sequential analysis using SIGMA/W and VADOSE........... 46
CHAPTER 4. LABORATORY STUDY ON THE BEHAVIOUR OF INTERFACE BETWEEN THE ENERGY PILE MATERIAL AND SOIL 48
4.1 Influence of moisture content on the shear strength parameters of the interface using direct shear tests at room temperature (Δ T=0°C)……………………...50
4.2 Test material.. 50
4.3 Steel plate 54
4.4 Experimental plan and testing apparatus 55
4.5 Interface test under isothermal condition 56
4.5.1 Test results and discussion.. 57
4.5.1.1 Shear stress versus horizontal displacement 57
4.5.1.2 Vertical displacements at the interface shear strength parameters at various temperatures 59

4.5.1.3 Shear strength of soil-steel plate interface 60
4.6 Test machine to study the behaviour of interface under coupled thermo-mechanical loading conditions.... 62
4.6.1 Thermal plate 63
4.6.2 Numerical analysis of heat transfer in the modified interface apparatus . 64
4.6.2.1 Thermal boundary conditions 64
4.6.2.2 Arrangement of the holes.. 65
4.6.2.3 Thermal properties of materials... 66
4.6.2.4 Temperature contours in the steel plate and soil specimen..... 66
4.6.2.5 Temperature vs. time 67
4.6.2.6 Discussion of the results of numerical analysis 69
4.6.3 Setup for thermal loading 70
4.7 Soil-pile interface tests at different temperatures and unsaturated conditions.... 72
4.7.1 Thermal effects on the shear strength parameters of soil-pile interface with low degree of saturation.. 72
4.7.1.1 Shear stress versus horizontal displacement 74
4.7.1.2 Shear strength parameters.. 78
4.7.1.3 Thermal effect on the volume of the normally consolidated soil sample 80
4.7.2 Thermal effects on the shear strength parameters of soil-pile interface with high degree of saturation.. 81
4.7.2.1 Shear stress versus horizontal displacement 81
4.7.2.2 Shear strength parameters... 84

4.7.2.3 Thermal effect on the volume of the overconsolidated soil sample 86
4.8 Numerical analysis of interface tests (overconsolidated soil samples) 86
4.8.1 Analysis domain 86
4.8.2 Types of analysis and results 88
4.8.2.1 Deformation of domain 88
4.8.2.2 Temperature distributions in soil 89
4.8.2.3 Suction values in overconsolidated soil sample 90
4.8.2.4 Interface shear strength 92
4.8.2.5 Calculation of shear strength of unsaturated soil using Vanapalli and Fredlund (2000) method 94
CHAPTER 5. NUMERICAL ANALYSIS OF THERMAL EFFECTS ON THE INTERFACE BEHAVIOUR OF AN ENERGY PILE 97
5.1 Geometry of an energy pile and analysis domain 97
5.2 Analysis and results 101
5.2.1 Thermo-mechanical behaviour of the pile 101
5.2.1.1 Axial stress in the pile 101
5.2.1.2 Axial strain in the pile 103
5.2.1.3 Radial strain in the pile 103
5.2.1.4 Thermal effect on the bearing capacity of energy pile 104
5.2.2 Thermo-mechanical behaviour of the soil 105
5.2.2.1 Thermal effect on the horizontal stresses acting on the pile–soil interface 105
5.2.2.2 Volumetric water content 111

5.2.2.3 Matric suction 111

5.2.2.4 Temperature distribution in the soil 112

5.2.2.5 Heat flux in the soil 114

5.3 Fully coupled THM analysis of energy piles using finite element code PLAXIS 2D 115

5.3.1 Validation of procedures used in the present study in utilizing PLAXIS.116

5.3.1.1 First validation (Mechanical loading) 117

5.3.1.2 Second validation (Thermo -mechanical) 119

5.3.1.3 Third validation (Thermo –hydro-mechanical couplings). ... 122

5.3.2 Analysis of an energy pile 126

5.3.2.1 Saturation of soil 126

5.3.2.2 Matric suction 128

5.3.2.3 Temperature distribution in the soil 131

5.3.2.4 Thermal effect on the bearing capacity of energy pile 133

5.3.2.4.1 Saturated soil conditions 133

5.3.2.4.2 Unsaturated soil conditions 137

5.3.2.5 Heat flux in the soil 140

CHAPTER 6. SUMMARY AND CONCLUSIONS OF THE PRESENT STUDY 142

6.1 Summary and conclusions…. 144

6.2 Major contributions 146

REFERENCES 146

APPENDIX A 155

Formulation of THM processes in PLAXIS 155

LIST OF TABLES

2.1 Summary of small-scale experimental studies investigating the thermal effects on load-displacement behaviour of energy piles (from Olgun et al. 2014b) 17

2.2 Summary of values of thermal conductivity and specific heat capacity of various soils (from Hamdhan and Clarke 2010) 23

2.3 Common Soil-water characteristic curves equations 34

4.1 Water content, density, void ratio, degree of saturation and suction for each specimen 52

4.2 Parameters of α, n, m for kaolin-sand mixture with temperatures 54

4.3 Thermal properties of materials 66

4.4 Water content, void ratio, degree of saturation at initial state, degree of saturation after heating and shearing, and the peak shear strength for normally consolidated soil samples 73

4.5 Shear strength parameters at various temperatures and matric suction 79

4.6 Water content, void ratio and degree of saturation at the initial state, as well as after heating, and shearing the overconsolidated soil samples at confining pressure of 100 kPa. Corresponding peak shear strength values are provided in the last column.. 81

4.7 Shear strength parameter at various temperatures for overconsolidated soil samples.85

4.8 Suction values in soil at the interface under different normal load and temperatures..91

4.9 Apparent cohesion and internal frictions with different temperatures 95

4.10 Shear strength of unsaturated soil under different thermal conditions 95

4.11 Shear strength of unsaturated interface under different thermal conditions 96

5.1 Model parameters of the soil in the mechanical analysis 99

5.2 Thermal parameters of soil and pile... 99

5.3 Shaft resistance of the pile at 15^{o}C 108

5.4 Shaft resistance of the pile at 25^{o}C 109

5.5 Shaft resistance of the pile at 36^{o}C 110

5.6 Heat flux in saturated and unsaturated conditions (GeoStudio) 115

5.7 Mechanical parameters of soil and pile (from Al-Khazaali et al. 2016).................. 117

5.8 Mechanical parameters of soil (from Laloui et al. 2006).. 123

5.9 Thermal parameters of soil and pile (from Laloui et al. 2006)............................... 123

LIST OF FIGURES

1.1 Construction record of energy piles in the UK (after Amis and Loveridge 2014)....... 2

1.2 Schematic view of geothermal energypiles system (from Laloui et al. 2006)............. 3

2.1 Schematic view of a geothermal energy pile 7

2.2 Geological profile of the site (from Laloui et al. 2006).. 10

2.3 Thermal-mechanical loading in the field test (from Laloui et al. 2006).................... 10

2.4 Thermo-mechanical vertical stresses in the pile (from Laloui et al. 2006) 11

2.5a Effect of thermal loading and surrounding soil on pile behaviour during heating without end restraint (after Bourne Bourne-Webb et al. 2009) : (a) axil thermal strain profiles; (b) axil thermal load profiles; (c) thermally mobilised load profile .. 12

2.5b Effect of thermal loading and surrounding soil on pile behaviour during heating with different degrees of end restraint (after Amatya et al. 2012): (a) axil thermal strain profiles; (b) axil thermal load profiles; (c) thermally mobilised load profile . 13

2.6 Load- displacement curves for energy piles under different elevated temperatures in the centrifuge test (from McCartney and Rosenberg 2011)...................................... 15

2.7 Predominant heat transfer mechanisms in soil influenced by grain size and saturation (after Farouki 1986) 21

2.8 The equilibrium of a pile shaft element (a) mechanical load (b) mechanical and thermal load (from Abuel-Naga et al. 2015).. 26

2.9 Development of the ground thermal regime at 1, 8 and 24-month periods for flow velocities of 0.16 m/day (from Tolooiyan and Hemmingway 2012)........................ 28

2.10 Combined effects of temperature and suction on the evolution of the preconsolidation pressure of a sandy silt: (a) decrease with temperature and (b) increase with suction. The normalized preconsolidation pressure is the preconsolidation pressure measured at a given temperature T and suction, s, over the established preconsolidation pressure at ambient and saturated conditions (T_0 and s =0). se is the air-entry suction (from Salager et al. 2008) 30

2.11 Effect of (a) temperature and (b) suction on the shape of coupled mechanical yield limits (from Francois and Laloui 2009) 31

2.12 Thermal effect on SWCC of FEBEX bentonite (from Villar and Gómez-Espina 2009) 32

2.13 Components of pile bearing capacity 35

2.14 Numerical model for energy pile load and displacement analysis: (a) model for mechanical load; (b) external forces mobilized by mechanical loading; (c) model for thermal load; (d) external forces mobilized by thermal loading (from Knellwolf et al. 2011) 38

3.1 Mechanisms of heat transfer between energy piles and the ground (from Abdelaziz et al. 2011) 40

3.2 THM processes of soil-pile interface (modified from Jing 2003) 41

3.3 Thermal conductivity in response to degree of saturation of a sandy soil and a clay soil, both with n = 0.3, and dry particle thermal conductivities of 7.9 W/m K, and 1.9 W/m K, respectively (Johansen 1977) 44

4.1 Temperature and volumetric moisture content distribution along the soil specimen under temperature gradients (ΔT=33°C) (from Evgin and Svec 1988)........ 49

4.2 Grain size distribution of the kaolin-sand mixture 51

4.3 Static compaction curve of kaolin-sand mixture…………… 51

4.4 Variations in void ratio versus effective stress curve of soil sample with w=17.5%
at 23°C ……………. 53

4.5 SWCC curves for kaolin-sand mixture T= 8, 23, 35°C ……………. 54

4.6 Modified direct shear apparatus for testing interfaces(ΔT=0°C)………………......... 53

4.7 3-D cyclic interface testing apparatus with temperature control ……………. 54

4.8 Shear stress versus horizontal displacement of soil-steel plate interface with various
moisture contents (Normal stress = 150 kPa) ……………. 56

4.9 Shear stress versus horizontal displacement of soil-on-soil tests
(Normal stresses = 150 kPa) 56

4.10 Vertical displacement versus horizontal displacement of soil-steel plate interface
(Normal stress = 150 kPa) …………... 57

4.11 Shear stress versus normal stress at failure for soil–steel plate interface and
soil–on-soil samples at w=17.5%……………. 58

4.12 Shear stress versus normal stress at failure for soil–steel plate interface under
various moisture contents 58

4.13 Arrangement of plates for thermal loading of interface machine……………....... 59

4.14 Geometry of the thermal plate (dimensions in cm) ……………. 60

4.15 Counter-bore o-ring connections……………. 61

4.16 Numerical model: soil domain, steel and the thermal plate, and boundary
conditions…………….. 62

4.17 Temperature contours of steel interface plate and soil (2 holes) ……………....... 63

4.18 Temperature contours of steel interface plate and soil (3 holes) ……………....... 64

4.19 Temperature contours of steel interface plate and soil (4 holes) ……………....... 67

4.20 Temperature vs. time at the middle of interface plate (2 holes) ……………........ 68

4.21 Temperature vs. time at the middle of interface plate (3 holes) ……………........ 68

4.22 Temperature vs. time at the middle of interface plate (4 holes) ……………........ 69

4.23 Effect of insulation layer on the heat transfer from the thermal plate……………. 70

4.24 Thermal loading arrangment for 3-D cyclic interface testing apparatus 71

4.25 Numerical result compared with test data (4 holes) ……………........................... 72

4.26 Temperature vs. time in the soil during the heating from 23 ^{o}C to 35 ^{o}C................ 73

4.27 Temperature vs. time in the soil during the cooling from 23 ^{o}C to 15 ^{o}C 74

4.28 Shear stress versus horizontal displacement of soil-steel plate interface at 8°C (Normal stress = 60 kPa) …………….. 75

4.29 Shear stress versus horizontal displacement of soil-steel plate interface at 15 °C (Normal stress = 60 kPa) …………….. 75

4.30 Shear stress versus horizontal displacement of soil-steel plate interface at 23 °C (Normal stress = 60 kPa) …………….. 76

4.31 Shear stress versus horizontal displacement of soil-steel plate interface at 35 °C (Normal stress = 60 kPa) …………….. 76

4.32 Shear stress versus horizontal displacement of soil-steel plate interface with various temperatures (Normal stress = 60 kPa) ……………... 77

4.33 Shear stress versus horizontal displacement of soil-steel plate interface with various temperatures (Normal stress = 80 kPa) ……………... 77

4.34 Shear stress versus horizontal displacement of soil-steel plate interface with various temperatures (Normal stress = 100 kPa) ……………... 78

4.35 Failure envelopes of the interface between kaolin-sand mixture and the steel plate with temperatures at normally- consolidated condition... 79
4.36 Height of the normally consolidated soil sample during heating 80
4.37 Shear stress versus horizontal displacement of soil-steel plate interface with various temperatures (Normal stress = 60 kPa) …………….. 82
4.38 Shear stress versus horizontal displacement of soil-steel plate interface with various temperatures (Normal stress = 80 kPa) …………….. 83
4.39 Shear stress versus horizontal displacement of soil-steel plate interface with various temperatures (Normal stress = 100 kPa) ……………... 84
4.40 Failure envelopes of the interface between kaolin-sand mixture and the steel plate with temperatures at overconsolidated condition ……………. 85
4.41 Height of the overconsolidated soil sample during heating.................................... 86
4.42 Schematics of the geometry used in the FE analysis of interface tests ……………88
4.43 Horizontal displacements in soil domain (Normal stress=80kPa and T= 35°C) ….89
4.44 Temperature distribution in soil (Normal stress=80kPa and the interface plate is at T= 35°C) ……………. 89
4.45 Temperature vs. time at point A on the interface plate during the heating to35°C... 90
4.46 Suction distribution in soil domain (Normal stress=80kPa and T= 35°C) 91
4.47 Maximum shear stress distribution in soil domain (Normal stress=80kPa and T= 35°C) 92
4.48 Shear stress versus horizontal displacement of soil-steel plate interface with various temperatures (Normal stress = 60 kPa) …………….. 93
4.49 Shear stress versus horizontal displacement of soil-steel plate interface with various

temperatures (Normal stress = 80 kPa) ……………... 93

4.50 Shear stress versus horizontal displacement of soil-steel plate interface with various temperatures (Normal stress = 100 kPa) ……………... 94

5.1 Schematics of pile–soil analysis domain (GeoStudio)……………. 98

5.2 Boundary conditions (GeoStudio)……………. 100

5.3 A heating–cooling cycle of loading with time (From Laloui et al. 2006)…. 101

5.4 Axial stress in the pile under saturated and unsaturated conditions during thermo-hydro-mechanical processes at ΔT=21°C (GeoStudio)……………..................... 102

5.5 Axial strains in the pile at ΔT=21°C under saturated and unsaturated conditions (positive for expansion)(GeoStudio) 103

5.6 Radial strains in the pile under mechanical and thermal mechanical loading (GeoStudio)... 104

5.7 Bearing capacity of the pile versus vertical displacement of the pile during the heating process GeoStudio). 105

5.8 Figure 5.8. Horizontal normal stresses acting on the pile-soil interface along the pile shaft during heating process (PLAXIS) (a) Saturated condition (b) Unsaturated condition…………………………………………………………..107

5.9 Variation of volumetric water content in the soil at points along the radial direction after thermal loading of 21°C (GeoStudio).. 111

5.10 Variation of matric suction in the soil along the radial direction after 12 days of thermal loading increment of 21°C (GeoStudio).. 112

5.11 Temperature distributions in the soil after 12 days of heating (GeoStudio).......... 113

5.12 Temperature distributions in the soil (A-A section) as a function of time (r = horizontal distance from soil-pile interface) (GeoStudio) 113

5.13 Heat flux distributions in the horizontal direction as a function of time along section A-A (GeoStudio)……….. 114

5.14 A numerical model setup (PLAXIS)…………….. 118

5.15 Measured and calculaated results of load versus axial displacement of the model pile (PLAXIS)……………... 119

5.16 Experimental setup (After Tang et al. 2014) ……………. 120

5.17 Schematics of pile–soil analysis domain (PLAXIS)…... 121

5.18 Deformation of pile during heating and cooling processes (PLAXIS)................. 121

5.19 Schematics of solution region for validation (Dimensions are from Laloui et al. 2006).. 124

5.20 Vertical stresses in the pile at ΔT = 15°C (PLAXIS).. 125

5.21 Thermal pile uplift during a heating process (PLAXIS)....................................... 125

5.22 Distribution of degree of saturation in soil after heating the pile to 32°C for 12 days (PLAXIS)... 127

5.23 Distribution of degree of saturation in soil after cooling the pile to11°C for 16 days (PLAXIS)... 128

5.24 Suction distributions in soil after heating the pile to 32°C for 12 days (PLAXIS)…………….. 129

5.25 Suction distribution in soil after cooling he pile to 11°C for 16 days (PLAXIS)…………... 130

5.26 Matric suction in the soil along pile shaft during a heating-cooling cycle (PLAXIS).. 131

5.27 Temperature distribution in the soil after 12 days of heating (PLAXIS)…. 132

5.28 Temperature distributions in the soil after 16 days of cooling (PLAXIS)........... 133

5.29 Bearing capacity of the pile versus vertical displacement of the pile head at 15°C (GeoStudio and PLAXIS) 134

5.30 Bearing capacity of the pile versus vertical displacement of the pile head at 25°C (GeoStudio and PLAXIS) 134

5.31 Bearing capacity of the pile versus vertical displacement of the pile head at 36°C (GeoStudio and PLAXIS) 135

5.32 Developments of failure points in the soil around the pile with increments of vertical displacements (D_y) applied on pile head at 15°C (PLAXIS)................................. 136

5.33 Bearing capacity of the pile versu s vertical displacement of the pile head at 15°C (PLAXIS)…..…….. 138

5.34 Bearing capacity of the pile versus vertical displacement of the pile head at 25°C (PLAXIS)…..…….. 139

5.35 Bearing capacity of the pile versus vertical displacement of the pile head at 36°C (PLAXIS)…..…….. 140

5.36 Heat flux distributions in the horizontal direction with the time along section

A-A. (PLAXIS) 141

LIST OF APPENDICES

APPENDIX A 155

CHAPTER 1

INTRODUCTION

1.1. Statement of Problem

Due to the growing global energy demand, depleting natural resources and the adverse effects of greenhouse gas emissions from oil/gas consumption, there is a rapidly developing trend around the world to explore alternative energy sources. Renewable geothermal energy is one such alternative energy source for the 21st century. Geothermal energy can be used for heating and cooling buildings by making use of pile foundations. The benefit of using this approach is that it takes advantage of the structural piles that were already slated to be built, thus reducing the costs of installation of the geothermal system.

The first energy pile installations in Austria started in 1984 as reported by Brandl (2006). In the subsequent decades energy piles have been installed in many countries such as Sweden, Denmark, Germany, Netherlands, United Kingdom, Switzerland, China, Japan, United States and Canada. Figure 1.1 shows the rate of increase in construction of energy piles in the UK over a 7 year period.

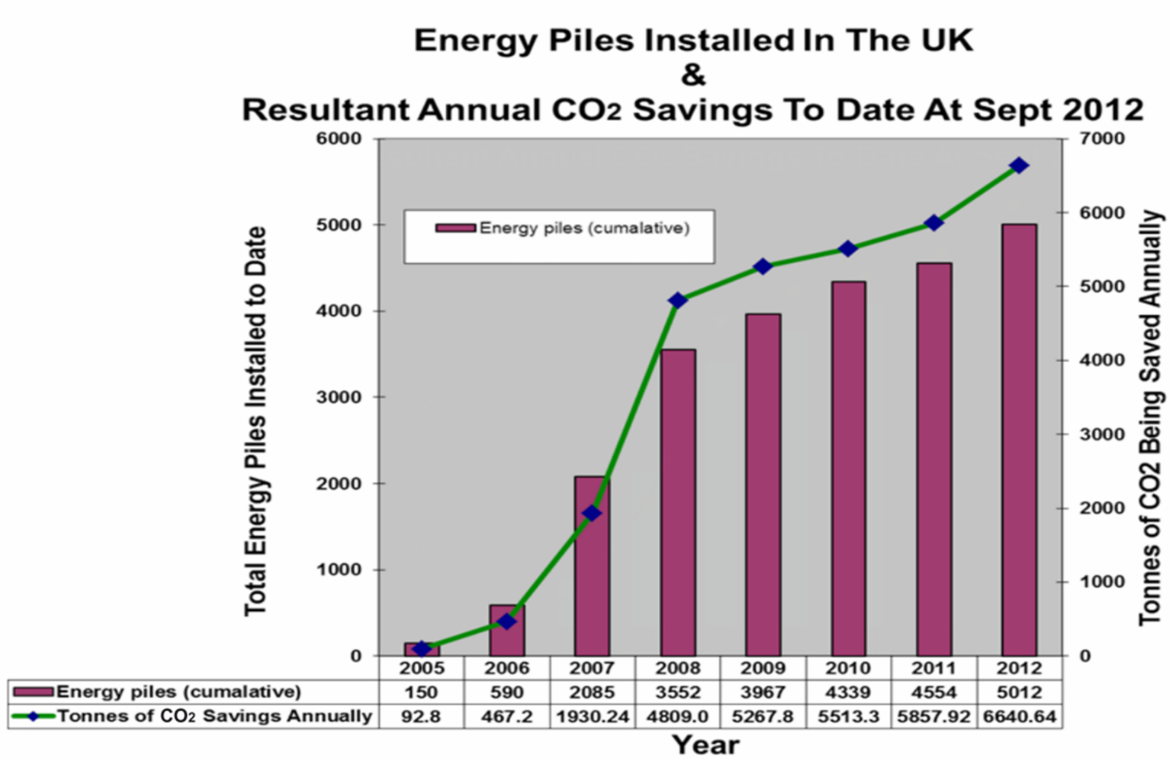

Figure 1.1. Construction record of energy piles in the UK (after Amis and Loveridge, 2014)

Although Energy Piles are a relatively new innovative renewable energy technology (Brandl, 1998), they are gaining popularity with annual increases of 10% in applications around the world (Curtis et al. 2005). In this technology, the foundation piles serve not only as load bearing structures but also as heat exchangers. The piles contain fluid circulation tubes. Water or another fluid, such as ethylene glycol, is used as the heat transport medium. Heat from the superstructure or soil is transferred through the tubes. Thermal energy is fed into the ground for cooling of the building in the summer and withdrawn from the soil for heating purposes during the winter. The fluid is generally circulated through a heat pump, similar to those used in residential and commercial facilities as illustrated in Figure 1.2.

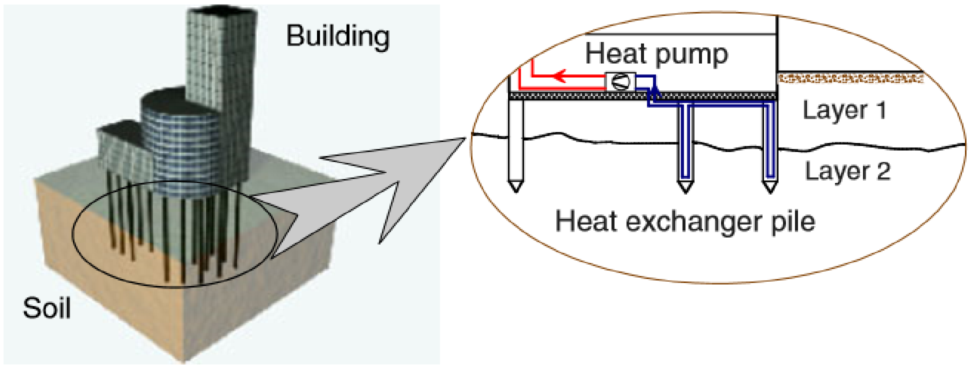

Figure 1.2. Schematic view of geothermal energy piles system (from Laloui et al. 2006)

Once an energy pile system is installed, the pile-soil interface undergoes thermal loading (heating/cooling cycles), mechanical loading (stress/deformation), and hydraulic loading (fluid flow and change in suction). These three processes affect each other. For example, heating may cause an increase in shaft resistance of a pile; on the other hand, cooling may cause reduction in soil resistance to lateral movement of the pile near the ground surface (Olgun and McCartney, 2014). The interface behaviour will have an impact on the bearing capacity of piles and the efficiency of heat transfer of the energy pile.

In the present investigation, the behaviour of a pile material–unsaturated soil interface is studied by performing laboratory tests where the interface is subjected to mechanical loading coupled with thermal loading (heating or cooling) using the modified 3-D Cyclic Interface Testing Apparatus (Fu et al. 2013). Friction angle and adhesion at the interface are determined from the laboratory tests as combined effects of temperature, matric suction, and net normal stress acting on the interface.

Numerical analyses in 2-D are performed to study (a) the interface behaviour during coupled thermo-hydro-mechanical (THM) processes, (b) the thermal behaviour of a full scale energy pile using commercial finite element codes developed for solving multi-physics problems.

At the initial stages of this study, thermal effects on the behaviour of energy piles under saturated and unsaturated conditions were analyzed by using SIGMA/W and VADOSE/W finite element codes of GeoStudio 2012. Although these codes are not, in the true sense, coupled multi-physics FE codes, they are used sequentially to obtain results that will show the trends in pile behaviour. This numerical approach is used first to analyze the behaviour of an actual energy pile (Laloui et al. 2006) installed partially in unsaturated soil. The soil on the upper part of the pile is unsaturated. The moisture content and temperature distributions around a 10 m long, bored pile are calculated using transient analyses. Changes taking place in the stress state along the pile shaft and the bearing capacity of the pile at different temperatures are calculated.

In addition to the sequential finite element analysis, a fully coupled analysis is carried out using finite element code PLAXIS 2D. Three different simulations involving (1) mechanical loading only**,** (2) thermo-mechanical coupling, and (3) thermo–hydro-mechanical coupling are performed. In these simulations actual case studies available in the open literature are used. The purpose was to investigate the capabilities of the software (PLAXIS) and to establish correct usage of the procedures followed in the simulation of energy piles. Once, the capabilities of the software were established by the three simulations mentioned above, the research work continued to study the behaviour of the 10 m long generic energy pile installed in the kaolin-sand mixture (This is the same soil used in interface tests carried out in the laboratory). Numerical results of the fully-coupled method are compared with the results of sequential analysis.

The numerical analysis provided geotechnical information such as the bearing capacity of the pile with and without the effect of temperature. Some other results, essential for the design of energy piles, were obtained from the numerical work. These results include: temperature effects on pile head movements, temperature induced stresses in the pile, amount of heat that can be stored or extracted from the ground as a function of time.

1.2. Study Objectives

The main objectives of this study are as follows:

1. To evaluate the effects of some important factors such as temperature, moisture content of soil (or suction), stress history of soil on the thermo-hydro-mechanical behaviour of an interface between a structural material and an unsaturated soil.

2. To investigate the effect of the above mentioned factors on the behaviour of energy piles.
3. To determine the usefulness of a sequential approach in the numerical analysis of energy piles and compare its results with a fully coupled finite element analysis.

1.3. Scope of study

In order to achieve the above objectives, the following tasks are undertaken in this study:

1.3.1 Laboratory experiments

(a) Perform direct shear type interface tests on an unsaturated soil mixture at various moisture contents to explore the effect of the soil moisture content on the shear strength of an interface between a soil mixture and a steel plate. These tests are conducted in room temperature. Thermal effects are not considered.

(b) Modify an existing interface machine (Fakharian and Evgin 1996) in order to explore the thermal effects on the behaviour of the interface between an energy pile material and soil mixture as explained by Fu et al. 2013. With these modifications, the behaviour of an interface can be studied under thermo-hydro-mechanical loading conditions.

(c) Investigate the combined effects of temperature, suction, and net normal stress changes on the parameters such as adhesion and friction angle of an interface between a soil mixture and a steel plate by using the modified 3-D Cyclic Interface Testing Apparatus.

1.3.2. Numerical analysis

1.3.2.1. Numerical simulation of interface tests using PLAXIS

In order to investigate whether the experimental findings could be obtained by calculations, the numerical analysis of interface tests were conducted. Commercial finite element code PLAXIS 2D was used to simulate the interface tests and establish any shortcomings, if any, for further developments in the case of discrepancies between measured and predicted results.

1.3.2.2. Coupled Simulations using PLAXIS

Three case studies, which are available in open literature, are simulated using PLAXIS 2D to establish correct procedures to be followed in the simulation of energy piles. The numerical analyses are conducted in stages to include progressively all physical processes, namely (1) mechanical load alone, (2) thermo-mechanical coupling, and (3) thermo-hydro-mechanical coupling.

1.3.2.3. Numerical analysis of a generic energy pile

A generic pile is used to do the following work: (1) Conduct a parametric study to investigate the thermal effects on the behaviour of the energy pile and soil-structure interaction. (2) Evaluate heat and moisture transfer in the soil as a function of time. (3) Calculate the thermally induced stress and strain changes in the pile and the surrounding soil. (4) Find out the amount of expansion and contraction in the pile and the soil. (5) Determine how the shaft resistance changes in response to variations in temperature. The sequential analysis is conducted using SIGMA/W and VADOSE/W. Fully coupled analysis is carried out by PLAXIS 2D finite element code to explore the behaviour of an energy pile in thermo-hydro-mechanical processes.

1.4. Outline of study

This thesis is organized in the following way:

Chapter 2 presents a literature review on energy piles.

Chapter 3 describes thermo-hydro-mechanical (THM) processes.

Chapter 4 gives the details of the modifications made on the interface machine and shows the results of laboratory tests performed to determine the temperature effect on the behaviour of an interface between the pile material and soil.

Chapter 5 presents the results of the coupled finite element analysis of a 10 m long generic energy pile.

Chapter 6 presents the conclusions of the research work.

CHAPTER 2

LITERATURE REVIEW ON ENERGY PILES

2.1. Energy piles

An energy pile is shown in Figure 2.1. The energy piles serve not only as load bearing structures but also as heat exchangers. The piles contain tubes through which a fluid (typically water or antifreeze) circulates. This technology is based on the fact that, heat can be transferred between a building and soil mass through energy piles. During the winter months, heat is extracted from the ground and released in the structure. During the summer the process is reversed and excess heat is stored in the ground to cool the building. A heat pump can be used to increase the temperature difference between the ground and the structure to heat/cool the air (Omer, 2008).

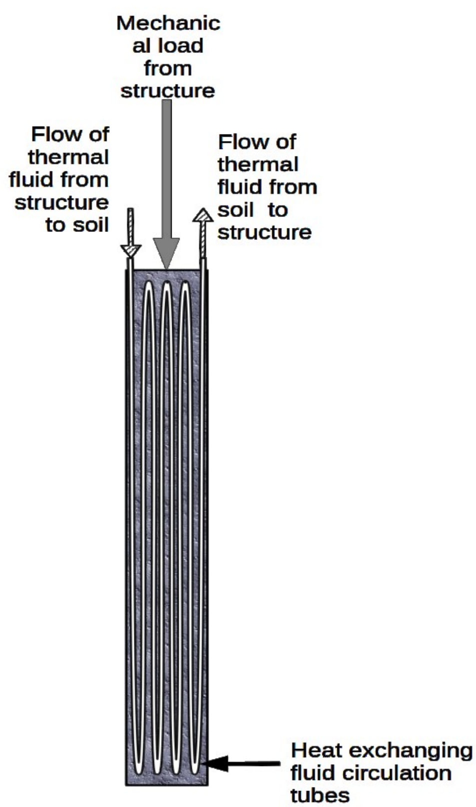

Figure 2.1. Schematic view of a geothermal energy pile

2.2. Types of energy piles

There are various pile types classified according to manufacturing and installation methods. Steel and more commonly built concrete piles are usually used as ground heat exchangers. In the laboratory experiments of this study, a steel pile-soil interface is considered. Steel energy piles provide some advantages compared with the conventional bored concrete piles as listed below:

1. Water can be used as a thermal medium with no risk of water leakage from piles due to the waterproof property of steel.
2. Steel foundation piles have higher heat conductivity than concrete foundation piles.
3. A steel pile can be manufactured in larger diameters than concrete piles.
4. A steel pile has some advantages in high-speed installations and no disposal of waste soil is required.

2.3. Benefits of energy piles

From an energy point of view, the advantages of using energy piles for the buildings are listed below:

- They use an alternative renewable energy resource.
- Cooling the building in summer directly with the coolness from the earth.
- An alternative source of energy without smoke and fumes–contributing to environmental protection.
- Applicable in most climates or region

2.4. Problems related to energy piles

Although energy pile systems have been successfully used in the world, there are no clear design guides providing how thermal actions are considered in terms of safety and serviceability of energy piles (Bourne-Webb et al. 2016). Empirical considerations are generally dominated in the geotechnical design of energy piles and the factor of safety is at least twice as large as that used for traditional piles without a heat exchanger (Amatya et al. 2012). The shear strength of the pile –soil interface has a significant effect on the factor of safety of energy piles. The change in shear strength of soil–pile interfaces under thermo-hydro-mechanical loads needs further investigation

(Laloui et al. 2003, 2006; Knellwolf et al. 2011). In particular, few analytical, physical or numerical tools are available to consider the coupled thermo-hydro-mechanical effects on the behaviour of pile-soil interfaces. In addition, not enough is known about the effect of temperature changes on the load carrying capacity of energy piles and the resulting changes in soil stress–strain response due to the heat transfer in and out of the energy piles (GSHP 2012). Therefore, it is necessary to investigate the behaviour of pile–soil interaction under various thermo-hydro-mechanical loading conditions. During heating and cooling cycles, energy piles as well as the surrounding soils expand and contract, and this movement changes the pile–soil interaction. In some cases it may result in unwanted consequences, such as additional building settlement, excessive axial tensile stresses, large compressive axial stresses or mobilization of limiting resistance on the pile shaft.

The following literature review provides an overview of previous attempts made by researchers to understand thermo-hydro-mechanical behavior of the energy piles.

2.4.1. Field tests on energy piles

Laloui et al. (2006) conducted an in-situ test on one of the piles of a five-story building under construction at Lausanne, Switzerland. The pile was equipped with a heating system, load cells, strain gauges, and thermometers. The drilled pile diameter was 0.96-1.1 m in diameter and 25.8m long. The geological profile of the site is shown in Figure 2.2. At each step of the building construction, the temperature of the pile was increased by 15°C and then the system was cooled down to the initial temperature. The first test (T1) was performed before starting the construction when the pile head was free to move. The other tests (T2 to T7) correspond to the heating/recovery test at the end of each construction stage as shown in Figure 2.3. The displacements of the pile head and variation of axial stresses along the pile under different pile head loads during heating/cooling tests were measured. The test results showed that the thermally (Ther.)-induced axial stress in the pile is higher than that caused by the mechanical (Mech.) load alone as shown in Figure 2.4. Their test results also showed that the mobilized shaft resistance increased with the temperature increase.

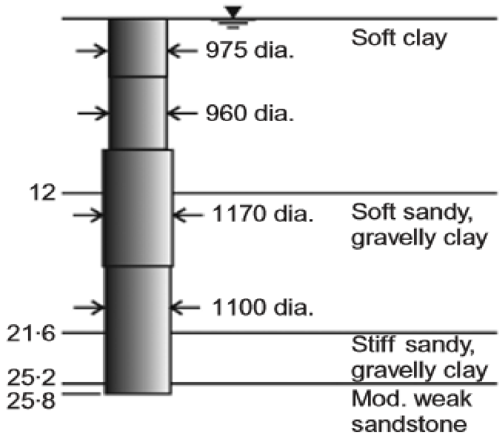

Typical soil properties

Soft clay	γ = 19·6 kN/m^3 c_u = 15–20 kPa
Soft sandy, gravelly clay	γ = 19·1 kN/m^3 c_u = 20–30 kPa
Stiff sandy, gravelly clay	γ = 21·6 kN/m^3 c_u = 70–150 kPa
Mod. weak. sandstone	γ = 25 kN/m^3 UCS = 12 MPa

Figure 2.2. Geological profile of the site (from Laloui et al. 2006)

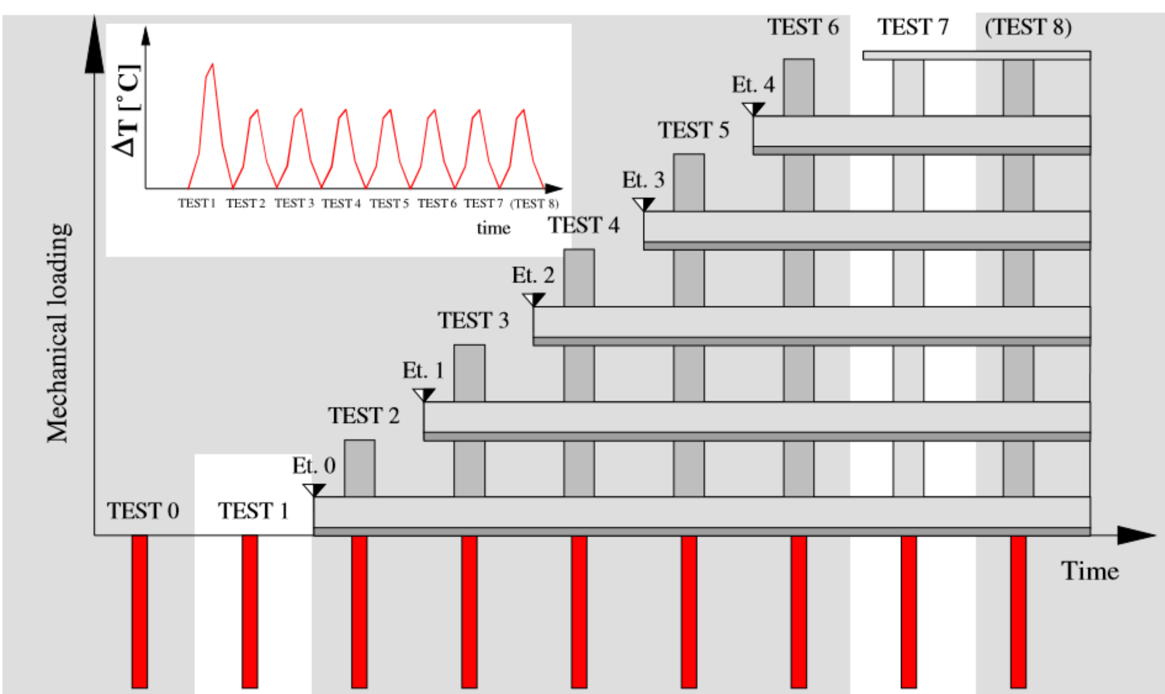

Figure 2.3. Thermo-mechanical loading in the field test (from Laloui et al. 2006)

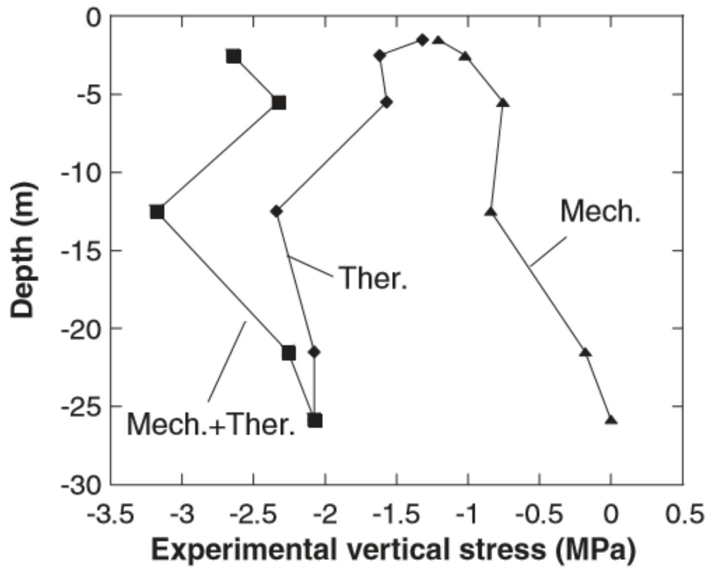

Figure 2.4. Thermo-mechanical vertical stresses in the pile (from Laloui et al. 2006)

Bouazza et al. (2013), Singh et al. (2015) and Wang et al. (2014) conducted a full-scale in situ static load test on an energy pile installed at Monash University, Melbourne, Australia in a sandy profile. The pile was 0.6 m in diameter and 16 m long. They found that the pile shaft capacity increased when the pile was heated and returned to the initial capacity when the pile was cooled. No loss in pile shaft capacity was observed after heating and cooling cycles.

Bourne-Webb et al. (2009) and Amatya et al. (2012) conducted an in-situ test on an energy pile. The pile was 0.55 m in diameter and 23 m in length. It was installed in London Clay. A constant mechanical load was applied at the pile head. The thermal loading was varied between -2.5°C and 36°C. Effect of thermal loading and surrounding ground on pile behaviour during heating with no end restraint is shown in Figure 2.5a. The effect of end restraint of the same pile is shown in Figure 2.5b. It was found that the end restraint condition strongly influenced the axial load distribution developed in the pile in response to heating or cooling.

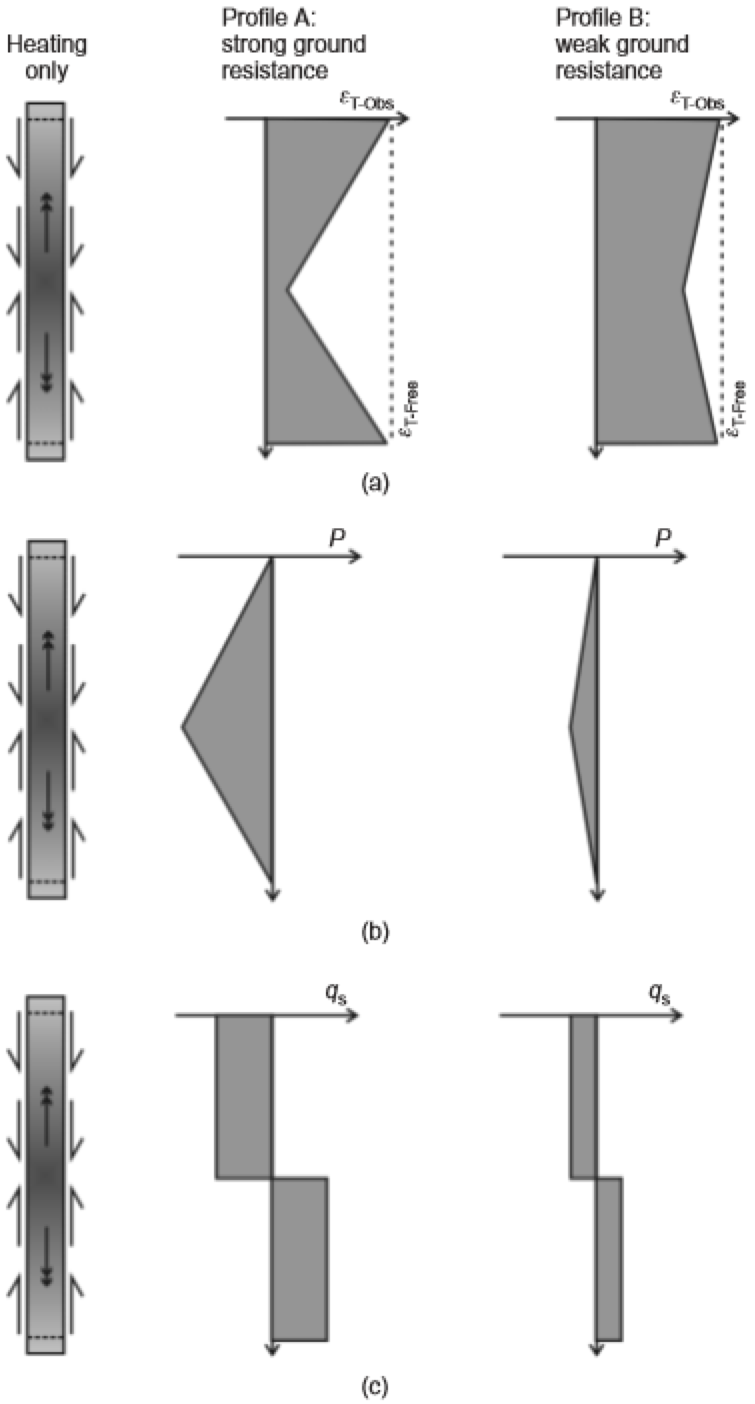

Figure 2.5a. Effect of thermal loading and surrounding ground on pile behaviour during heating with no end restraint (after Bourne-Webb et al. (2009): (a) axial thermal strain profiles; (b) axial thermal load profiles; (c) thermally mobilised load profiles.

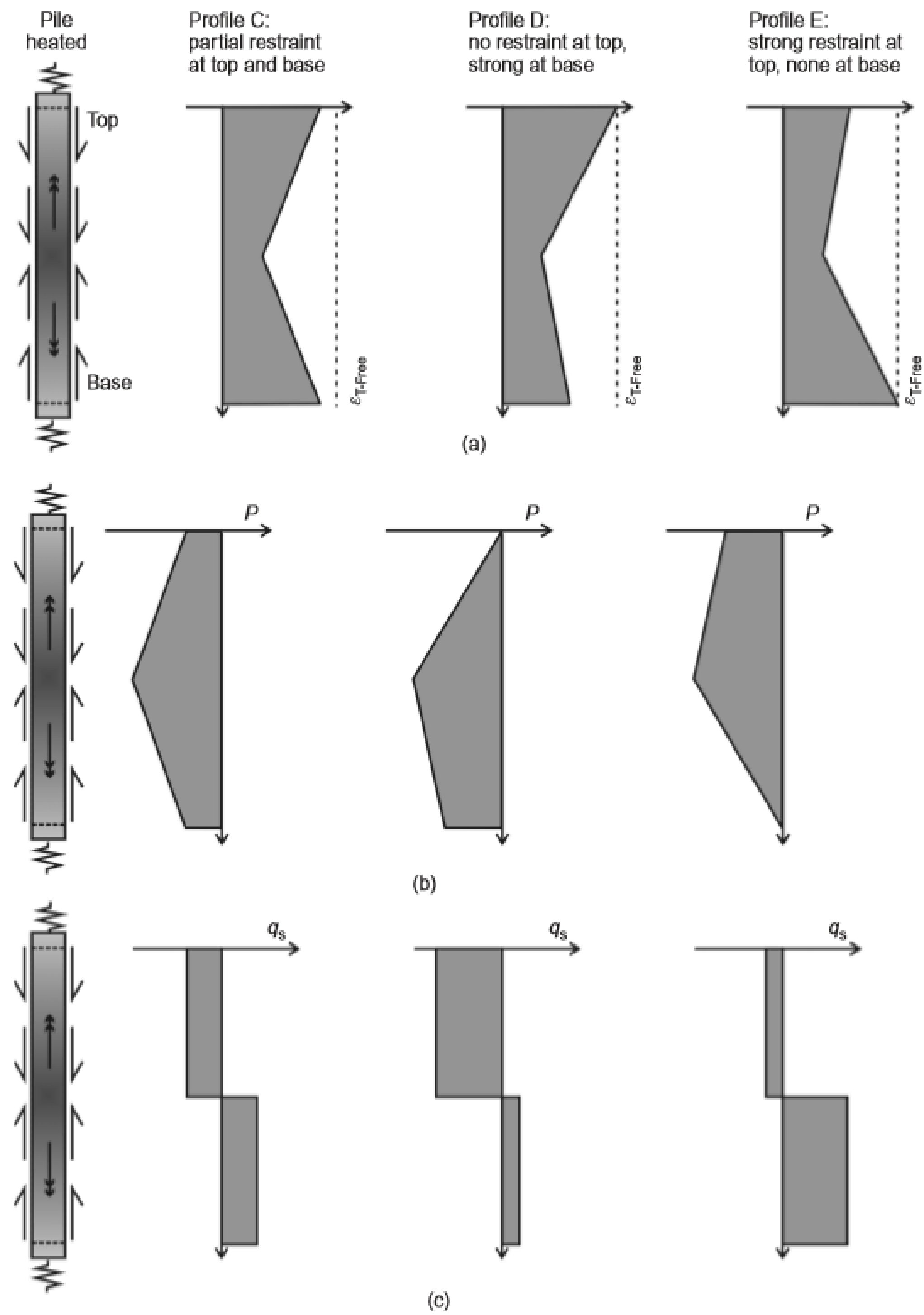

Figure 2.5b. Effect of thermal loading and surrounding ground on pile behaviour during heating with different degrees of end restraint (after Amatya et al. 2012): (a) axial thermal strain profiles; (b) axial thermal load profiles; (c) thermally mobilised load profiles.

Murphy and McCartney (2015) reported a thermo-mechanical evaluation of two full-scale energy foundations during heating and cooling operations for two years of an 8-story building in Denver, Colorado, USA. The thermally induced axial strain during the first year of heating and cooling were elastic and recoverable, but in the second year, plastic deformations took place at the interface.

Murphy et al. (2014, 2015) presented the results of a combined thermal response test on full-scale energy foundation beneath a new building at the U.S. Air Force Academy. They pointed out that, for a temperature increase of 18°C, the maximum thermally induced axial stress ranged from 4.0 to 5.1 MPa, which was approximately 25 % of the compressive strength of concrete, and the maximum upward displacement ranged from 1.4 to 1.7 mm. They concluded that these upward displacements would not cause angular distortions sufficient enough to cause structural or aesthetic damage of the building.

2.4.2. Laboratory tests

A number of experimental and analytical studies have been conducted in the past to investigate the thermo-mechanical behaviour of energy piles, including thermal effects on soil behaviour and shear stress at the soil-pile interface due to thermo-elastic pile deformations (Brandl 2006, Laloui et al. 2006, Bourne-Webb et al. 2009, and Knellwolf et al. 2011).

2.4.2.1. Centrifuge tests

McCartney et al. (2010) carried out load tests on semi-floating energy piles in a centrifuge using unsaturated Bonny silt compacted around the pile. The test pile was heated to different temperatures before applying the structural load. Their study demonstrates the effect of temperature on the load-displacement behaviour of energy piles. Figure 2.6 shows that the pile has an increased capacity at higher temperatures. Goode et al. (2014) conducted similar centrifuge experiments but using dry Nevada sand and observed no change in ultimate side shear resistance with increasing temperature. Stewart and McCartney (2012, 2014) used a centrifuge modeling approach to investigate the thermo-mechanical response of soil-structure interaction.

The test results showed that during successive heating-cooling cycles, slight decreases in upward head displacement were observed due to changes in the stiffness of the unsaturated soil from thermally induced water flow away from the foundation and potential downdrag effects. However, little change in the thermally induced axial stress was observed during the heating-cooling cycles. Ng et al. (2015) reported a series of centrifuge tests on aluminum energy piles in medium dense saturated sand. The pile load tests showed that pile capacities increased by 13% and 30% with increasing temperatures of 15°C and 30°C, respectively. It was noted that with an increasing temperature, shaft resistance increased but at a reducing rate. The explanation for this behaviour was given as follows. At a higher temperature, toe resistance increased more rapidly than shaft resistance due to a larger downward expansion of the pile.

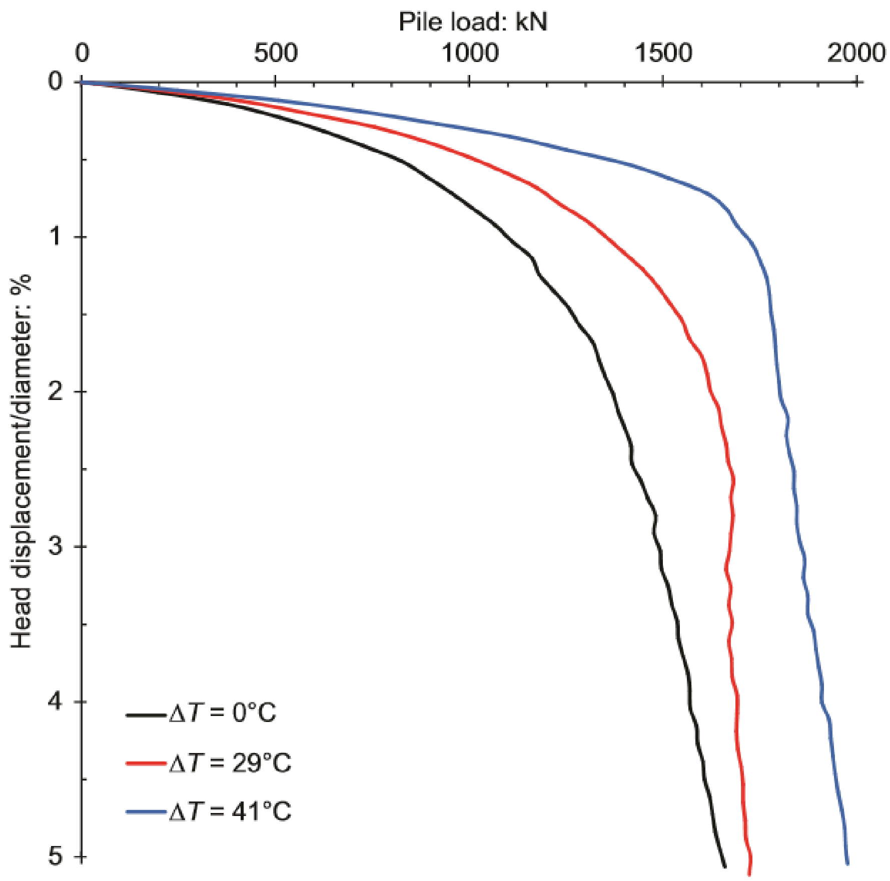

Figure 2.6 Load- displacement curves for energy piles under different elevated temperatures in the centrifuge test (from McCartney and Rosenberg 2011)

2.4.2.2. Model scale pile tests

Laboratory tests on model scale piles have been used to study the thermo-mechanical behaviour of soil-pile interaction for energy piles. Wang et al. (2011, 2012) performed tests on small-scale piles at different temperatures using loosely compacted dry and unsaturated N50 fine sand. The tests results showed no change in shaft resistance with dry sand and a decrease in shaft resistance with the unsaturated sand at elevated temperatures. Kramer and Basu (2014) conducted similar small-scale tests using dry F50 Ottawa sand and noted a slight increase (~5%) in pile capacity at increased temperatures. Yavari et al. (2014) conducted an experimental study on a model pile with 20 mm diameter embedded in dry sand. The behaviour of the axially loaded pile under thermal cycles was investigated. After applying the axial load on the pile head, the pile temperature was varied between 5 and 30^{o}C. It was noted that heating under low axial load induced heave and cooling induced settlement of the pile head. However, at higher axial loads, irreversible settlement of the pile head was observed after a few thermal cycles. The test results showed that thermal cycles modified significantly the mobilized skin friction along the pile. It was found that at the energy pile–soil interface, temperature decrease leads to a decrease in shaft resistance of the axially loaded pile. The effect of heating and cooling cycles on the settlement of a pile was studied by Kalantidou et al. (2013). The test results showed an additional settlement after the first heating cycle and irreversible settlement of the pile head after multiple thermal cycles.

Centrifuge tests and model scale tests provided important information about the behaviour of energy piles. A summary of experimental studies investigating thermal effects on the load-displacement behaviour of energy piles is shown in Table 2.1.

Table 2.1 Summary of small-scale experimental studies investigating the thermal effects on load-displacement behaviour of energy piles (from Olgun et al. 2014b)

Study	Model	Soil type	Pile	ΔT (°C)	Pile capacity
McCartney and Rosenberg (2011)	Centrifuge (24g)	Bonny silt (compacted) w=13.2% ϕ'=32°	Concrete D=76.2mm (1.8m) H=381mm (9.1m)	29 / 41	40% increase in side shear resistance with heating
Wang et al. (2011)	Laboratory (1g)	N50 Fine sand (loosely compacted) Cu=1.47，Cc=1.21 w=0.5%	Steel tube D=25.4mm t=1.2mm	20	50% decrease in side shear resistance with heating
		300WQ Silica flour (loosely compacted) Cu=4.8, Cc=2.13 w=21.5%, 24%	Pile surface is coated with a layer of N50 fine sand using epoxy resin		10% to 50% decrease in side shear resistance with heating
Wang et al. (2012)	Laboratory (1g)	N50 Fine sand (loosely compacted) Cu=1.47, Cc=1.21 w=0%, 2%, 4%	Steel tube D=25.4mm t=1.2mm Pile surface is coated with a layer of N50 fine sand using epoxy resin	20/40	w=0% – No change in side shear resistance w=2%, 4% – Reduction in side shear resistance
Goode et al. (2014)	Centrifuge (24g)	Dry Nevada sand e=0.75, ϕ=35° G=30MPa ν=0.3	Concrete D=63.5mm (1.5m) H=342.9mm (8.2m)	7 / 12 / 18	No change in ultimate capacity with heating
Kramer and Basu (2014)	Laboratory (1g)	Dry F50 Ottawa sand (fine silica sand) Cu=1.8, Gs=2.65	Concrete D=100mm H=1.22m	20	Slight increase in pile capacity (~5%) with heating Decrease in pile head stiffness with heating

2.4.3. Numerical analysis of energy piles

A large number of researchers attempted to understand the behaviour of energy piles in coupled thermo-hydro-mechanical processes by theoretical and numerical methods. Ouyang et al. (2011) conducted numerical back-analysis of an energy pile test at Lambeth College, London and observed that the thermal loading caused changes in the confining stress and shear stiffness properties at the pile-soil interface. Ghasemi-Fare and Basu (2013) performed heat transfer analysis of energy piles using finite difference method and reported that initial temperature difference between the ground and circulation fluid, thermal conductivity of soil, and radius of circulation tube are identified to be the most important parameters that affect thermal efficiency of an energy pile. Dupray et al. (2014) performed a coupled multi-physics finite element analysis to investigate thermo-hydro-mechanical behaviour of an energy pile and found out that the heating–cooling cycles have a significant influence on the changes of pore water pressure in the low-permeability soils around the energy pile. Saggu and Chakraborty (2013) investigated the effect of soil properties on the behaviour of energy piles during the cyclic thermal loading. They reported that the shaft resistance did not change significantly under thermo-mechanical loading in loose sandy soil; however, an increase in shaft resistance occurred for piles in the dense sand. Houston et al. (2015) performed a study on thermally induced settlements for an energy pile on unsaturated soil and reported that soil suction, net normal stress, and temperature are of key importance in estimating the settlements.

Suryatriyastuti et al. (2014) took into account two different conditions of contact between soil and pile: perfect contact and sliding contact using frictional interface elements. The numerical results showed that temperature–induced mechanical behaviour of pile and soil is strongly related to the condition of contact between them.

Rotta et al. (2015) carried out thermo-hydro-mechanical finite element analysis of an energy pile in saturated sand. They pointed out that plasticity is a key part of the constitutive models of soil and of pile–soil interface to capture the null point movements along the length of energy piles. In their numerical study, they used thin layer of finite elements to simulate the pile–soil interface and found that these types of elements are suitable to represent the pile–soil interfaces under different magnitudes of thermal and mechanical loads. Numerical results showed that plastic strains occur at the pile-soil interface. This may affect the mechanisms of shear resistance mobilization at the pile shaft.

Wang et al. (2015) conducted an axisymmetric fully coupled thermo-poro-mechanical (TPM) finite element analysis of soil–structure interaction between an energy pile and unsaturated silt. The model consists of three main physical processes: non-isothermal pore water and gas flow, heat transport in the soil mixture, and poro-elasto-plastic deformations. The numerical results showed that thermally-induced liquid water and water vapor flow inside the soil induced significant changes in suction and volumetric water content especially near the soil-foundation interface. For example, volumetric water content decreased from an initial value of 0.226 to approximately 0.18 near the interface after heating.

Caulk et al. (2016) set up a three dimensional model to explore the interaction between an energy pile and soil by using COMSOL Multiphysics finite element software. The numerical results indicated that the energy pile configuration has an impact on the heat transfer. For example, heat transfer increased by up to 8% for an even energy pile layout compared to an uneven layout. Meanwhile, even energy pile layouts had even cross-sectional temperature distributions, which corresponded to higher energy pile performance.

Olgun et al. (2014a) carried out finite element analyses to investigate the long-term performance of energy piles and progression of temperatures within the ground around the pile. The analyses indicated that the nature and degree of temperature progression around an energy pile was directly related to the seasonal energy demand. It was seen that temperature changes induced to the ground were minimal for cases where respective energy demands during winter and summer are balanced.

Olgun et al. (2014b) numerically examined if the lateral stress acting on the pile-soil interface increased due to thermal effects. They concluded that thermally induced increase in lateral stress is a major factor affecting shaft resistance and the load–displacement behaviour of energy piles. The results demonstrated that the increase in contact pressure induced only by radial thermal expansion of the pile is small in magnitude and therefore would not result in significant increases in shaft resistance.

2.4.4. Effect of temperature change on the behaviour of soil

There are three principal mechanisms in heat transfer: conduction, convection and radiation.

Conduction

Conduction is heat transfer by means of molecular agitation within a material without any motion of the material as a whole. According to Fourier's Law, the heat flux per unit area, q_{cond}, generated by conduction, may be written as:

$$q_{cond} = -\lambda \Delta T \tag{2.1}$$

where λ is the thermal conductivity of the medium, T is the temperature and Δ is the gradient operator.

Convection

Convection is heat transfer by mass motion of a fluid such as liquid or vapour when the heated fluid is caused to move away from the source of heat, carrying energy with it. In soils, it is usually assumed that the soil structure (solid phase) is static and thus convection effects are only attributed to liquid and vapour transport.

The heat flux generated by liquid convection is then given as:

$$q_{lconv} = c_l \rho_l \, v_l \, (T-T_o) \tag{2.2}$$

where c_l is the specific heat capacity of soil water, ρ_l is the density of soil water, v_l is the vector of water velocity and T_o is the reference temperature. This equation is also known as Newton's Law of convection.

Similarly, the heat flux generated by vapour convection can be written as:

$$q_{vconv} = c_v \rho_l \, v_v \, (T-T_o) \tag{2.3}$$

where c_v is the specific heat capacity of soil vapour and v_v is the vector of vapour velocity.

Radiation

Thermal radiation is energy transfer by the emission of electromagnetic waves which carry energy away from the emitting object. The temperature of the radiating body is the most important factor, the flow of heat being proportional to the fourth power of the absolute temperature. The flux of energy radiating from an object e (T) can be expressed by the Stefan-Boltzmann Law:

$$e(T) = \sigma T^4 \tag{2.4}$$

where the Stefan-Boltzmann constant, σ, is 5.67036×10^{-8} $W/m^2.K^4$ and T is the absolute temperature.

2.4.4.1 Heat transfer in soils

These three types of heat transfer may occur within soils. Conduction is usually the dominant process when no significant ground water flows are present (Rees et al. 2000). Convection and radiation may become important in the soils with large grain sizes where the pore spaces are sufficiently large to allow these two processes occur. Changes of volumetric moisture content may also have significant effect on heat transfer in fine grained unsaturated soils as shown in Figure 2.7.

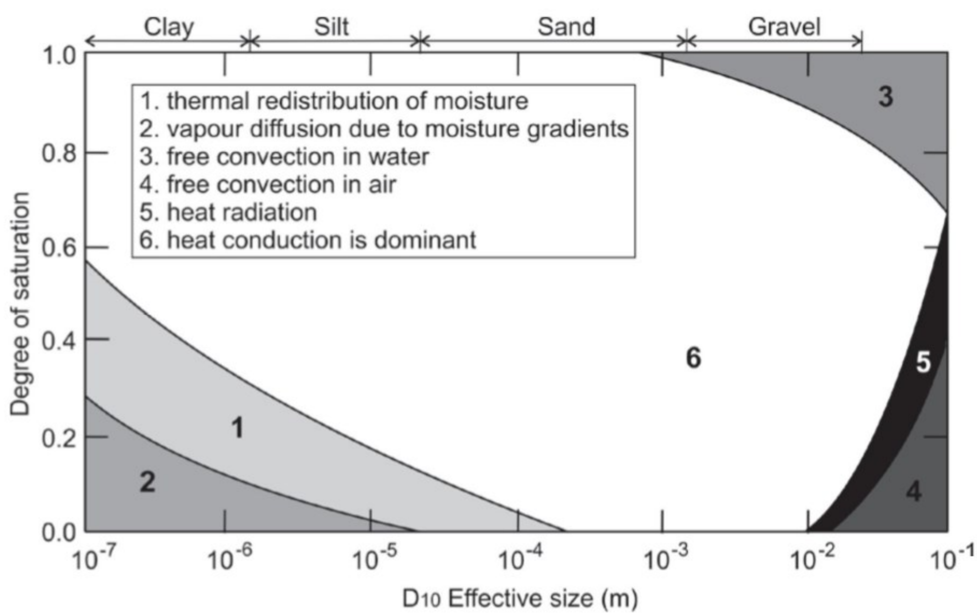

Figure 2.7 Predominant heat transfer mechanisms in soil influenced by grain size and saturation (after Farouki 1986)

2.4.4.2 Thermal characteristics of soil

The thermal conductivity and specific heat capacity are two main thermal characteristics of soil. The thermal conductivity is defined as the quantity of heat that flows through a unit area in a unit time under a unit temperature gradient, which governs the flow of heat through the soil.

Thermal conductivity can be defined mathematically as Fourier's law. Thermal conductivity (λ or k) is the capacity of the body to conduct or spread heat.

$$k = \frac{QL}{A\Delta T} \tag{2.5}$$

where thermal conductivity is k in W/m K, the amount of heat transfer through the material is Q in J/S or W, the area of the body is A in m^2, the difference in temperature is ΔT in K.

The specific heat capacity of a substance is the amount of heat required to raise one gram of the substance by one degree Celsius. The specific heat capacity can be defined as follows.

$$C_s = \frac{Q}{m \times \Delta T} \tag{2.6}$$

where Cs is specific heat capacity, Q is heat, m is mass, ΔT is change in temperature.

The saturation and dry density of a soil have significant effects on thermal conductivity. An increase in either the saturation or dry density of a soil will result in an increase in its thermal conductivity as shown in Table 2.2.

Table 2.2. Summary of values of thermal conductivity and specific heat capacity of various soils (from Hamdhan and Clarke 2010)

Soil type	Water content (%)	Dry density (Mg/m^3)	Thermal conductivity (W/m K)	Specific heat capacity (J/kg K)
China CLAY (D) (sat.)	46.2	1183	1.52	2362
China CLAY (D) (dry)	0	1390	0.25	800
Sandy CLAY	26.5	1494	1.61	1696
Sandy CLAY	19.5	1757	2.45	1459
Soft grey fine sandy CLAY	54.6	1067	4.20	2646
Soft grey fine sandy CLAY	41.4	1231	3.03	2200
Stiff dark grey sandy gravely CLAY	10.1	2088	3.69	1141
Stiff dark grey sandy gravelly CLAY	9.6	2161	3.28	1125
Course SAND (dry)	0	1800	0.25	800
Course SAND (sat.)	20.2	1730	3.72	1483
Medium SAND (dry)	0	1700	0.27	800
Medium SAND (sat.)	20.2	1730	3.34	1483
Fine SAND (dry)	0	1600	0.15	800
Fine SAND (sat.)	24.6	1613	2.75	1632

2.4.5 Thermal effects on the behaviour of soil-pile interfaces

Yavari et al. (2016) investigated the effect of temperature changes on the shear strength of soils and the soil-structure interfaces. A conventional direct shear apparatus was modified by adding a temperature control system. The structural component of the interface was made of concrete. Both sand and clay samples in saturated state were used in their experiments. Tests were done at temperatures of 5, 20, and 40^{o}C. Initially, all samples were consolidated to 100 kPa. Subsequently, the normal stress was lowered to a smaller value ranging from 5 kPa to 80 kPa before shearing commenced. Therefore, all tests were carried out on overconsolidated soil samples. They concluded that the effect of temperature on the shear strength of sand, clay, and the clay concrete interface is negligible for the temperature range 5 to 40^{o}C.

Di Donna et al. (2016) conducted laboratory experiments to study (a) the cyclic mobilization of the shear strength of the soil-pile interface that is induced by thermal deformation of the pile and (b) the direct influence of temperature variations on the soil and soil-pile interface behaviour. The structural component of the interface was made of concrete. Both sand and soil samples were used in the experiments. They concluded that the sand-concrete interface was affected by cyclic degradation but not affected directly by temperature. However, the response of the clay-concrete interface changed at different temperatures. The strength of the interface increased with increasing temperature. Most of the increase in strength was due to a large amount of increase in adhesion. In fact, the interface friction angle reduced slightly.

Murphy and McCartney (2014) measured the impact of temperature on the shear stress–displacement curves for soil–concrete interfaces using a new modified borehole shear device in drained condition. The results from the laboratory tests indicate that temperature does not have a major impact on the peak shear strength and friction angle.

Xiao et al. (2014) studied the shear behavior of a silty soil and soil- concrete interface subjected the temperature changes. The conventional direct shear device was placed in a temperature controlled chamber. The effect of cyclic temperature change was investigated. They pointed out that shear strength of silt is proportional to the temperature and increase with the cyclic thermal loads. They also observed that thermal-strengthening behavior of the unsaturated silty soil was presented under the cyclic temperature variation. However, they did not consider the impacts of suction and thermal effects on the shear strength of the interface.

2.4.6. Coupled analysis of thermo-hydro-mechanical behaviour of an energy pile

Due to heating and cooling cycles, the energy pile and the surrounding soil would expand or contract and consequently the pile–soil interface behaviour will be affected. Abuel-Naga et al. (2015) studied the potential temperature effects on pile–soil interaction. Figure 2.8 shows the equilibrium of a pile shaft element and its surrounding soil under only mechanical load and under the combination of mechanical and thermal loads. They stated that, in order to predict dPr/dT and dPs/dT and the corresponding strains, it is necessary to conduct a coupled thermo-hydro-mechanical analysis in soil–pile interaction for energy pile.

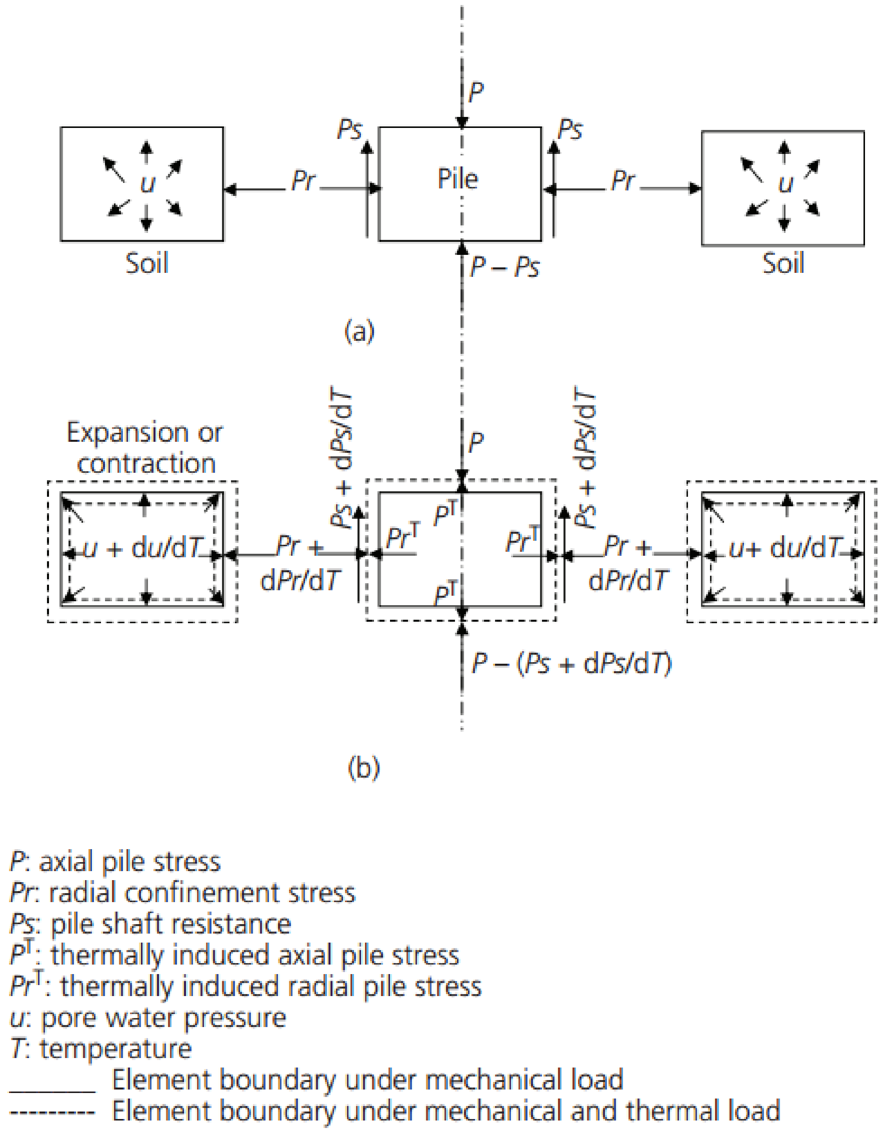

Figure 2.8. The equilibrium of a pile shaft element (a) mechanical load (b) mechanical and thermal load (from Abuel-Naga et al. 2015)

The authors describe their model as quoted in the following.

"*In the axial direction of the energy pile, the thermally induced axial pile stress PT is a function of thermal expansion coefficient and elastic modulus of concrete as well as the pile restrained condition (Bourne-Webb et al., 2012). The thermally mobilised interface shear stress change at the soil–pile interface dPs/dT depends on the differential thermally induced axial strain between the pile and the surrounding soil, the temperature effect on the interface shear coefficient and the radial confinement effective stress Pr and its thermal evolution dPr/dT. In fact, dPr/dT depends on the differential thermally induced radial strain between the pile and the surrounding soil, the effect of temperature on the lateral earth pressure coefficient of soil and the thermally induced* *pore water pressure. In addition, dPr/dT and dPs/dT could also be functions of cyclic heating and cooling properties.*

Based on the above conceptual understanding of the temperature effects on pile structural behaviour, it can be concluded that the design of an energy pile should be conducted using a coupled thermo-hydromechanical soil–structure interaction model that is able to predict dPr/dT and dPs/dT and the corresponding strains. Therefore, the proper design of an efficient energy pile should involve (i) thorough understanding of the thermo-mechanical properties of soils and (ii) use of a special design approach that considers the structural function of the pile under cyclic temperature conditions."

Abuel-Naga et al. (2015) also provided a literature review of thermo-mechanical behavior of saturated clays. A summary of their review work is given below.

1. The volumetric strain change in saturated fine-grained soils subjected to temperature changes depends on the stress history. The normally consolidated clays contract irreversibly and nonlinearly upon heating. The highly overconsolidated clays exhibit reversible expansion following the heating/cooling cycles.
2. The undrained shear strength of normally consolidated clays increases as the temperature increases.
3. The secant modulus of normally consolidated clays increases as the soil temperature increases.
4. The hydraulic conductivity of soils increases as the temperature increases. This behavior is attributed to the thermally induced change in the pore fluid viscosity.
5. Pore water pressure changes as a result of temperature change. The stress level and history affect the thermally induced pore water pressure change. The authors provide the following points: "*(i) the rate of the thermally induced pore water pressure increase with temperature is nonlinear; (ii) a higher consolidation pressure produces a larger pore water pressure increase for a given temperature increase, (iii) the rate of increase in the thermally induced pore water pressure is stress history dependent (OCR) and tends to decrease as the OCR increases and (iv) the thermally induced pore water pressure of the normally consolidated specimens was reversible whereas the overconsolidated specimens showed an irreversible behaviour.*"

Claesson and Eskilson (1998) performed a study on the influence of groundwater flow across heat exchanger and concluded that the thermal effect of natural groundwater movements is negligible at low groundwater flow rate (0.0013 m/day). However, Tolooiyan and Hemmingway (2012) reported that a moderate groundwater flow (0.16 m/day) across a site can lead to a significant change in the development of the sub-surface thermal regime as shown in Figure 2.9. Katzenbach et al. (2008) analyzed the coupling of heat transfer and water flow processes in the energy piles installed in Frankfurt, Germany and concluded that the horizontal groundwater flow results in the deflection of isotherms in the downstream direction, resulting in a larger thermally influenced area in the downstream direction of the energy pile.

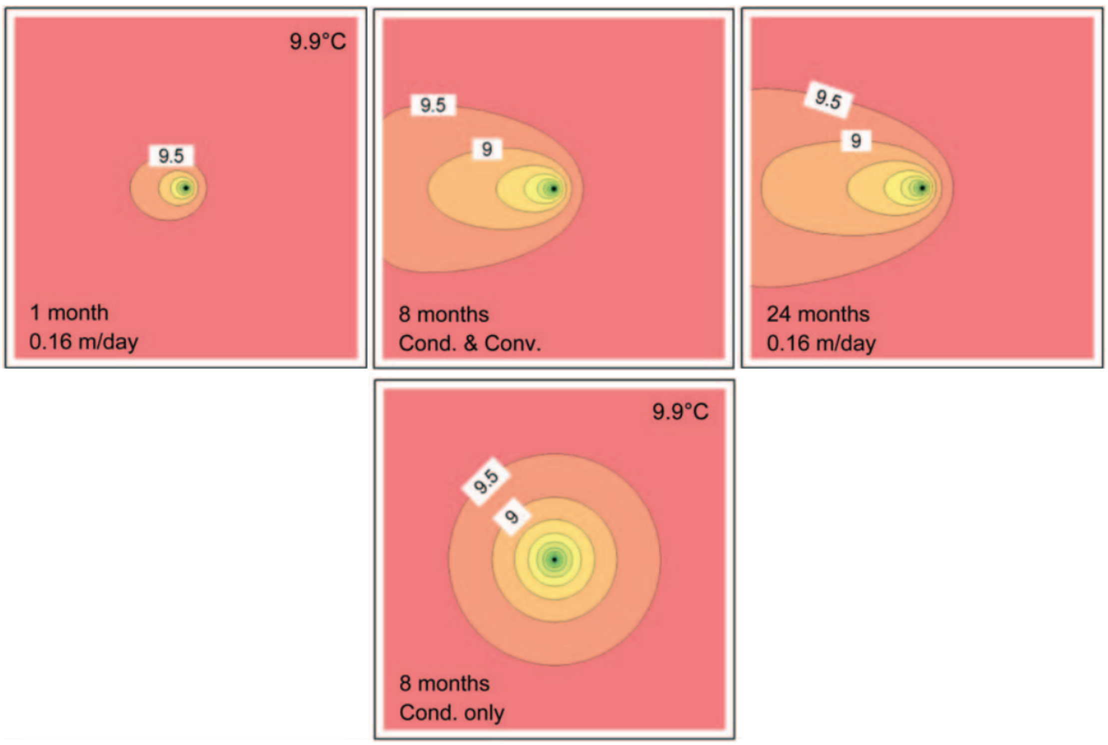

Figure 2.9. Development of the ground thermal regime at 1, 8 and 24-month periods for flow velocities of 0.16 m/day (from Tolooiyan and Hemmingway 2012)

Most of the thermo-hydro-mechanical models used to simulate the behaviour of energy piles assume that the surrounding soil is under a saturated condition. In real life, an unsaturated soil condition is always a possibility. For instance, the groundwater table may be significantly below the ground surface, in addition to which its level may also change seasonally. The heat transfer between the pile and soil results in moisture movement and the degree of saturation is redistributed. A study was carried out by Arson et al. (2013) to explore the effect of debonding and the presence of air pockets at the soil–pile interface in heat transfer from the thermal piles in dry sand. They observed that air pockets at the pile–soil interface have an insulating effect and reduce the heat transferred to the ground. They also pointed out that debonding has a critical effect on the mechanical performance of the pile due to loss of frictional resistance. It is clear that there is a need to conduct the thermo-hydro-mechanical analysis under unsaturated conditions.

2.4.6.1 Effect of temperature and suction on strength of unsaturated soil

Salager et al. (2008) conducted an experimental study to investigate the combined effects of suction and temperature on the preconsolidation pressure, *pc*, of a sandy silt. This study indicated that increasing temperature causes preconsolidation stress decrease, the shear strength decrease, whereas a suction increase leads to preconsolidation stress increase, the shear strength increase, when suction higher than the air-entry value as shown in Figure 2.10.

Uchaipichat and Khalili (2009) carried out temperature and suction controlled shear tests on an unsaturated soil. They found that at a constant suction, an increase in temperature caused a reduction in the size of the yield locus, the thermal softening of shear strength of unsaturated soil occured. On the other hand, at a constant temperature, an increase in matric suction caused an expansion of the yield locus, the suction hardening of shear strength took place.

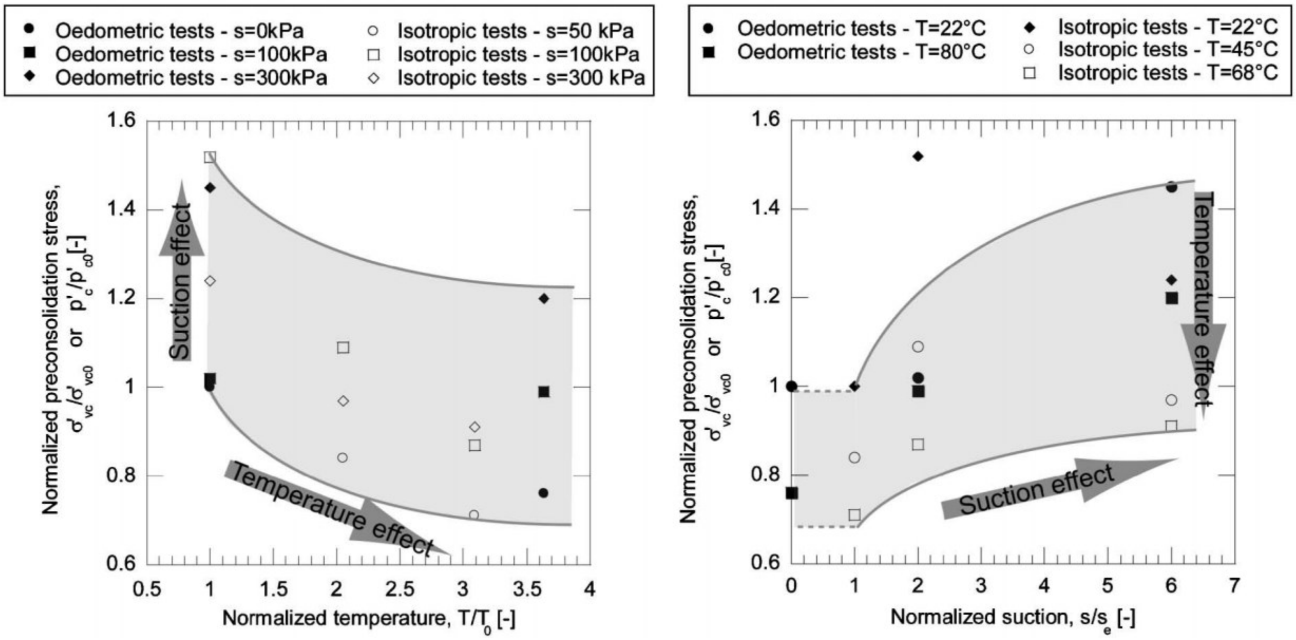

(a) (b)

Figure 2.10. Combined effects of temperature and suction on the evolution of the preconsolidation pressure of a sandy silt: (a) decrease with temperature and (b) increase with suction. The normalized preconsolidation pressure is the preconsolidation pressure measured at a given temperature T and suction, s, over the established preconsolidation pressure at ambient and saturated conditions (T_0 and s =0). s_e is the air-entry suction (from Salager et al. 2008)

Francois and Laloui (2008) developed a constitutive model, based on their experimental data, for unsaturated soils under non-isothermal conditions. Considering mechanical irreveribilities induced by stress-strain, suction or temperature variations, this model used the generalized effective stress, the temperature and the suction as state varialbles to fully simulate the THM constitutive behaviour of materials within an elasto-plastic framwork. The elastic deformation was induced by the effective stress and temperature variations through thermo-elasticity. The plastic deformation was caused by two coupled dissipative processes: an isotropic and a deviatoric plastic strain mechanisms affected by the temperatuare and suction through the evolution of the proconsolidation pressure. Figure 2.11 (a) shows the effect of temperature on the shape of mechanical yield limits. It is noted that the yield limit of soil decreases with the temperature increase. However, the yield limit of soil increases with the suction incease as show in Figure 2.11 (b).

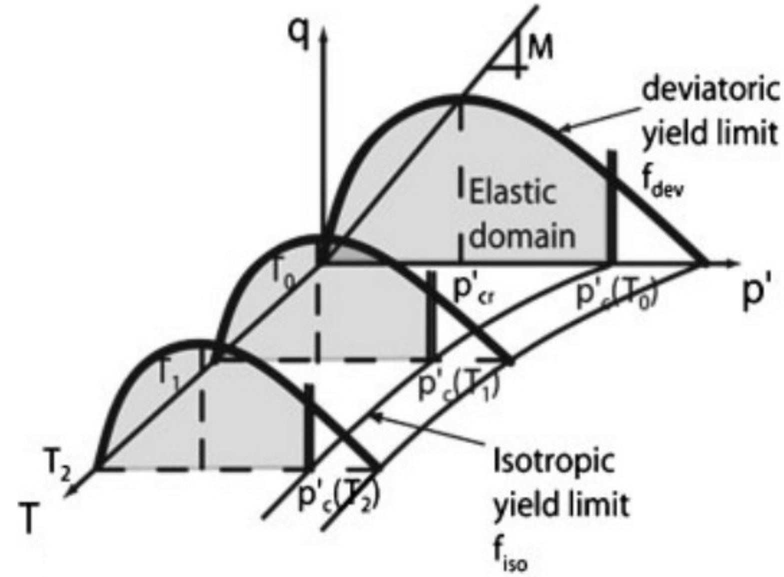

(a)

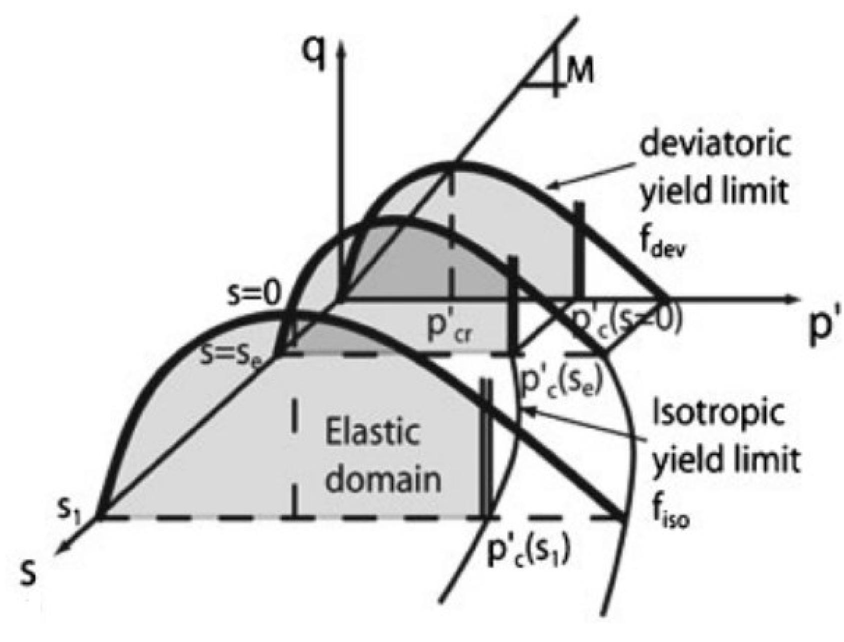

(b)

Figure 2.11. Effect of (a) temperature and (b) suction on the shape of coupled mechanical yield limits (from Francois and Laloui 2009).

2.4.6.2 Temperature effect on soil water characteristic curve (SWCC)

The soil water-characteristic curve (SWCC) is defined as the relationship between soil matric suction and degree of saturation, or gravimetric water content or the volumetric water content (Buckingham 1907; Williams 1982). Physical properties such as water permeability, and shear strength of unsaturated soils are a function of the SWCC. The study of the behaviour of unsaturated soils under non-isothermal conditions requires an understanding of how the soil water characteristic curve (SWCC) changes as a function of temperature. The effect of temperature on SWCC of a compacted soil has been investigated in several studies. Grant and Salehzadeh (1996), She and Sleep (1998) reported that an increase in temperature leads to a decrease in degree of saturation for a given suction. They pointed out that changes in the soil–water contact angle lead to a reduction in the air entry value. Elevated temperatures make a shift in the SWCC to lower degrees of saturation as shown in Figure 2.12. The same trend of shifting a SWCC due to temperature effect was reported in a number of studies (Romero et al. 2001, Salager et al. 2007, Uchaipichat and Khalili 2009, Romero et al. 2003, Villar and Gómez-Espina 2009).

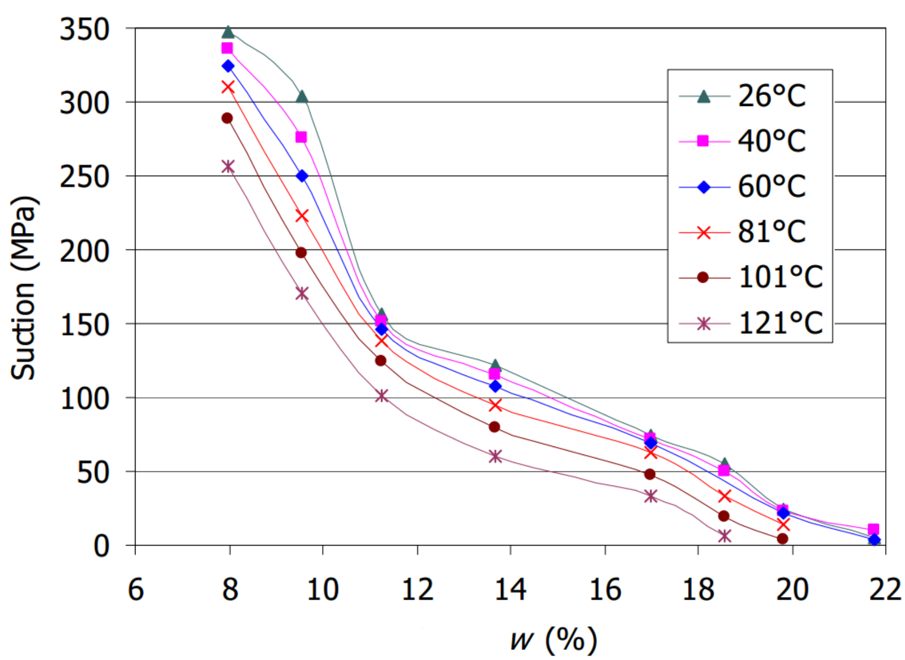

Figure 2.12. Thermal effect on SWCC of FEBEX bentonite (from Villar and Gómez-Espina 2009)

Many empirical, analytical and statistical models in the literature have been proposed for the mathematical representation of the SWCC (Brooks and Corey 1964; van Genuchten 1980; Fredlund and Xing 1994; Leong and Rahardjo 1997). Among these extensive models, the Brooks and Corey (1964), van Genuchten (1980), and Fredlund and Xing (1994) equations shown in Table 2.3 are found to be more practical for geotechnical engineering applications (Sillers et al. 2001).

The SWCC estimation using the Fredlund and Xing (1994) equation has more flexibility in case of mathematical attributions (Sillers et al. 2001; Chin et al. 2010). The fitting parameters, *a*, *n* and *m* in this equation, can be distinguished from the effect of the other two parameters which leads to a greater flexibility (Sillers et al. 2001).The *n* and *m* parameters are generally associated with the shape (slope) of the SWCC. Experimental data published by Wu et al. (2004) and Salager et al. (2006) showed that the measured SWCC at two different temperatures have similar slopes and are parallel to each other. Therefore, the temperature changes have little impact on the values of *n* and *m.* While the parameter *a* is associated with the air entry value, which is affected by the changes of temperature. Roshani and Sedano (2016) developed an expression for the parameter *a* of the Fredlund and Xing model as a function of temperature as expressed in the following:

$$\alpha_T = \alpha_{(T=20)} \times 7.22 \times 10^{-5} \times \frac{(658.2 - 2.509 \times T - 4.606 \times 10^{-3} \times T^2)}{(0.117 - 0.00153 \times T)} \tag{2.7}$$

where a_T is the Fredlund and Xing parameter at a desirable temperature, T is a temperature (^oC), and $a_{T=20\,^oC}$ is the value of the *a* parameter at reference temperature.

Table 2.3 Common Soil-water characteristic curves equations

References	Equations
Brooks and Corey (1964)	$\theta_\omega = \theta_r + (\theta_s - \theta_r)(\frac{a_{bc}}{\psi})^{b_{bc}}$
van Genuchten (1980)	$\theta_\omega = \theta_r + \frac{\theta_s - \theta_r}{(1 + \alpha_{vg}\psi^{b_{vg}})^{c_{vg}}}$
Fredlund and Xing (1994)	$\theta_\omega = \theta_r + \frac{\theta_s - \theta_r}{(ln(e + (\frac{\psi}{\alpha_f})^{n_f}))^{m_f}}$

Note: θ is the volumetric water content; θ_s is the saturated volumetric water content, θr is the residual volumetric water content, a, n, m, α, b, are fitting parameters and ψ is the soil suction in kPa.

2.5. Analysis of pile capacity

The soil-pile interface can be considered as a zone of intense localization of shear strains (Cichy et al. 1987). The interface behaviour will have an impact on the bearing capacity of piles and efficiency of heat transfer of energy piles. The ultimate shearing resistance at the interface between soils and pile material is relevant to the stability of piles as shown schematically in Figure 2.13.

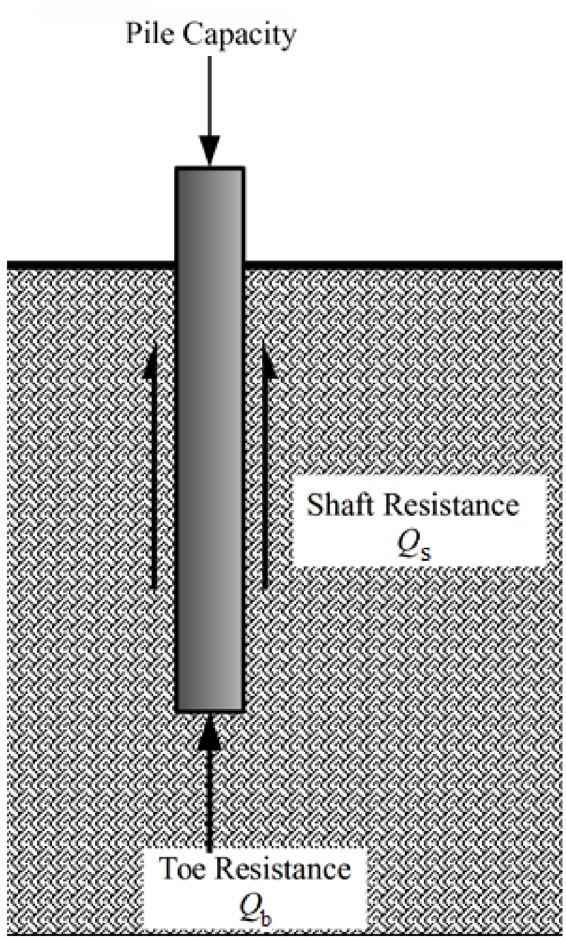

Figure 2.13. Components of pile bearing capacity

The capacity (Q_u) of a pile depends on the toe resistance (Q_b) and shaft resistance (Q_s) as shown in Figure 2.13. The shaft resistance can be determined by Equation 2.8.

$$Q_S = \Sigma\, r_s\, p\, \Delta L \qquad (2.8)$$

where Q_s is the shaft resistance, p is perimeter of the cross section of the pile, ΔL = incremental length of the pile.

$$r_s = f_1 + f_2 \qquad (2.9)$$

where r_s is the interface shear strength, or unit shaft friction, for the pile, f_1 is the friction contribution to the interface strength, f_2 is the adhesion between the soil mixture and pile.

$$f_1 = K\,\sigma'_v\,\tan\delta \tag{2.10}$$

where K is effective earth pressure coefficient, σ'_v is effective vertical stress at the depth under consideration, δ is the interface friction angle.

2.5.1 Bearing capacity of piles in unsaturated soils (without temperature effect)

Vanapalli and Taylan (2012) studied the influence of matric suction on the shaft resistance of a model scale single pile. Based on the experimental results, they modified the conventional α, β, and λ methods to estimate the total shaft resistance of piles in unsaturated soils. The equation used for the calculation of shear strength in their analysis will be discussed later in Section 4.8.2.5. There are many publications in the literature related to the topic of bearing capacity of piles in unsaturated soils. Because the temperature is an additional factor in determining the bearing capacity of energy piles, the further literature (review given in the following pages) on methods of bearing capacity calculations will include only those related to energy piles.

2.5.2 Bearing capacity of piles in unsaturated soils (with temperature effect)

Based on load-transfer method, Knellwolf et al. (2011) proposed thermomechanical load transfer method to consider the thermal effects on toe resistance (Q_b) and shaft resistance (Q_s) of an energy pile. The pile is discretized in a number of segments based on various soil layers with distinct properties and the variation of the soil properties with depth as shown in Figure. 2.14. The calculation of the thermomechanical response of the heat exchanger pile was achieved by the following steps. First, the stress state and the pile displacements were calculated due to mechanical loading; this state was viewed to as the initialization state. Then, from the initialization state, the pile responses were calculated due to the thermal loading (heating or cooling occurring during heat exchange). An iterative procedure allowed the thermal strains and the associated additional efforts, when the pile was subjected to both axial mechanical loading and temperature changes, to be quantified.

Based on the work by Knellwolf et al. (2011), Chen and McCartney (2016) developed a thermo-mechanical load transfer method in nonlinear conditions. They pointed out that the important step is to identify the null point (NP) location (the location of zero thermal displacement in an energy pile undergoing a uniform temperature change). Once the NP was identified, the status of axial strain and stress in the energy pile was iteratively computed to reach equilibrium in the upper and lower parts of the pile, considering compatibility of displacements between the soil and pile.

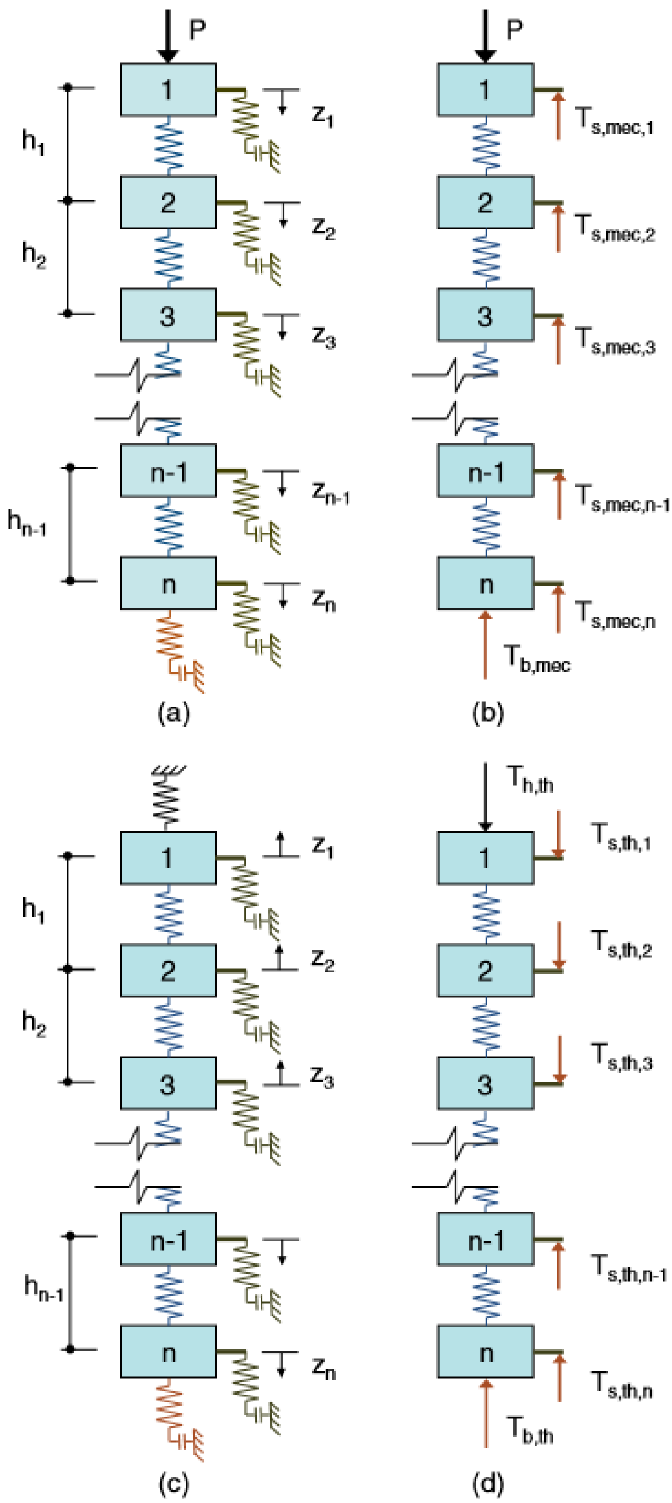

Figure 2.14. Numerical model for energy pile load and displacement analysis: (a) model for mechanical load; (b) external forces mobilized by mechanical loading; (c) model for thermal load; (d) external forces mobilized by thermal loading (From Knellwolf et al. 2011).

2.6. Conclusions of literature review

Conclusions of the present literature review are as follows.

- Deformation characteristics and shear strength of unsaturated soils are influenced mainly by the capillary forces. The capillary forces are complex functions of the soil properties (particle and pore size), degree of saturation and the properties of the multiphase fluid interface (air-water surface tension, contact angle) with the temperature.
- In relation to the behaviour of unsaturated soil-structure interfaces, the surface roughness and the type of structural material are added factors to all other influential factors related to unsaturated soils.
- Thermo-hydro-mechanical processes are coupled processes. For that reason, the temperature, matric suction, stress states, and stress history in laboratory experiments and field tests have to be known to reach valid conclusions.
- Temperature increase may reduce the strength of fine grained unsaturated soils.
- Increasing suction causes an increase in shear strength of unsaturated soils.
- Thermally induced increase in lateral stress is a major factor affecting shaft resistance and the load–displacement behaviour of energy piles.

CHAPTER 3

COUPLING OF THERMO-HYDRO-MECHANICAL PROCESSES TAKING PLACE AT THE SOIL STRUCTURE INTERFACES

The mechanisms of heat transfer between energy piles and the ground are described as follows:

1) Heat conduction within the pile (H1),
2) Heat conduction within the soil (H2), and
3) Heat flow via subsurface fluid flow (H3).

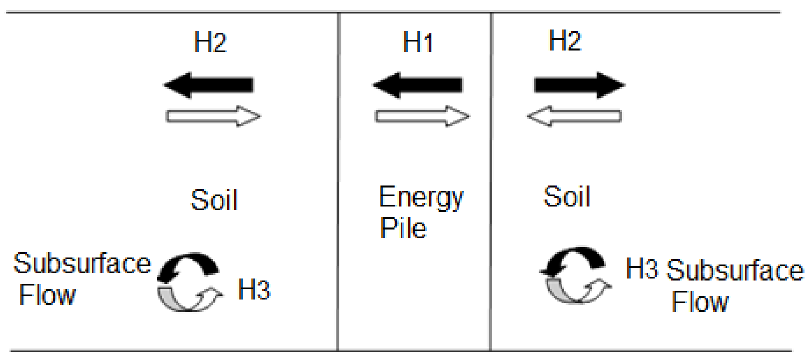

Figure 3.1. Mechanisms of heat transfer between energy piles and the ground (from Abdelaziz et al. 2011)

As schematically shown in Figure 3.1, heat transfer occurs in two directions reflecting the heat injection into the ground during cooling operations (dark arrows) and heat extraction from the ground during heating operations (white arrows).

Once an energy pile system is set up, the pile-soil interface is subjected to thermal loading (heating/cooling cycles), mechanical loading (stress/deformation) and hydraulic loading (fluid flow). These processes are complex events. One process affects the initiation and progress of the others as shown in Figure 3.2. The material parameters also change during the coupling. This study will focus on the thermo-hydro-mechanical (THM) processes in the pile-soil interface.

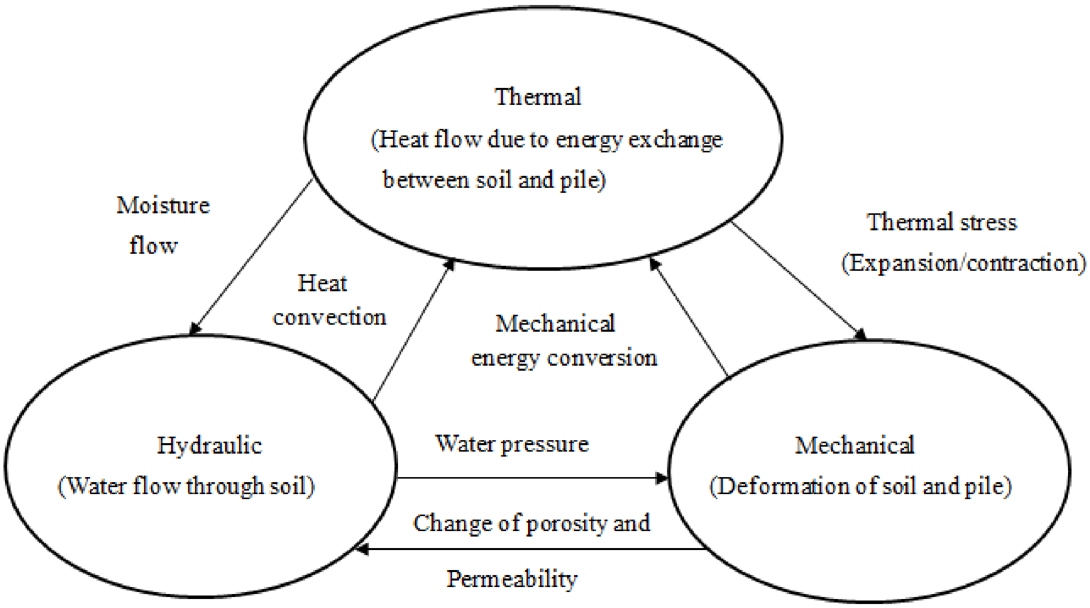

Figure 3.2. THM processes of soil-pile interface (modified from Jing 2003)

3.1. Mathematical formulation

A numerical model for a porous media with multi-physic processes is employed in this study. This model is based on the momentum conservation, mass conservation and energy conservation laws. Fully–coupled equations are used to describe the evolution of pore water pressure, solid displacement and heat flow under mechanical, hydraulic and thermal loading. The equations used in PLAXIS software are provided in Appendix A.

3.1.1. Static equilibrium (momentum conservation)

Soil equilibrium equation is expressed by

$$\mathrm{div}(\boldsymbol{\sigma}) + \mathbf{b} = 0 \tag{3.1}$$

where $\boldsymbol{\sigma}$ is the total stress tensor with tensile stresses taken as positive; and $\boldsymbol{b}$ is the body force vector, which is equal to $\rho_{sat}\mathbf{g}$ if the only body force is gravity. ρ_{sat} is the total average mass density and it is determined from

$$\rho_{sat} = n\rho_f + (1 - n)\rho_s \tag{3.2}$$

where ρ_s, ρ_f are the mass density of the solids and the fluid phases, respectively, and n is the porosity;

$\mathbf{g}$ is the vector of acceleration of gravity.

The strain increments that are related to stress increments consist of components due to suction, temperature and stress changes.

The behaviour of the solid matrix is assumed to be governed by the generalized effective stress tensors σ' through combinations of mechanical stresses and fluid pressures (Dupray et al. 2013):

$$\sigma' = \sigma - p_g I + S_r (p_g - p_w) I \tag{3.3}$$

where I is the identity matrix, S_r is degree of saturation, p_w is the pore pressure and p_g is the gas pressure; the term (σ - p_gI) is called the net stress, whereas (p_g - p_w) is the matrix suction.

In Lagrangian approach, the Cauchy strain tensor is used:

$$\varepsilon = \frac{1}{2}(L - L^T) \tag{3.4}$$

where $L = \frac{\partial u}{\partial X}$ is the displacement (u) gradient defined in the global axis (X). This strain tensor is related to the generalized effective stress tensor through the mechanical constitutive model:

$$\sigma' = D : \varepsilon \tag{3.5}$$

where D is the mechanical constitutive matrix which depends on the Young's modulus, E, and Poisson's ratio, v in the case of linear elastic relationships. This equation can be written in incremental form due to the non-linear behaviour of the solid matrix. Thus the momentum conservation equation takes the form

$$\mathrm{div}(D : \varepsilon) + \mathrm{grad}\,p_g - S_r \mathrm{grad}\,(p_g - p_w) + \rho_{sat} g = 0 \tag{3.6}$$

3.1.2. Fluid flow (Mass conservation)

Richards' equation is used to model the flow in variably saturated media. Wilson (1980) modified his equation, and later by Milly (1982). Equation (3.7) is very general and allows for time-dependent changes in both saturated and unsaturated conditions.

$$\frac{1}{\rho}\frac{\partial}{\partial x}\left(D_V\frac{\partial \mathrm{Pv}}{\partial \mathrm{x}}\right)+\frac{1}{\rho}\frac{\partial}{\partial y}\left(D_V\frac{\partial \mathrm{Pv}}{\partial \mathrm{y}}\right)+\frac{\partial}{\partial x}\left(k_x\frac{\partial(\frac{P}{\rho g}+y)}{\partial \mathrm{y}}\right)+\frac{\partial}{\partial y}\left(k_y\frac{\partial(\frac{P}{\rho g}+y)}{\partial \mathrm{y}}\right)+\mathrm{Q}$$
$$=\lambda\frac{\partial P}{\partial t} \tag{3.7}$$

where P is the capillary pressure; Pv is the vapor pressure of soil moisture; k_x and k_y are the hydraulic conductivities in the x- and y-directions, respectively; Q is the boundary flux, D_V is the vapour diffusion coefficient, y is the elevation head, ρ is the density of water, g is the gravitational acceleration, t is time, and λ is a decay constant.

3.1.3. Heat flow (Energy conservation)

From Fourier's linear law, the two major forms of heat flow, convection and conduction, are combined using the following general differential equation (3.8):

$$\mathrm{L}_V\frac{\partial}{\partial x}\left(D_V\frac{\partial \mathrm{Pv}}{\partial \mathrm{x}}\right)+\mathrm{L}_V\frac{\partial}{\partial y}\left(D_V\frac{\partial \mathrm{Pv}}{\partial \mathrm{y}}\right)+\frac{\partial}{\partial x}\left(k_x\frac{\partial \mathrm{T}}{\partial \mathrm{y}}\right)+\frac{\partial}{\partial y}\left(k_y\frac{\partial \mathrm{T}}{\partial \mathrm{y}}\right)+\mathrm{Q}_t+\rho \mathrm{c}V_x\frac{\partial T}{\partial x}+\rho \mathrm{c}V_y\frac{\partial T}{\partial y}$$
$$=\lambda_t\frac{\partial T}{\partial t} \tag{3.8}$$

where ρc is the volumetric specific heat, $\mathrm{P_v}$ is the vapor pressure of soil moisture, k_x and k_y are the thermal conductivities in the x and y directions, respectively, V_x and V_y are the Darcy velocities of water flow in the x and y directions, respectively, $\mathrm{D_v}$ is the vapour diffusion coefficient, Q_t is the thermal boundary flux, and L_v is the latent heat of vaporization, t is time, and T is the temperature, and λ_t is a decay constant.

Heat capacity and thermal conductivity of soils are strongly influenced by their degree of saturation. Johansen (1977) proposed an empirical relationship to predict soil thermal conductivity,

$$k = \left(k_{water}^{n} k_{soild}^{1-n} - \frac{0.137\rho_d + 64.7}{2650 - 0.947\rho_d}\right)(0.7logS_r + 1) + \frac{0.137\rho_d + 64.7}{2650 - 0.947\rho_d} \qquad (3.9)$$

where k_{water} and k_{solid} are thermal conductivities of water and solid, respectively; n is the porosity; S_r is the degree of saturation; ρ_d is the dry density of soil, kg/m^3.

Figure 3.3 shows the thermal conductivity in response to varying degree of saturation for a sandy soil compared to a clay soil (Johansen, 1977).

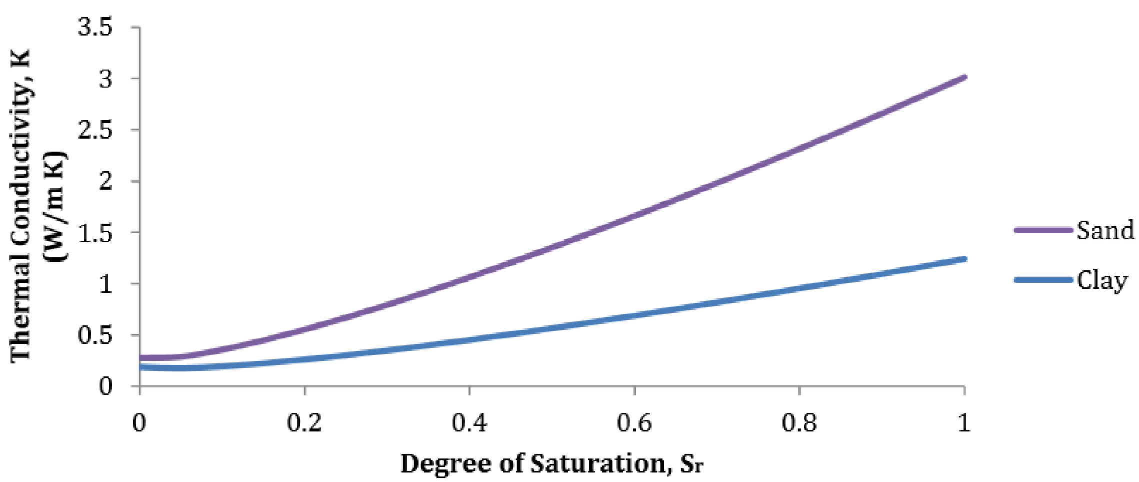

Figure 3.3. Thermal conductivity in response to degree of saturation of a sandy soil and a clay soil, both with n = 0.3, and dry particle thermal conductivities of 7.9 W/m K, and 1.9 W/m K, respectively (Johansen 1977).

In order to eliminate the logarithmic dependence on degree of saturation, Cote and Konrad (2005) modified Johansen's (1977) model and proposed a new empirical equation.

$$k = (k_{water}^{n} k_{solid}^{1-n} - \chi 10^{-\eta}) \left[\frac{\kappa S_r}{1 + (\kappa - 1) S_r}\right] + \chi 10^{-\eta} \tag{3.10}$$

where χ and η relate to particle shape effect, and κ accounts for soil texture effect. For fine and medium sands, 1.7 W m^{-1} K^{-1} for χ, 1.8 for η and 3.55 for κ were suggested by Cote and Konrad (2005) and these values were adopted in the model predictions.

To sum up, the Equation (3.6) is governing the static equilibrium. The Equation (3.7) is used to control the fluid flow and Equation (3.8) is used to describe the heat flow. They are coupled throughout the dependent variables of solid displacement vector, pore water pressure and temperature in the medium.

In this study, two finite-element software packages known as SIGMA/W and VADOSE/W of GeoStudio 2012 by Geo-Slope International Ltd are integrated to solve equations (3.6), (3.7) and (3.8) which are used to mathematically describe the thermo–hydro-mechanical processes in 2-dimensional analyses. SIGMA/W is a finite-element program, which has been designed for the analysis of sub-surface stress and deformation problem. VADOSE/W is a finite-element program capable of simulating sub-surface thermal-hydrogeological problems such as pore-water evaporation and recharge, heat transfer and mass movement under both steady-state as well as transient-state.

3.2. Material constitutive models

In this study, the pile is assumed to behave as a linear elastic material. The stress–strain response of soil is modeled using the Elastic-Plastic model in SIGMA/W. Stresses are directly proportional to strains until the yield point is reached. Beyond the yield point, the stress-strain curve is horizontal.

Mohr-Coulomb yield criterion is used as the yield function for the Elastic-Plastic model. The following equation provides a common form of the Mohr-Coulomb criterion expressed in terms of stress invariants I_1, J_2 and Θ (Chen and Zhang, 1991). Equation 3.11 represents the yield function.

$$F = \sqrt{J_2}\,\mathrm{L}_V \sin\left(\theta + \frac{\pi}{3}\right) - \sqrt{\frac{J_2}{3}}\cos\left(\theta + \frac{\pi}{3}\right)\sin\emptyset - \frac{I_1}{3}\sin\emptyset - c\cos\emptyset = 0 \quad (3.11)$$

Where:

$$J_2 = \frac{1}{6}\,[(\sigma_x - \sigma_y)^2 + (\sigma_y - \sigma_z)^2 + (\sigma_z - \sigma_x)^2] + \tau^2{}_{xy} + \tau^2{}_{yz} + \tau^2{}_{zx}$$

$$\rightarrow second\ invariant\ of\ deviatoric\ stress\ tensor$$

$$\theta = \frac{1}{3}\cos^{-1}\{\frac{3\sqrt{3}}{2}\frac{J_3}{J_2^{3/2}}\} \rightarrow Lode\ angle$$

$$J_3 = \sigma_x^d\sigma_y^d\sigma_z^d - \sigma_z^d\tau^2{}_{xy} - \sigma_y^d\tau^2{}_{zx} - \sigma_x^d\tau^2{}_{yz}$$

$$\rightarrow third\ invariant\ of\ deviatoric\ stress\ tensor$$

where

$$\sigma_x^d = \sigma_x - \frac{I_1}{3}$$

$$\sigma_y^d = \sigma_y - \frac{I_1}{3}$$

$$\sigma_z^d = \sigma_z - \frac{I_1}{3}$$

$$I_1 = \sigma_x + \sigma_y + \sigma_z \rightarrow first\ stress\ invariant$$

3.3. Sequential analysis using SIGMA/W and VADOSE

The integration of SIGMA/W and VADOSE/W analyses is achieved in the following way: at first, a mechanical process for the interaction between an energy pile and soil is analyzed (parent analysis) using SIGMA/W; after the parent analysis, the model uses VADOSE/W to continue with the analysis of processes of heat transfer and fluid flow. In other words, one process is analyzed after another process after updating the required parameters. The analysis is a sequential type, but not a fully coupled thermo-hydro-mechanical analysis. However, the analysis of one process (say thermal analysis) is divided into small steps to integrate with the analysis of the other processes (say mechanical) for several times. After each step, the material parameters are changed for the next integration, which is viewed as the sequential analysis method. For example, the temperature loading is divided into several increments ($\Delta T=\sum\Delta T_i$). After the thermal analysis under the condition of ΔT_i by VADOSE/W, the material parameters in the model are changed and the mechanical analysis is conducted by SIGMA/W again. After that the analysis of thermal processes under the condition of ΔT_{i+1} is carried out by VADOSE/W. The sequential analysis method needs the material parameters changing with the temperature. By performing the analysis sequentially, the shear strength parameters of the soil are updated as a function of temperature from lab tests. Soil-Water Characteristics Curves (SWCC) at different temperatures are used to describe the behaviour of unsaturated soil in VADOSE/W. The method proposed by Roshani and Sedano (2016) is used to obtain SWCC at different temperatures.

CHAPTER 4

LABORATORY STUDY ON THE BEHAVIOUR OF AN INTERFACE BETWEEN AN ENERGY PILE MATERIAL AND SOIL

In this study, laboratory experiments are carried out to investigate the behaviour of an interface between an energy pile material and soil. Two types of tests are conducted as described in the following:

(a) To explore the effect of the soil moisture content on (a) the shear strength of an unsaturated soil mixture and (b) the shear strength of an interface between the unsaturated soil mixture and a steel plate, a series of tests are conducted using a conventional direct shear machine and a modified conventional direct shear type interface machine.

(b) To investigate the effects of temperature, matric suction, net normal stress, and stress history on the interface parameters i.e. adhesion and friction angle, a series of interface tests are conducted using the modified 3-D Cyclic Interface Testing Apparatus developed earlier by Fakharian and Evgin (1996). This interface machine did not have the capability of applying temperature changes on the test samples. As part of the present investigation, Fu et al. (2013) made the necessary modifications to add this capability to the testing machine.

Temperature gradients in the unsaturated soils cause water to migrate in the liquid and vapor phases from the warmer regions to the colder regions. The following example is given to illustrate this phenomenon.

A laboratory investigation about the physics of heat and moisture transfer in compacted Mackenzie Silt samples was conducted by Evgin and Svec (1988). Tests were conducted on a soil sample which was 111mm long and 75 mm high. The initial thermal conductivity of the soil was equal to 1.58 W/m K. First, the soil was placed in a fully instrumented soil container at a volumetric moisture content of 0.17 at room temperature (20^{o}C). During the experiment, the left boundary of soil sample was kept at 41.2^{o}C and the right boundary was maintained at 8.2^{o}C.

After two hours of testing, the volumetric moisture content distribution along the sample was measured. The results are shown in Figure 4.1. It was noted that the volumetric moisture content of the soil near the worm end of the soil column reduced to about 0.07 from the initial value of 0.17; however, the volumetric moisture content at the cold end increased to about 0.22. Similar processes would take place at the soil-pile interfaces due to heating/cooling cycles of energy piles.

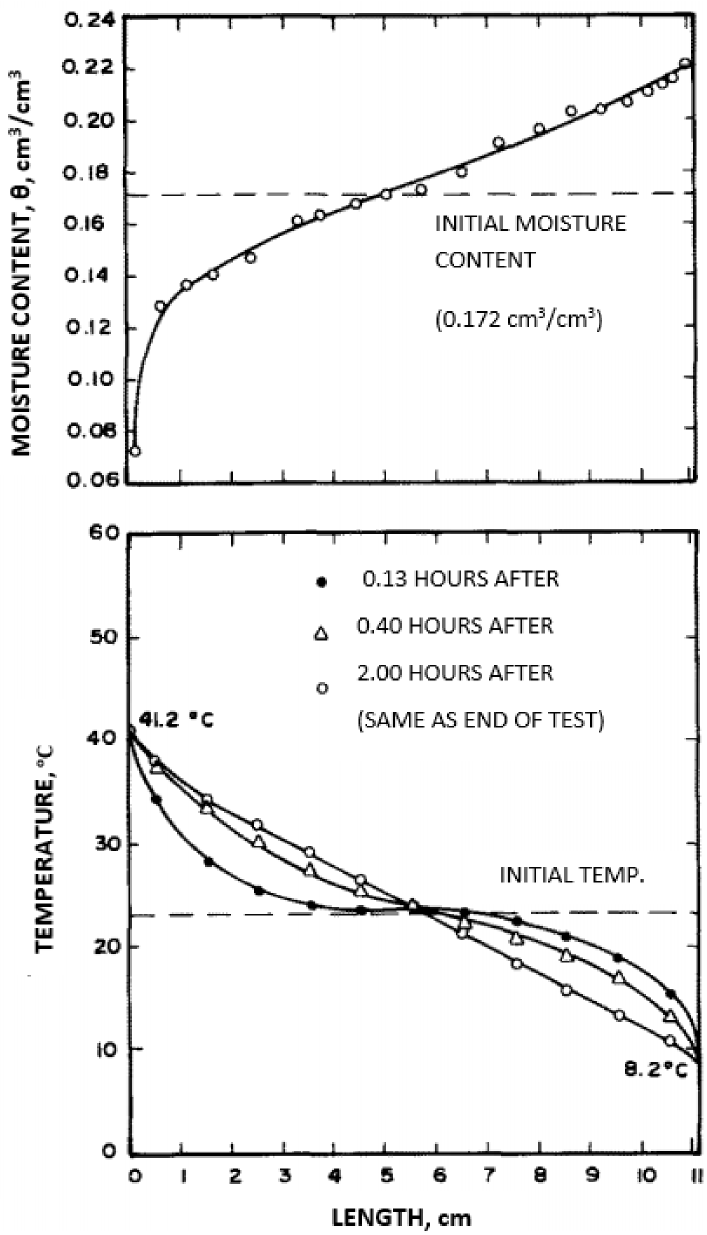

Figure 4.1. Temperature and volumetric moisture content distribution along the soil specimen under a temperature gradient (ΔT=33°C) (from Evgin and Svec 1988).

4.1. Influence of moisture content on the shear strength parameters of the interface using direct shear tests at room temperature (ΔT=0°C)

The moisture content of the soil plays an important role not only in the heat transfer rate but also in the load transfer characteristics of the soil-pile interface. In this study, the effects of the soil moisture content on the shear strength of an interface between a soil mixture (kaolin-sand) and a steel plate are investigated.

Direct shear type interface tests are performed to determine the influence of moisture content on the friction angle and adhesion at the interface. In addition, for the purpose of comparison, the shear stress versus displacement behaviour of the same soil mixture (no interface) is examined. The friction angle and cohesion of the soil mass are plotted as a function of the moisture content of the soil. It should be noted that these tests were conducted in a constant room temperature of 23^{o}C.

4.2. Test Materials

Kaolin-Sand Mixture

A literature survey indicates that clean sand is frequently used in laboratory studies concerning the stress-strain and shear strength behaviour of granular soils. However, field observations show that granular soils may contain a considerable amount of clay and/or silt. Therefore, the test material selected for this study is a kaolin-sand mixture prepared by mixing kaolin, fine sand and water. The commercial kaolin used in the experiments is produced by Edgar Minerals Inc. Clean fine sand is obtained from Merkley Supply Ltd. in Ottawa. The weight ratio of kaolin to sand was 1:3. The particle size distribution of the mixture is shown in Figure 4.2.

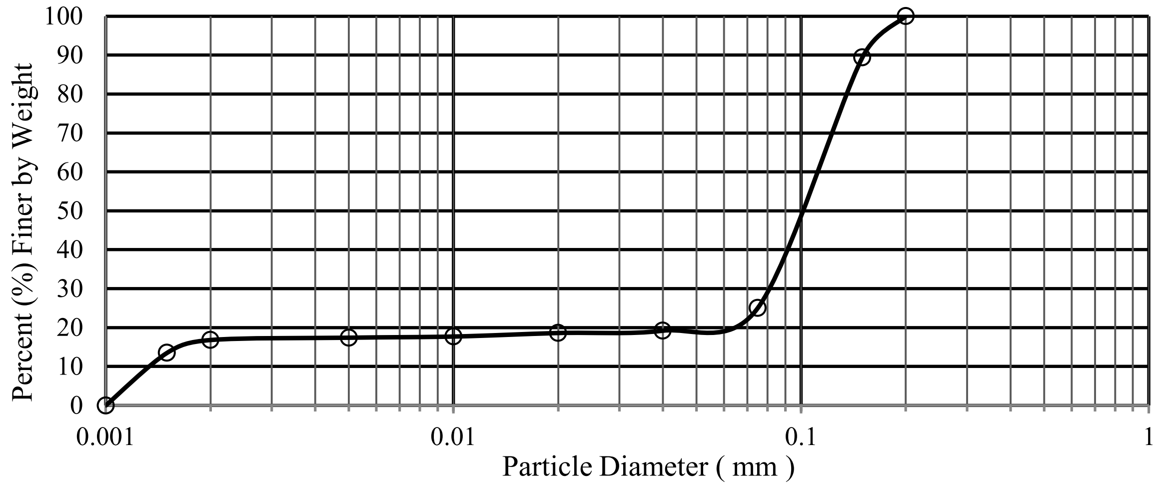

Figure 4.2. Grain size distribution of the kaolin-sand mixture

In the present research, soil samples were prepared in a consolidation ring using static compaction. The maximum normal stress that can be applied on the interface (i.e. the capacity of the machine) is 500 kPa. In order to leave some margin of safety, 375 kPa is chosen as the compaction stress. It is equal to about 45% of the Proctor's energy.

The compaction curve shown in Figure 4.3 indicates that the optimum moisture content for this mixture was about 17.5% with a dry density of 1740 kg/m^3.

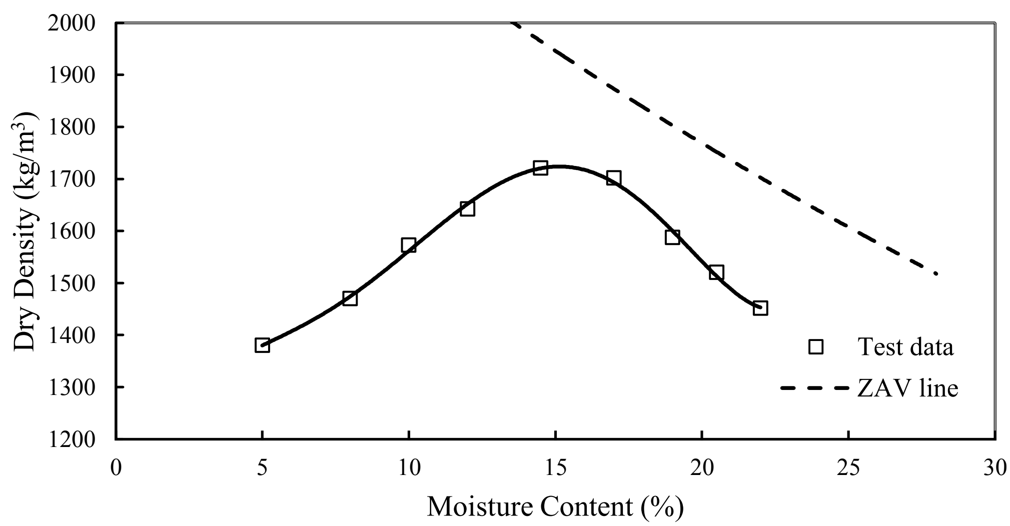

Figure 4.3. Static compaction curve of kaolin-sand mixture

In order to investigate the effect of the moisture content on the shear strength of the soil-steel plate interface, the samples of kaolin-sand mixture are prepared at moisture contents of 10%, 15%, 17.5%, and 21.5% in the laboratory with a controlled room temperature of 23°C. Water content, density, void ratio, degree of saturation and matric suction for each specimen are listed in Table 4.1.

In this study, the matric suction of soil specimens is measured by filter paper method ASTM 5298-10. Watman 42 filter papers are placed on the specimen, one at the top and another one at the bottom. Then the sample with the filter papers is stored in Ziploc bags and kept in a cooler where temperature remained constant for 24 hours. After that, the filter paper water content (w_{fp}) is obtained. Finally, the calibration information for Watman 42 filter paper is applied to determine the associated matric suction values.

ASTM calibration high suction range for:

$w_{fp} < 45.3\%$ $\qquad$ $\log(h) = 5.327 - 0.0779 * w_{fp}$

ASTM calibration low suction range for:

$w_{fp} > 45.3\%$ $\qquad$ $\log(h) = 2.412 - 0.0135 * w_{fp}$

where h is the matric suction, kPa.

Table 4.1 Water content, density, void ratio, degree of saturation and suction for each specimen

Specimen	Water Content (%)	Dry Unit Weight (kN/m^3)	Void ratio	Degree of Saturation (%)	Matric Suction (kPa)
1	10	15.7	0.60	45	68
2	15	16.9	0.58	70	34
3	17.5	17.2	0.56	85	21
4	21.5	14.3	0.66	88	15

The compression response of soil specimens are assessed by oedometer tests, with loading increments applied until settlement was negligible. The void ratio at the end of mechanical loading increment was calculated using the following steps:

1. The height of the soil solids, H_s, was first calculated using the following relationship:

$$H_S = \frac{H_i}{1 + e_i}$$

where H_i is the initial height of the specimen, and e_i is the initial void ratio.

2. The void ratio at any time during the test, e, was calculated from the height of soil solids and the measured height of the specimen using the following relationship:

$$e = \frac{H}{H_S} - 1$$

where H is the measured height of specimen during consolidation.

A typical consolidation curve of a soil sample with water content of 17.5% at room temperature is shown in Figure 4.4.

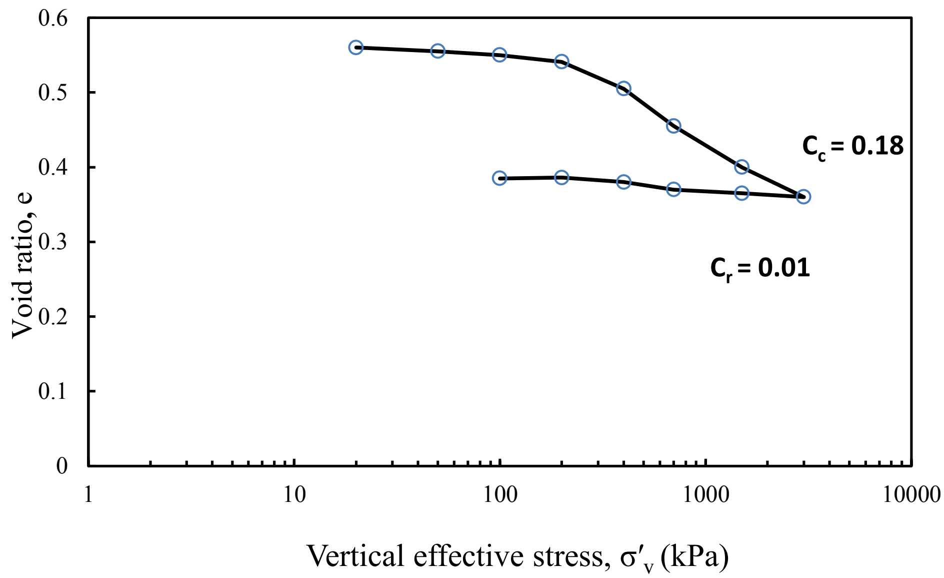

Figure 4.4. Variations in void ratio versus effective stress curve of soil sample with w=17.5% at 23°C

In this study, the drying–path soil water-characteristic curve (SWCC) at a temperature of 23^{o}C for kaolin-sand mixture is shown in Figure 4.5 (middle curve). It is generated by using Fredlund and Xing's equation fitted to experimental data obtained by filter paper method ASTM 5298-10 at 23^{o}C. The effect of temperature is included by changing the parameter α in Fredlund and Xing's equation using the equation of Roshani and Sedano (2016) (More information is given in Section 2.4). Table 4.2 shows the parameters α, n, m for the kaolin-sand mixture as calculated for three different temperatures.

Table 4.2 Parameters of α, n, m for kaolin-sand mixture with temperatures.

Temperature(°C)	θ_s	θ_r	α	n	m
23	0.39	0.07	35	2.39	0.58
8	0.39	0.07	43	2.39	0.58
35	0.39	0.07	22	2.39	0.58

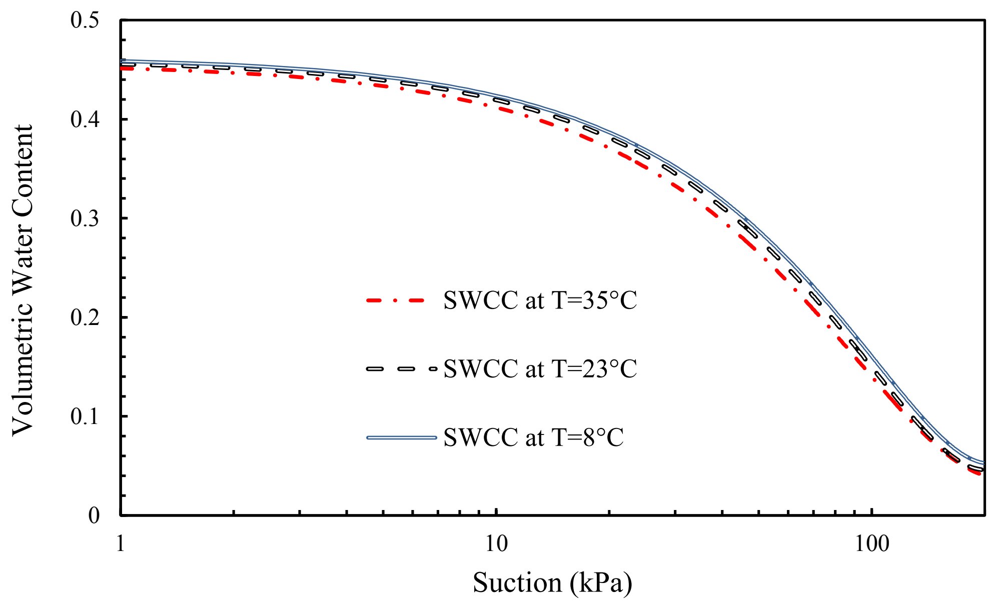

Figure 4.5. SWCC curves for kaolin-sand mixture at T= 8, 23, 35°C.

4.3. Steel plate

The average roughness (Ra) is the arithmetic average of the roughness profile. In engineering practice, typical steel piles have the roughness values ranging between 1 to 20 µm. In this study, the surface of steel plate used as part of the interface is sand blasted at the machine workshop at the University of Ottawa. The Ra is measured using a roughness tester. The average roughness (R_a) of the plate is 5.8 µm.

4.4. Experimental plan and testing apparatus

Two types of interface tests are conducted in this study. One type is performed at room temperature to investigate the effect soil water content on interface shear strength without the effect of temperature change. The tests are carried out using conventional direct shear apparatus as shown in Figure 4.6. The lab test results provided the strength and deformation parameters as well as the reduction factor needed in the numerical analysis of the interface tests using PLAXIS. In the numerical analysis of the energy piles, the results of the soil-on-soil tests and soil-steel plate interface tests (conducted at room temperature, ΔT=0°C) provided the necessary input parameters in the calculations.

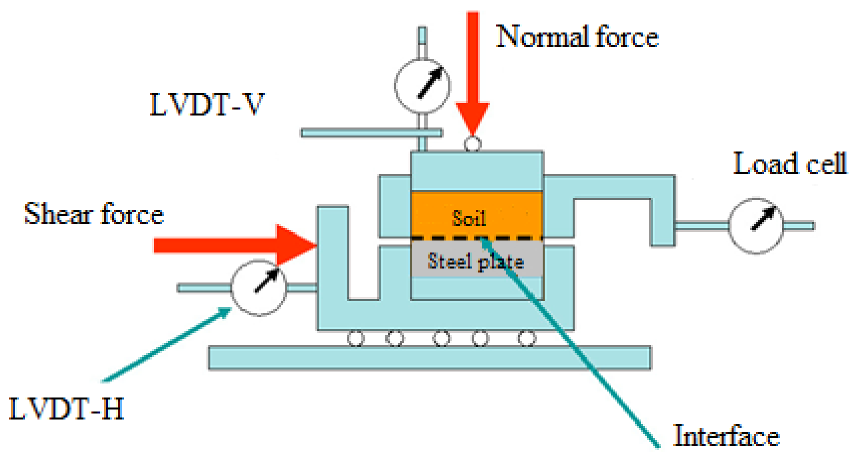

Figure 4.6. Modified direct shear apparatus for testing interfaces (ΔT=0°C).

The second type of tests is conducted to investigate the effect of temperature changes on interface behaviour using 3-Dimensional Cyclic Interface Testing Apparatus with Temperature Control as shown in Figure 4.7. More details about this machine are given in Section 4.6.

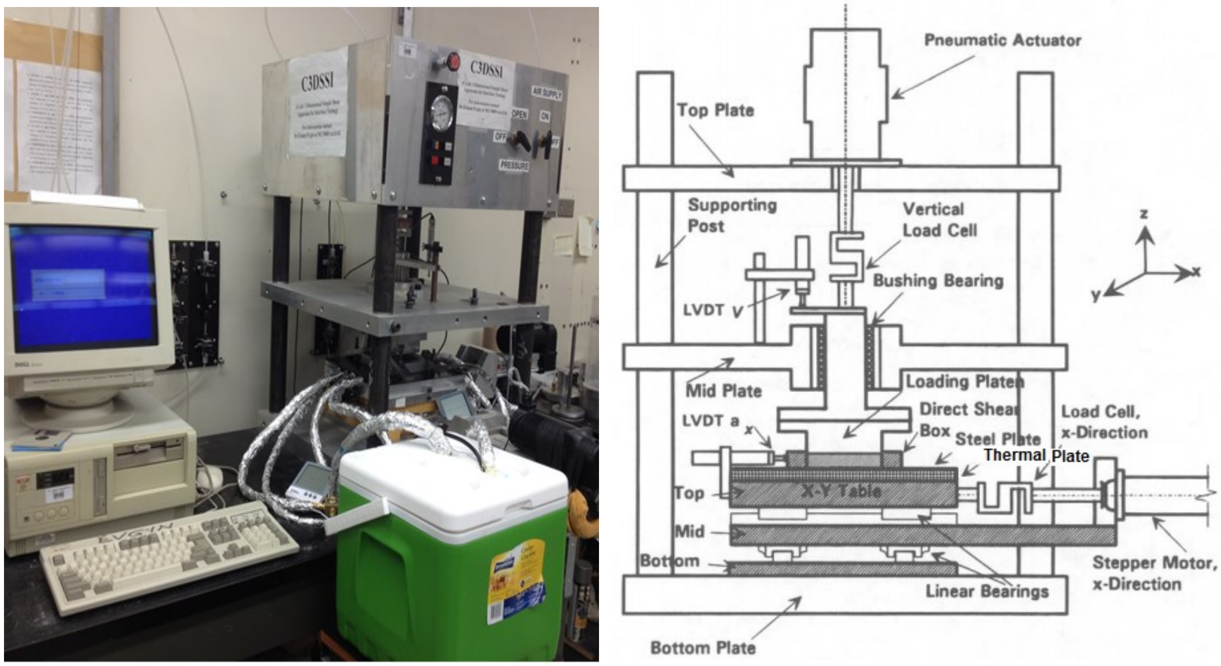

Figure 4.7. 3-D Cyclic Interface Testing Apparatus with Temperature Control

4.5 Interface tests under isothermal conditions

In the shear box, the bottom halve contains the steel plate, while the top half is filled with the kaolin-sand mixture. The interface is between the soil and the steel plate. The kaolin-sand mixture sample is compacted inside the shear box, and is then allowed to consolidate for about 20 minutes under normal stress equal to 45 kPa. After that time, there was no change in the sample height. It was assumed that the primary consolidation has already taken place. Shearing of the specimen begins after completion of the primary consolidation. The normal load acting on the sample remains constant during the shearing process. Tsubakihara et al. (1993) used 0.03 mm/min displacement rate for clay-steel interface tests in consolidated drained conditions. The clay content of their samples was 50%. In the present study, the clay content of the kaolin-sand mixture is 25%. For this reason, the shear displacement rate of 0.06 mm/min is used in the present experiments to correspond to drained conditions. All data regarding the test (shear force, horizontal and normal displacements) are collected using a computerized data logging system. The results are monitored and saved by LabView.

Interface shear tests were conducted on specimens with moisture contents of 10%, 15%, 17.5%, and 21.5%. For every soil-steel plate specimen, three tests were performed by applying normal stresses of 50, 100, and 150 kPa. Similarly, direct shear tests were conducted on soil samples for the purpose of comparison. There was no steel plate at the bottom half of the sample box. The box was filled with soil mixture only. These tests were also referred to as soil-on-soil tests.

4.5.1. Test results and discussion

The test results showing the effect of moisture content on the shear strength of the soil-steel plate interface are presented in this section. In the presentation, three types of graphs are used: the shear stress versus horizontal displacement curves, the vertical displacement versus horizontal displacement curves and the shear strength envelopes, which give shear strength parameters (adhesion, f, and friction angle, δ) of the interface.

4.5.1.1. Shear stress versus horizontal displacements

Figure 4.8 shows a typical relationship of shear stress versus horizontal displacement for the interaction between kaolin-sand mixture and the steel plate at moisture contents of 10%, 15%, 17.5% and 21.5%. The shear stress versus horizontal displacement curves from conventional direct shear tests performed on the soil mixture alone (i.e. soil-on-soil) are presented in Figure 4.9 for the purpose of comparison. The shear stress versus horizontal displacement curves of the interface between soil-steel plate show a similar trend and shape as those obtained from the tests on kaolin-sand mixture alone (Figures 4.8 and 4.9). However, the values of strength parameters obtained from the soil-on-soil tests are greater than those from soil-steel plate interface tests. This is due to the fact that sand grains tend to slide easily on the relatively smooth surface of the steel plate, which decreases the frictional resistance of the interface. This leads to lower peak shear strength of the interface than that of the soil mixture only.

As shown in Figure 4.8, the shear stress on the interface gradually increases with increasing horizontal displacement until the peak shear stress is reached. After the peak stress value, the strength reduces gradually and finally becomes more or less constant with increasing horizontal displacement. The experimental results show that as the moisture content increases and approaches to the optimum moisture content, the peak shear strength of the interface also increases to its largest value. However, for the interface with the moisture content larger than the optimum moisture content, the peak shear strength is reduced. It can also be noted that the sample at optimum moisture content has the steepest slope in the curves of shear stress vs horizontal displacement at the range from about 30 kPa to peak shear strength.

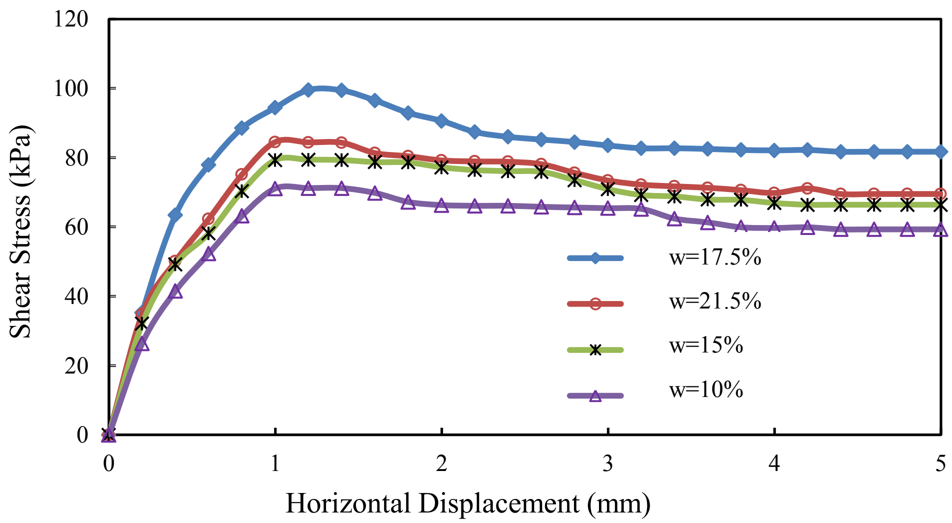

Figure 4.8. Shear stress versus horizontal displacement of soil-steel plate interface with various moisture contents (Normal stress = 150 kPa)

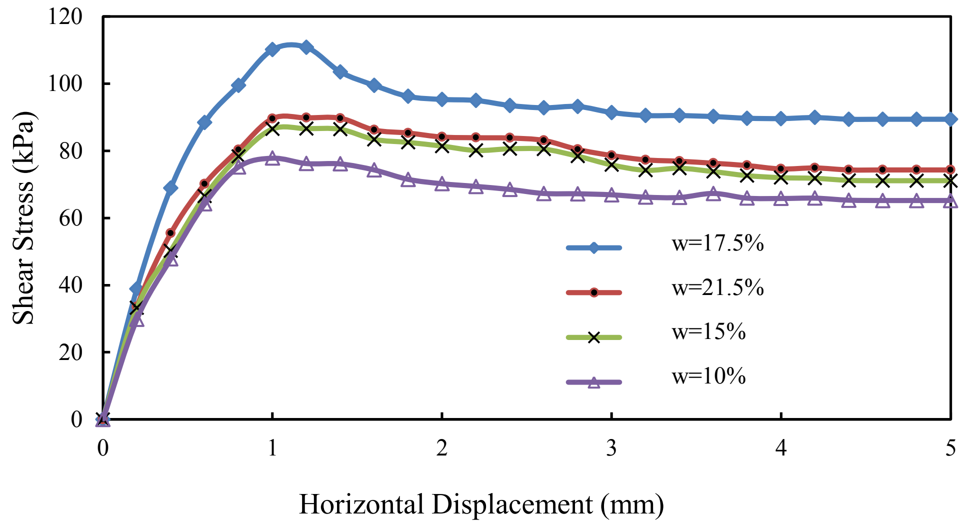

Figure 4.9. Shear stress versus horizontal displacement in soil-on-soil tests (Normal stress=150 kPa)

4.5.1.2. Vertical displacements in the soil mixture-steel plate interface tests

Figure 4.10 illustrates typical results of horizontal displacements versus vertical displacements in the interface tests between the kaolin-sand mixture and the steel plate. These results indicate that the vertical displacements at the top of the soil sample could be divided into two stages. During the first stage, all samples underwent a vertical compression. The amount of vertical displacements was smaller for the samples with moisture contents less than the optimum. During the second stage, two samples with low moisture contents exhibited expansion. However, the samples with high moisture contents continued to compress, but at a much smaller rate than the rates in the first stage.

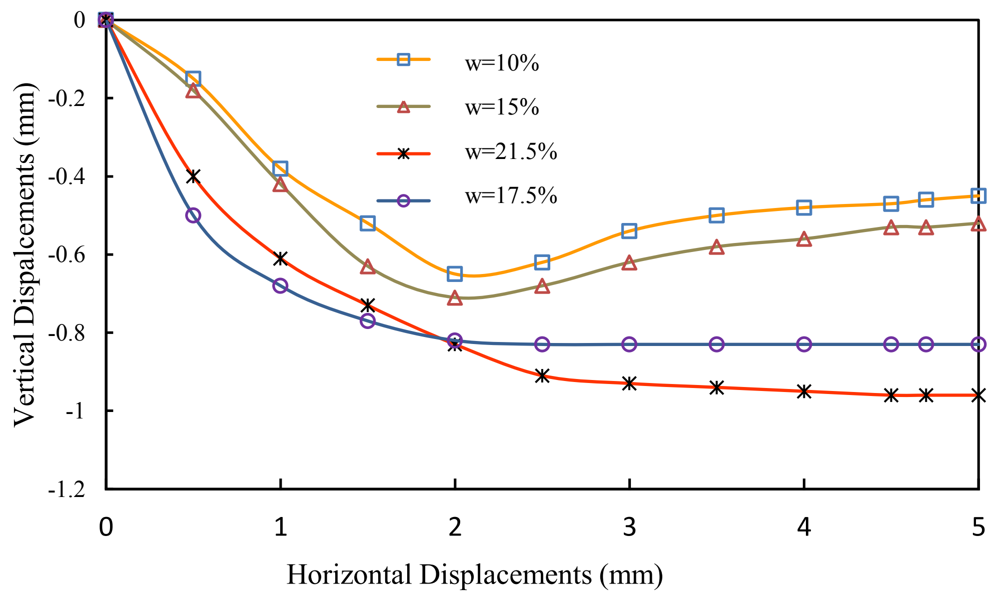

Figure 4.10. Vertical displacements versus horizontal displacements of soil-steel plate interface (Normal stress = 150 kPa)

4.5.1.3. Shear strength of soil-steel plate interface

The peak shear strength envelopes for the interface and the soil mixture alone are shown in Figure 4.11. These envelopes were obtained by fitting linear regression lines through each set of interface shear stress vs. normal stress data. The apparent cohesion and adhesion include the effect of the matric suction of the unsaturated soil.

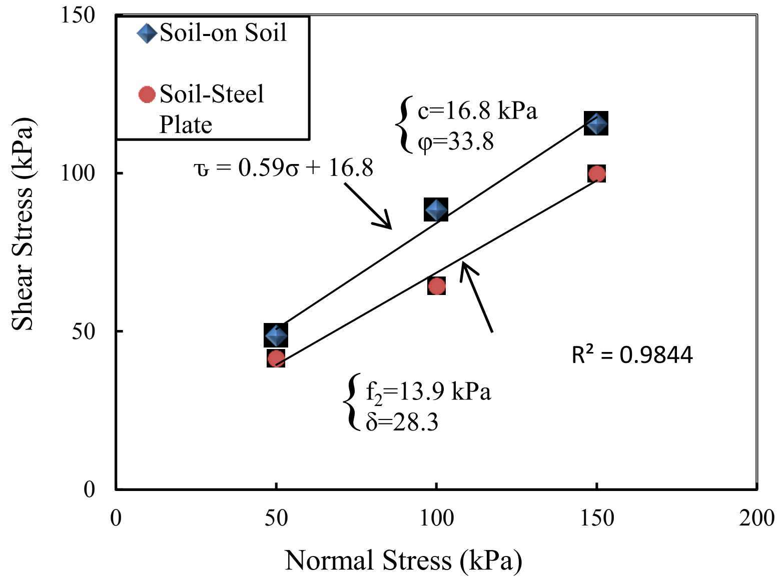

Figure 4.11. Shear stress versus normal stress at failure for soil–steel plate interface and soil-on-soil samples at w=17.5%

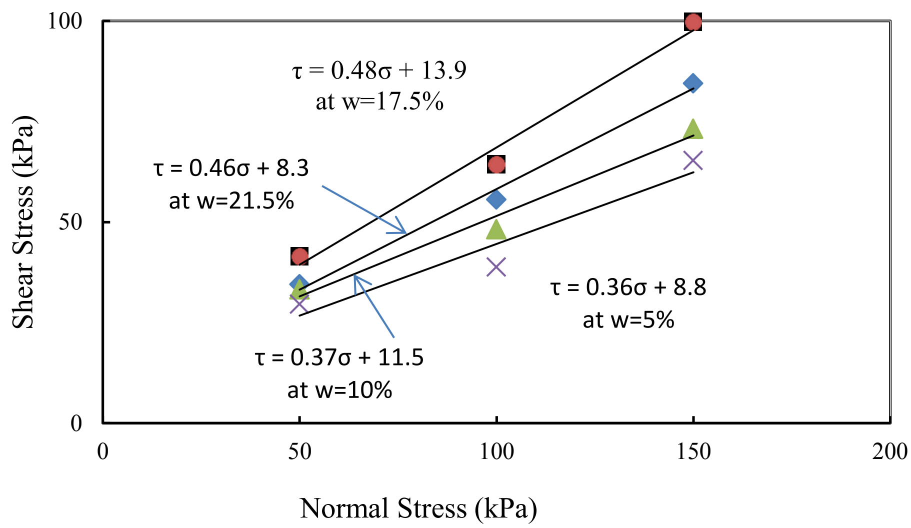

Figure 4.12. Shear stress versus normal stress at failure for soil–steel plate interface under various moisture contents

The peak shear strength envelopes for the interface under various moisture contents are shown in Figure 4.12. It is noted that the values of friction angle and adhesion increase with the increase in gravimetric moisture content until the sample reaches the optimum moisture content.

4.6. Test machine to study the behaviour of interfaces under coupled thermo-mechanical loading conditions

Experimental studies on the behaviour of interfaces have been conducted by various investigators such as Desai et al. (1985), Uesugi et al. (1989), Fakharian and Evgin (1996) and DeJong et al. (2003). These investigations have been carried out using several types of apparatus (i.e. direct shear, simple shear, and ring torsion) at room temperature. The effect of temperature (heating or cooling cycles) on the behaviour of interfaces is considered in the studies by Yavari et al. (2016), Di Donna et al. (2016), Murphy and McCartney (2014), Xiao et al. (2014). (More details in Section 2.4.5).

In order to explore the thermal effect on the behavior of interfaces between energy piles and soil, the interface tests are conducted in the geotechnical laboratories at the University of Ottawa. Before testing, it was necessary to modify the interface testing apparatus. Thermal boundary conditions are added in the apparatus. A thermal plate was placed under the steel interface plate to control the temperature of the interface plate. The thermal plate had four holes to circulate water at a desired temperature. The arrangement of steel interface plate and the thermal plate as part of the 3-Dimensional Cyclic Interface Testing Apparatus with Temperature Control is shown in Figure 4.13. The digital thermometer is mounted on center of the thermal plate.

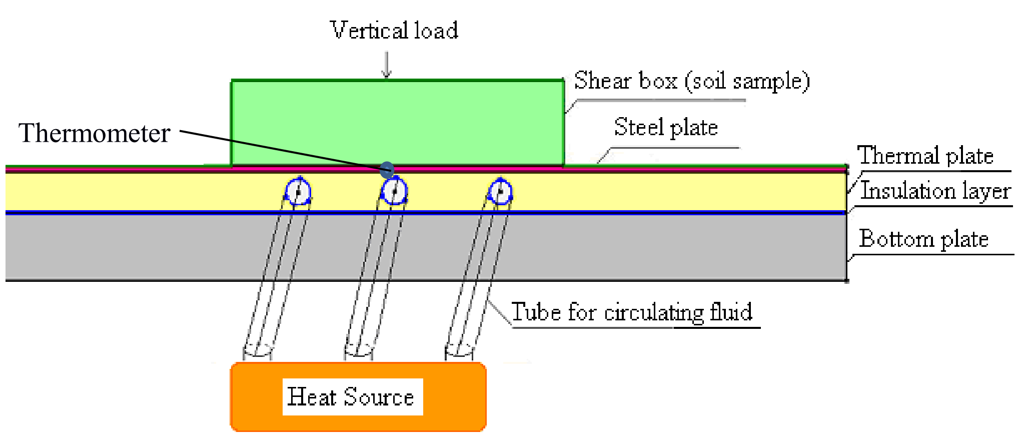

Figure 4.13. Arrangement of plates for thermal loading of interface machine

4.6.1. Thermal plate

The thermal plate is a piece of aluminum, 305 mm long, 305 mm wide, and 12 mm thick as depicted in Figure 4.14. The thermal fluid circulation holes are 6 mm in diameter and drilled through the plate. The holes are connected to ¼ inch polyurethane tubes through which a fluid (water in this case) is circulated. The circulating fluid is kept at a constant temperature in a heating (or cooling) reservoir, and provides a source/sink of heat to the thermal plate. Interface tests only begin once the interface has achieved a uniform temperature.

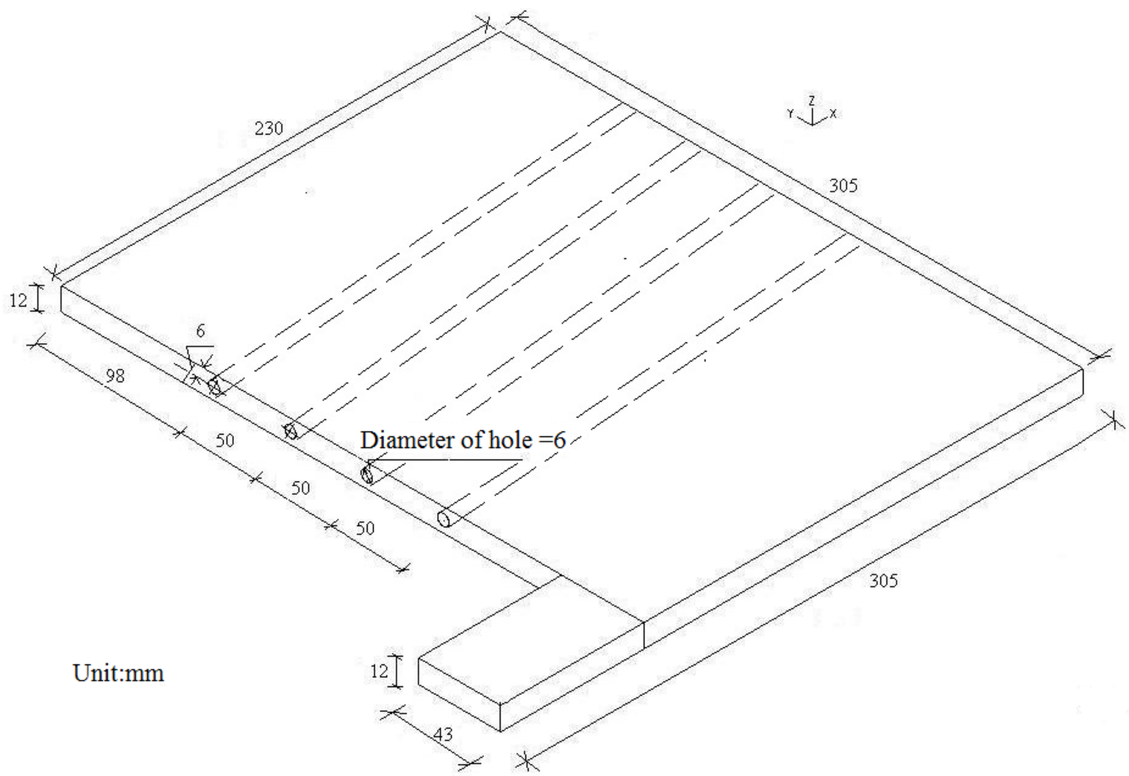

Figure 4.14. Geometry of the thermal plate (dimensions in mm)

Connection of holes of thermal plate to the ends of fluid circulation tubes is described next. An O-ring is fitted to the end of a polyurethane tube connected to each hole. To allow this, a 10 mm counter-bore, with a depth of 1.0 mm is drilled around each hole as shown in Figure 4.15. A small steel plate 3 mm thick, 12 mm wide and 48 mm long is screwed into the thermal plate to apply a positive pressure to the O-ring and ensure a good seal. The water at desired temperature is pumped into the thermal plate through 4 holes at the same time to heat the plate, and then flow back to the heat source.

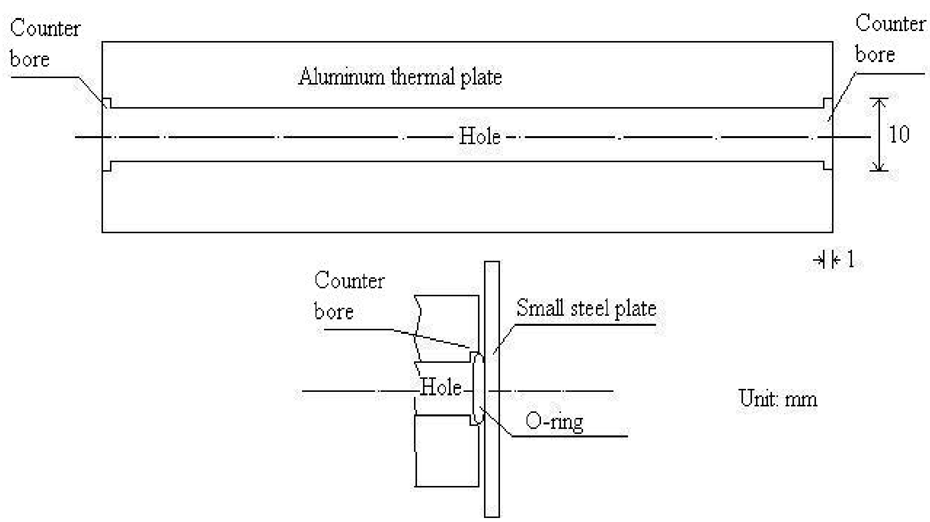

Figure 4.15. Counter-bore o-ring connections

4.6.2 Numerical analysis of heat transfer in the modified interface apparatus

In order to determine the effect of temperature on the interface behaviour, the temperature of the interface plate and the soil need to be kept constant at the required temperature. As described in the previous sections, constant temperature is achieved by circulating liquid through the holes drilled horizontally in the aluminum plate supporting the interface plate. Finite element analysis was used to determine the satisfactory number of holes. It was also important to find out the time required for the steady state condition to be reached. These analyses were conducted using the finite element codes of GeoStudio 2012.

4.6.2.1 Thermal boundary conditions

In the interface apparatus, the aluminum thermal plate is located at the bottom. The steel interface plate sits on top of the aluminum thermal plate. The soil container and the soil specimen are placed on top of the steel interface plate. Conduction heat transfer takes place between the thermal plate, steel plate and soil sample. Therefore, conductive boundary conditions are used as shown in Figure 4.16. The top surface of the shear box and a part of the steel plate are exposed to air and are treated as convective surfaces. This condition is taken into consideration in the numerical analysis. In real tests, the shear box is insulated and whole interface apparatus are covered to insulate from the air at room temperature. The thermal boundary conditions of the plate are as follows: the temperature of the holes in the aluminum thermal plate is constant, for example, 30°C. The initial temperature of both the aluminum and steel plates is 20°C which is the temperature of the temperature controlled room in which the experiments are conducted. The surface of the steel plate is treated as a convective surface; the convective heat transfer coefficient is assumed to be 1 J/sec/°C/m for this study. The analysis is conducted as a transient analysis for a duration of 1800 seconds to ensure that steady state conditions were achieved.

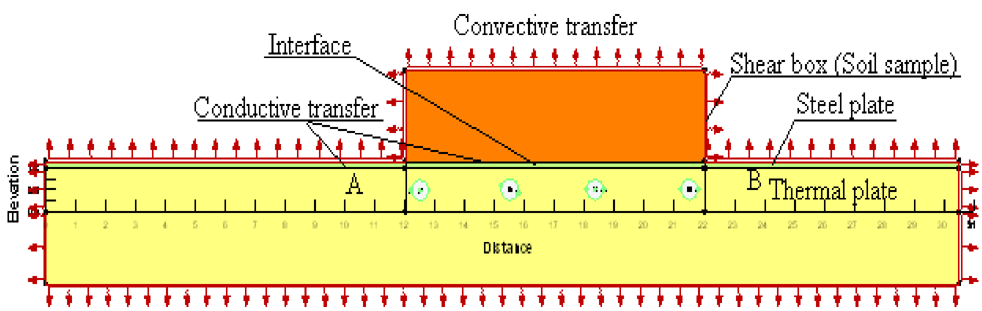

Figure 4.16. Numerical model: soil domain, steel and thermal plates, and boundary conditions

4.6.2.2 Arrangement of the holes

Numerical analyses have been conducted to determine the number of holes required between point A and point B (located near the bottom of the soil sample which has orange color as shown in the figure above), over a span of 150 mm, in order to adequately control the temperature of the interface as shown in Figure 4.16. The holes are 6 mm in diameter. Scenarios involving different number of holes and spacing were considered. The distance between two holes is 50 mm for the two-hole option, 37.50 mm for the three-hole option and 30 mm for the four-hole option (Figure 4.16).

4.6.2.3 Thermal properties of the materials used in the analysis

The thermal properties of materials are listed in Table 4.3.

Table 4.3. Thermal properties of materials

	Thermal plate	Steel plate	Soil sample	Insulation plate
Thermal conductivity (J/sec/m/°C)	237	45	2.5	0.05
Volumetric heat capacity (J/m³/°C)	2422	2250	2640	5200

4.6.2.4 Temperature contours in the steel plate and soil specimen

The temperature contours in the plate after 30 minutes of heating (1800 s) are shown in Figures 4.17 (2- holes), Figure 4.18 (3-holes) and Figure 4.19 (4-holes). Only in the case of the 4-hole scenario does the interface area reach the target temperature uniformly after heating. In the 2-hole and 3-hole scenarios, the interface area is not uniformly heated.

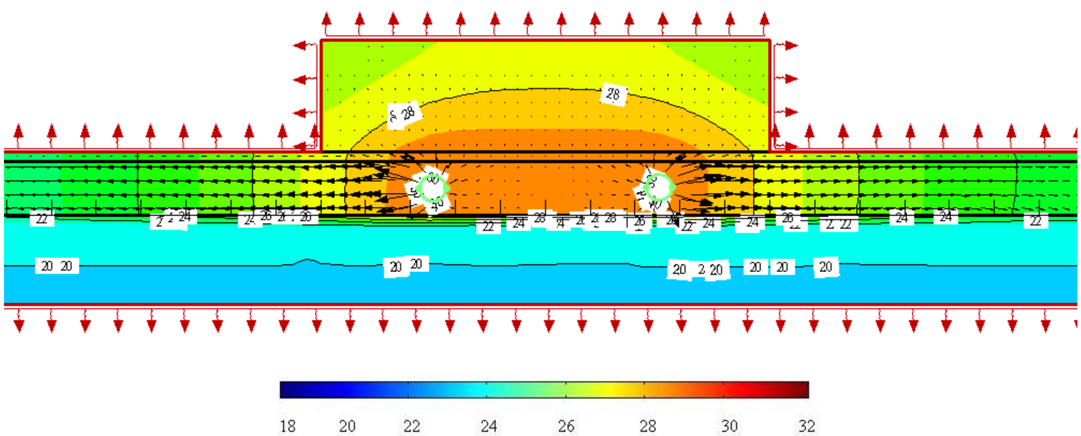

Figure 4.17. Temperature contours of steel interface plate and soil (2 holes)

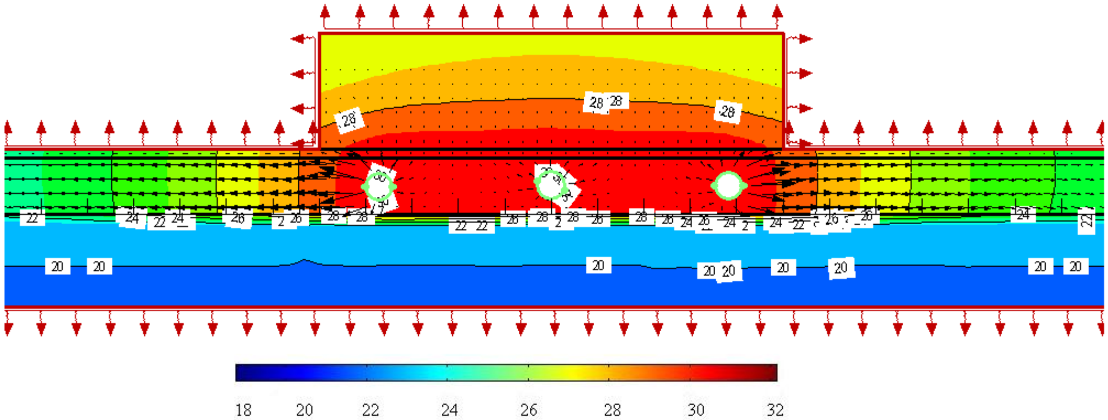

Figure 4.18. Temperature contours of steel interface plate and soil (3 holes)

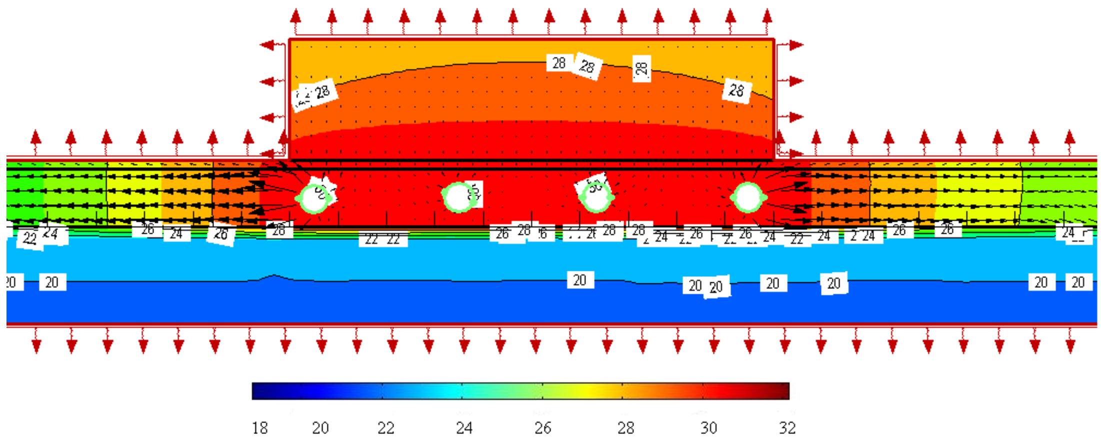

Figure 4.19. Temperature contours of steel interface plate and soil (4 holes)

4.6.2.5 Temperature vs. time

To compare the response time of the various scenarios, the temperature changes with time at two points across the plate (one is in the center, the other is at the edge of the plate) are plotted in Figure 4.20 (for 2-hole plate), Figure 4.21 (for 3-hole plate) and Figure 4.22 (for 4-hole plate). The 2-hole thermal plate cannot heat the interface area to the target temperature (30°C), reaching a maximum value of 29°C which it achieves after 10 minutes (600 seconds), approximately. The thermal plate with 3 holes can achieve 29.8°C after approximately 400 seconds of heating, while the 4 holes version can achieve the target temperature for the interface after 400 seconds of heating. Only the 4 holes scenario can therefore reach the target temperature.

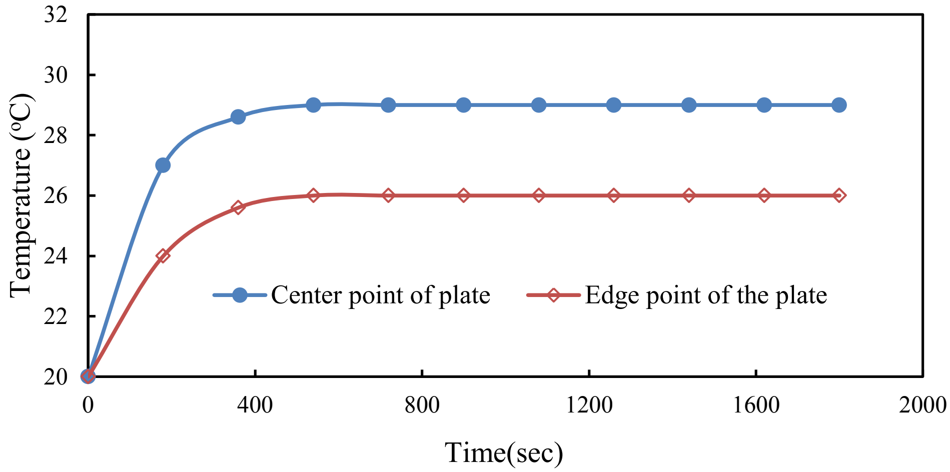

Figure 4.20. Temperature vs. time at two points across interface plate (2 holes)

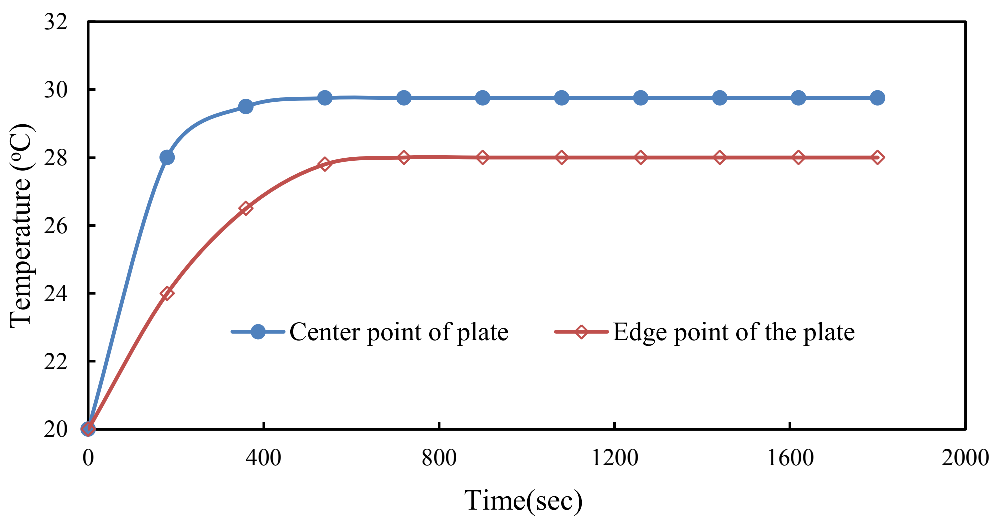

Figure 4.21. Temperature vs. time at two points across interface plate (3 holes)

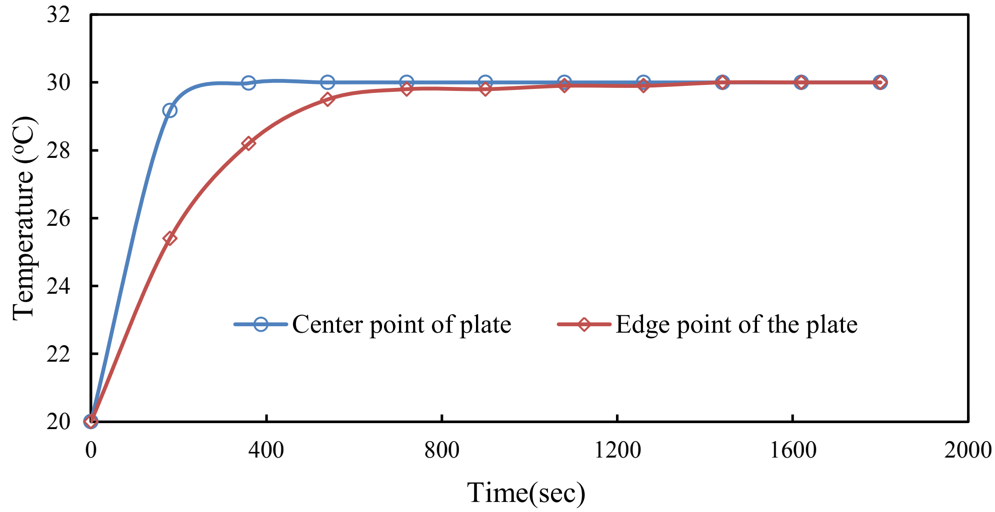

Figure 4.22. Temperature vs. time at two points across interface plate (4 holes)

4.6.2.6 Discussion of the results of numerical analysis

In order to reduce the heat transfer from the aluminum thermal plate to the support plate, an insulation layer is used (the thick dark line in Figure 4.23b). Finite element simulations are conducted with and without the use of the insulation layer. Figure 4.23 shows that in the absence of an insulation layer, a significant amount of heat is transferred to the support plate and only a small part of the soil reaches 30°C.

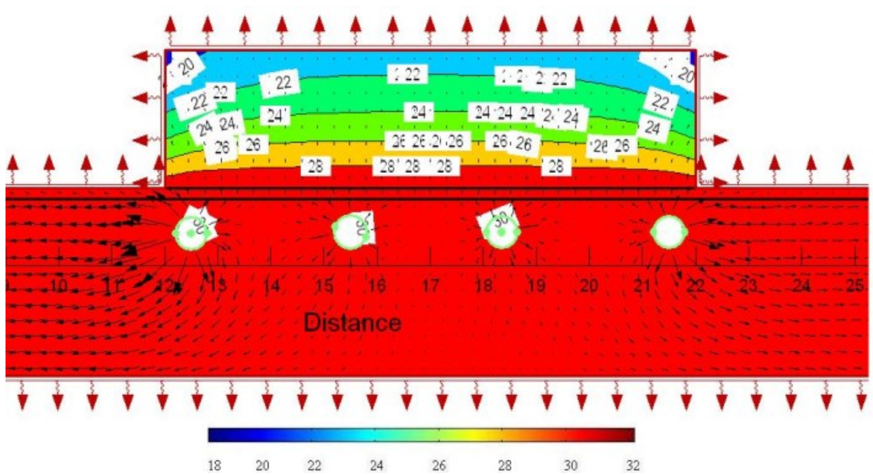

(a) Without insulation layer

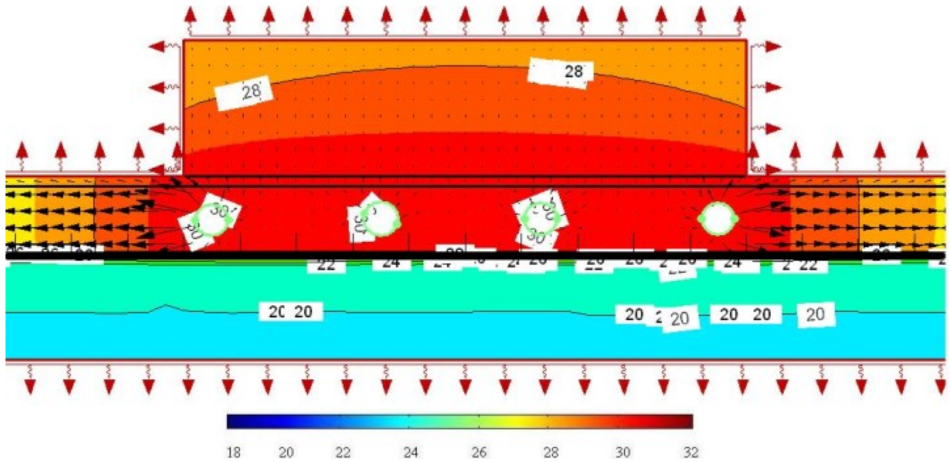

(b) With insulation layer

Figure 4.23. Effect of insulation layer on the heat transfer from the thermal plate

4.6.3 Setup for thermal loading

The setup with 4-hole thermal plate has been used to modify the C3DSSI as shown in Figure 4.24. The hot/cold water in the thermal source reservoir circulates through the thermal plate to achieve a controlled temperature at the interface.

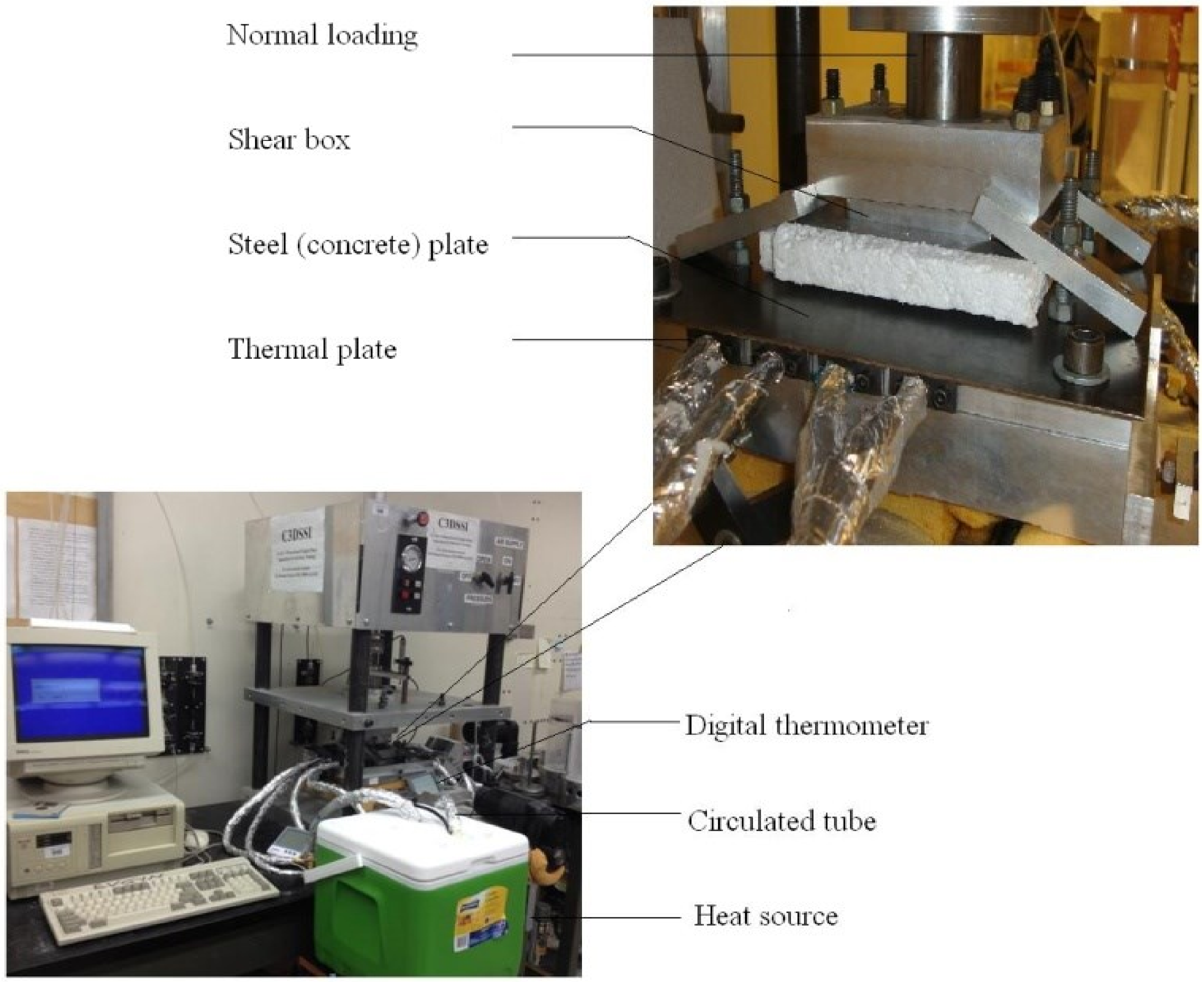

Figure 4.24. Thermal loading arrangement for 3-Dimensional Cyclic Interface Testing Apparatus

The temperature changes with time at the middle of the interface area have been measured in the laboratory and found to be in agreement with those predicted from the finite element analysis as shown in Figure 4.25. The temperature achieved in Figure 4.25 is lower than the target temperature, and the time to equilibrium slightly larger, however, this is attributed to the fact that when the measurements were taken, there was no soil specimen on the interface plate, and therefore a larger fraction of the interface was exposed to direct convective heat dissipation.

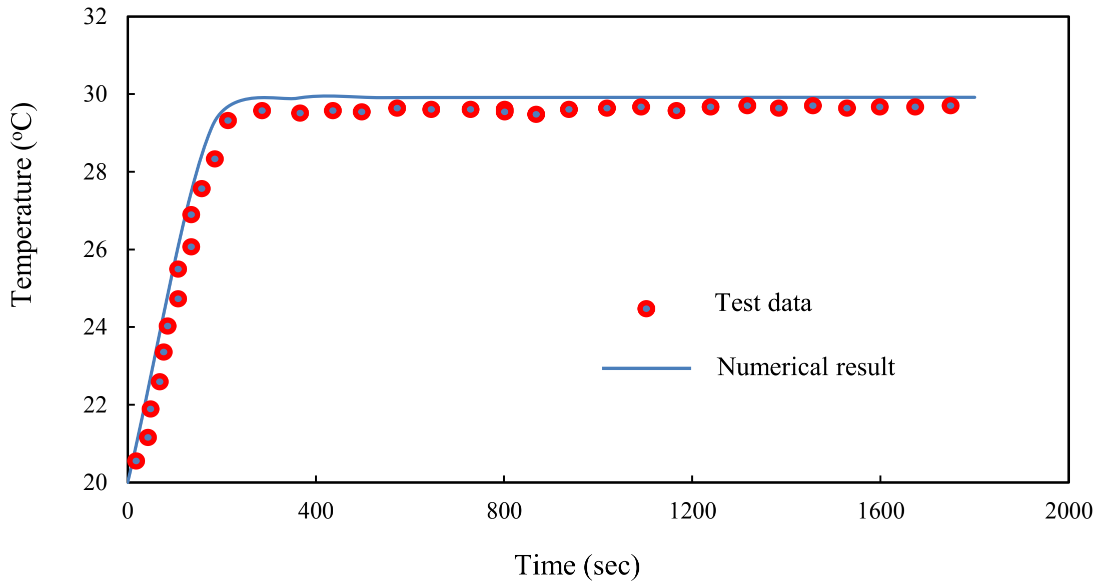

Figure 4.25. Numerical result compared with test data (4 holes)

4.7 Soil-pile interface tests at different temperatures and unsaturated conditions

The investigation of the effects of temperature and unsaturated condition on the shear strength of the soil-pile interface is carried out with the C3DSSITC apparatus. Displacements and forces are recorded automatically by transducers and a data acquisition system.

Interface shear tests were conducted on specimens with controlled interface temperatures of 8°C, 15°C, 23°C and 35°C. For every soil-steel plate specimen, three tests were performed by applying normal stresses of 60, 80, and 100 kPa.

4.7.1 Thermal effects on the shear strength parameters of soil-pile interface with low degree of saturation

The soil mixtures with initial moisture content of 10% were compacted in the shear box to achieve a dry unit weight of 15.7 kN/m^3 at room temperature of 23°C. Temperatures at three points in the soil are recorded during the heating/cooling tests. Point A is close to the bottom of the soil sample, Point B is in the middle and Point C is near the top of the soil sample.

Figure 4.26 shows the temperature changes with the time in the soil sample during the heating from 23^{o}C to 35^{o}C. Figure 4.27 shows the temperature changes with time in the soil sample during cooling from 23^{o}C to 15^{o}C. After each test, the water content of soil near the shearing surface was measured. The measured water contents of soil specimens at the end of experiments are 9.6 %, 9.8% for heating tests, and 10.5%, 10.8% for cooling test as shown in Table 4.4, which may be partially attributed to moisture migration due to temperature gradient.

Table 4.4 Water content, void ratio, degree of saturation at initial state, degree of saturation after heating and shearing, and the peak shear strength for normally consolidated soil samples

Temperature	w_i (%)	e_i	S_i (%)	e_h	e_f	w_f (%)	S_f (%)	Peak shear strength (kPa)
8	10	0.6	45	0.597	0.593	10.8	49.2	43.3
15	10	0.6	45	0.598	0.594	10.5	47.7	45.8
23	10	0.6	45	0.60	0.595	9.9	44.5	48.6
35	10	0.6	45	0.592	0.586	9.6	44.2	52.5

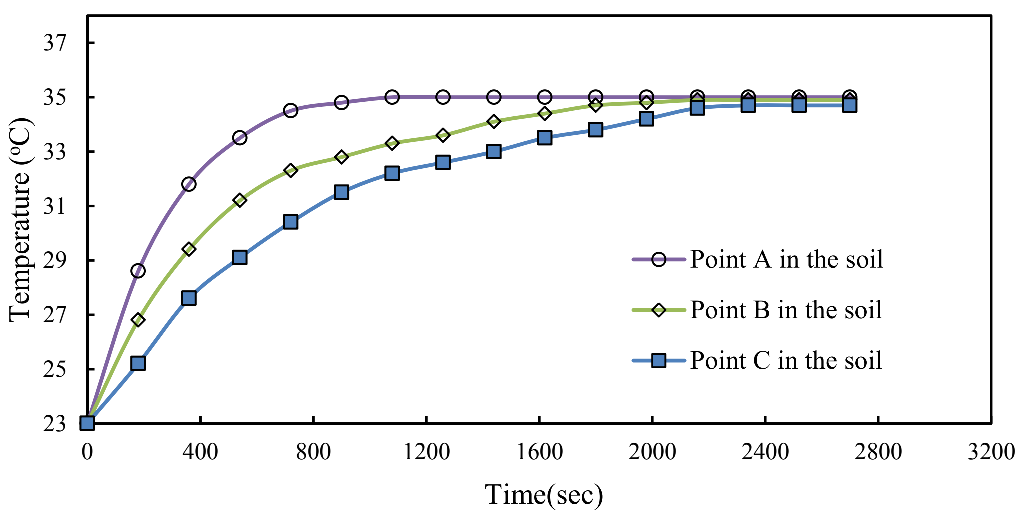

Figure 4.26. Temperature vs. time in the soil during heating from 23 ^{o}C to 35 ^{o}C

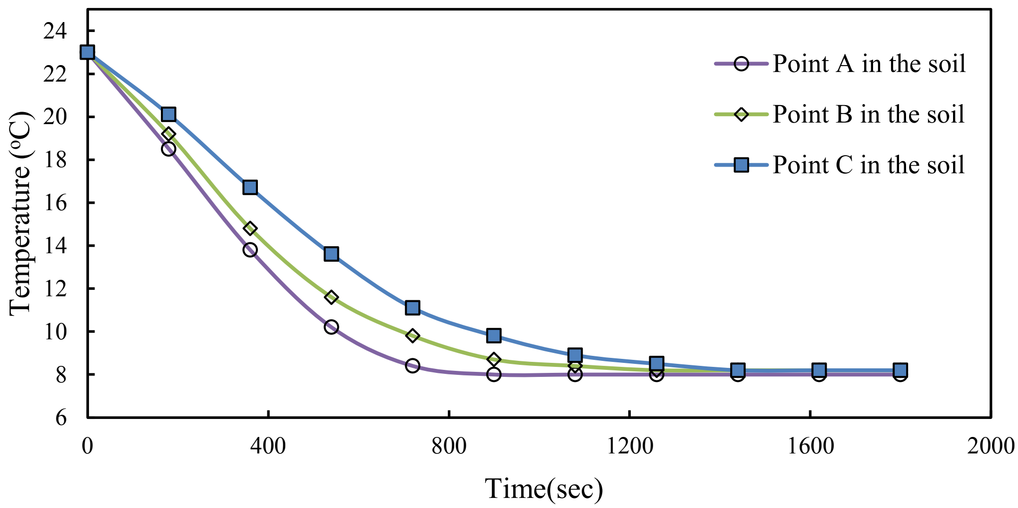

Figure 4.27. Temperature vs. time in the soil during cooling from 23°C to 15°C

4.7.1.1 Shear stress versus horizontal displacement curves

Figures 4.28 to 4.31 show a typical relationship of shear stress versus horizontal displacement for the interaction between kaolin-sand mixture and the steel plate at temperatures of 8°C, 15°C, 23°C and 35°C under 60 kPa normal stress. All shear stress versus displacement curves with various temperatures are presented together in Figure 4.32 (corresponding to 60 kPa normal stress) for the purpose of comparison. Similarly, Figures 4.33 and 4.34 show the shear stress versus horizontal displacement curves at various temperatures for 80 kPa and 100 kPa normal stress conditions. The shear stress versus horizontal displacement curves of the interface between the soil mixture and steel plates show that the shear strength of the interface increases with increasing temperatures. However, this observation is in contradiction with the findings of some other researchers. According to Figure 2.11(a), the strength of the soil decreases with increasing temperature. In order to explain the contradictory observations of the present study, the measured water contents of the soil (sampled next to the interface plate) at the end of each test (w_f) are provided below the label of the horizontal axis of Figures 4.28 to 4.31. It should be noted that the water contents decreased as the test temperature increased. This means that the suction increased as the water content decreased and temperature increased. Therefore, the combined effects of temperature and suction determine the outcome of the experiments. The increase in the strength due to increase in suction is more than the decrease in strength due to the increase in temperature.

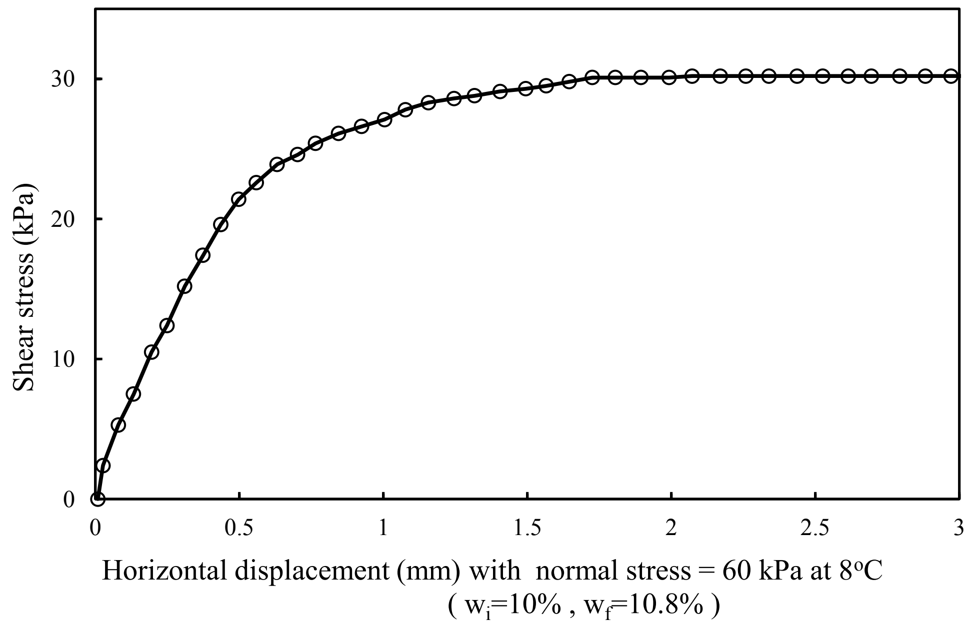

Figure 4.28. Shear stress versus horizontal displacement of soil-steel plate interface at $8^{o}C$ (Normal stress = 60 kPa)

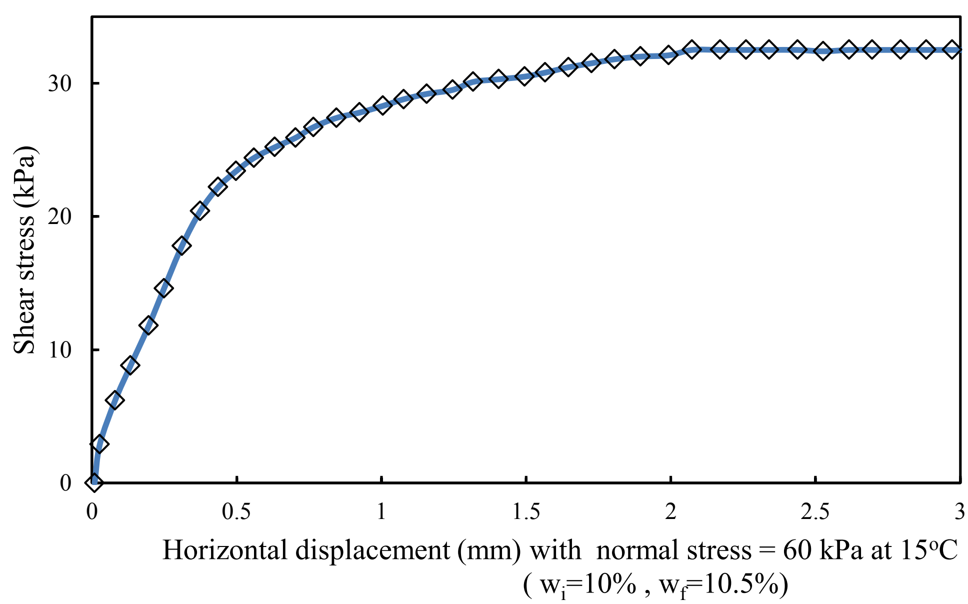

Figure 4.29 Shear stress versus horizontal displacement of soil-steel plate interface at $15^{o}C$ (Normal stress = 60 kPa)

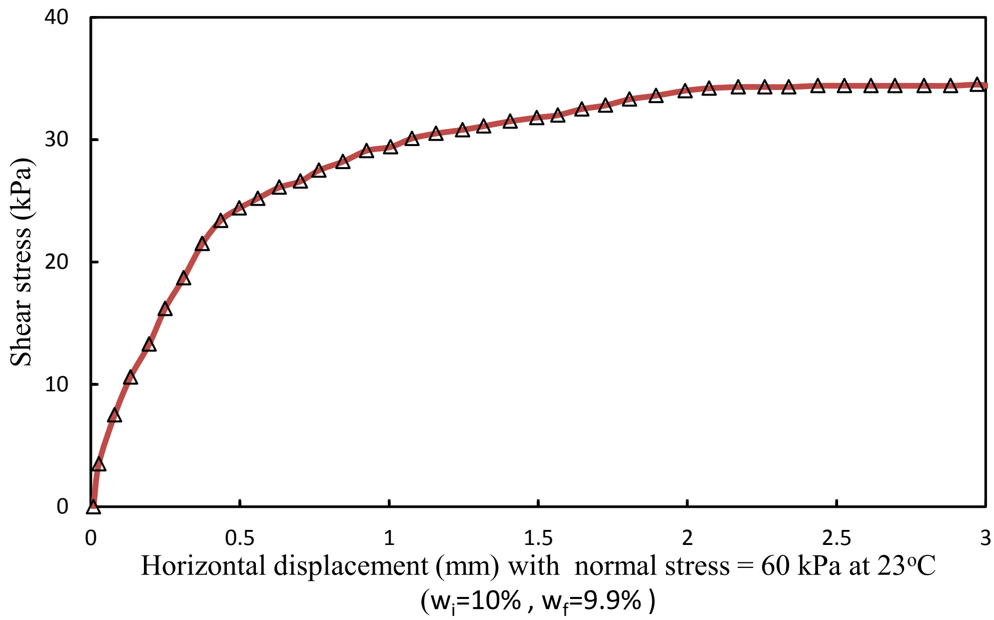

Figure 4.30. Shear stress versus horizontal displacement of soil-steel plate interface at 23°C (Normal stress = 60 kPa)

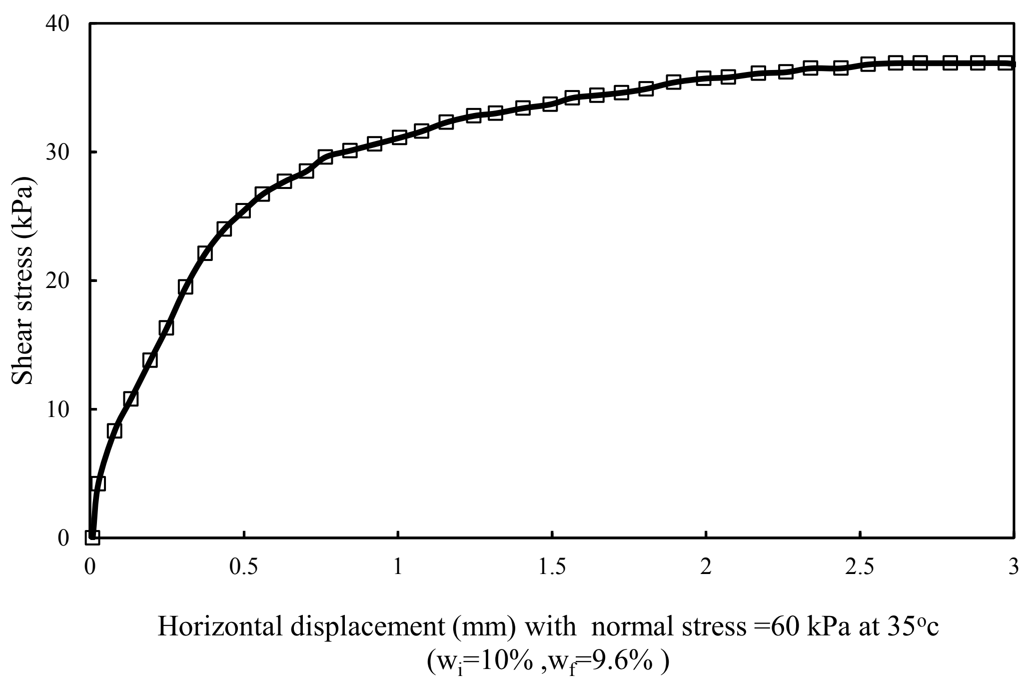

Figure 4.31. Shear stress versus horizontal displacement of soil-steel plate interface at 35°C (Normal stress = 60 kPa)

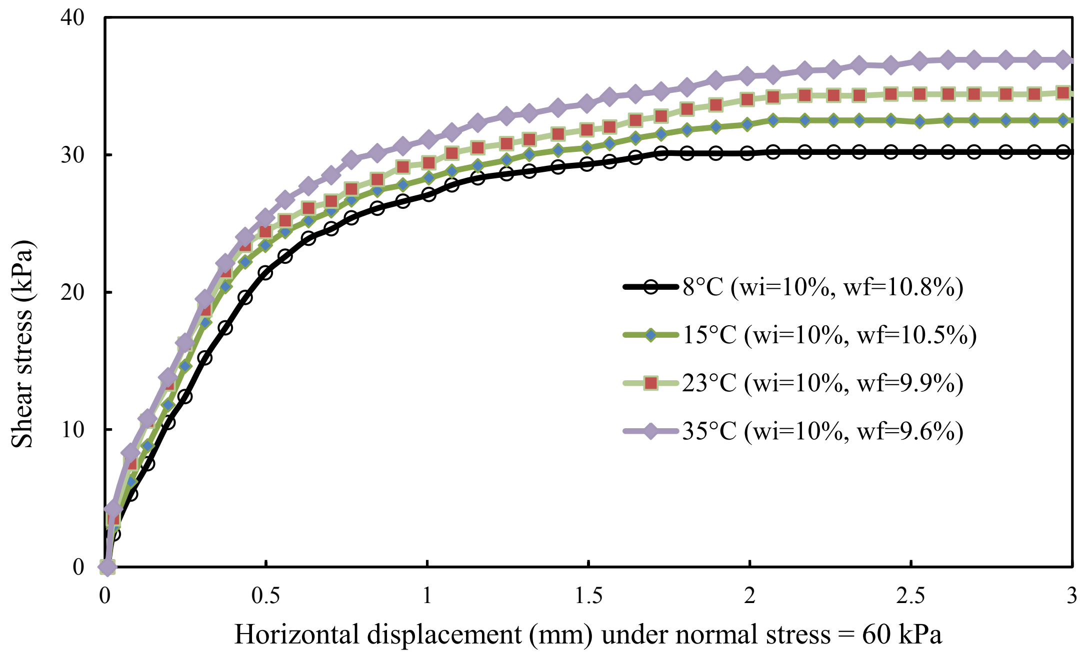

Figure 4.32. Shear stress versus horizontal displacement of soil-steel plate interface with various temperatures (Normal stress = 60 kPa)

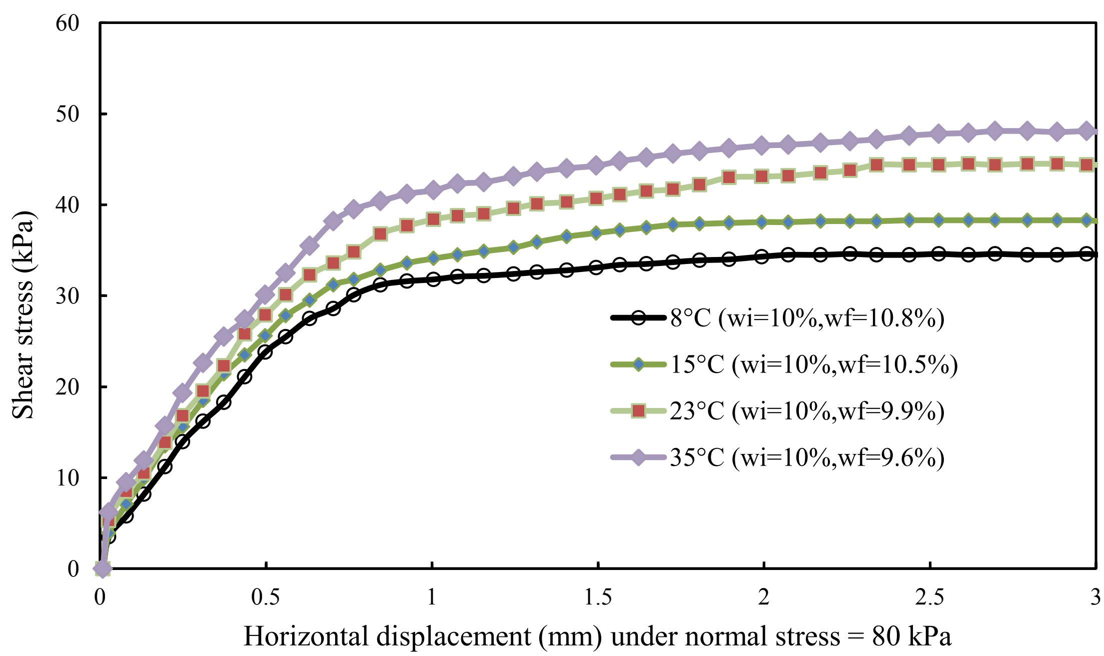

Figure 4.33. Shear stress versus horizontal displacement of soil-steel plate interface with various temperatures (Normal stress = 80 kPa)

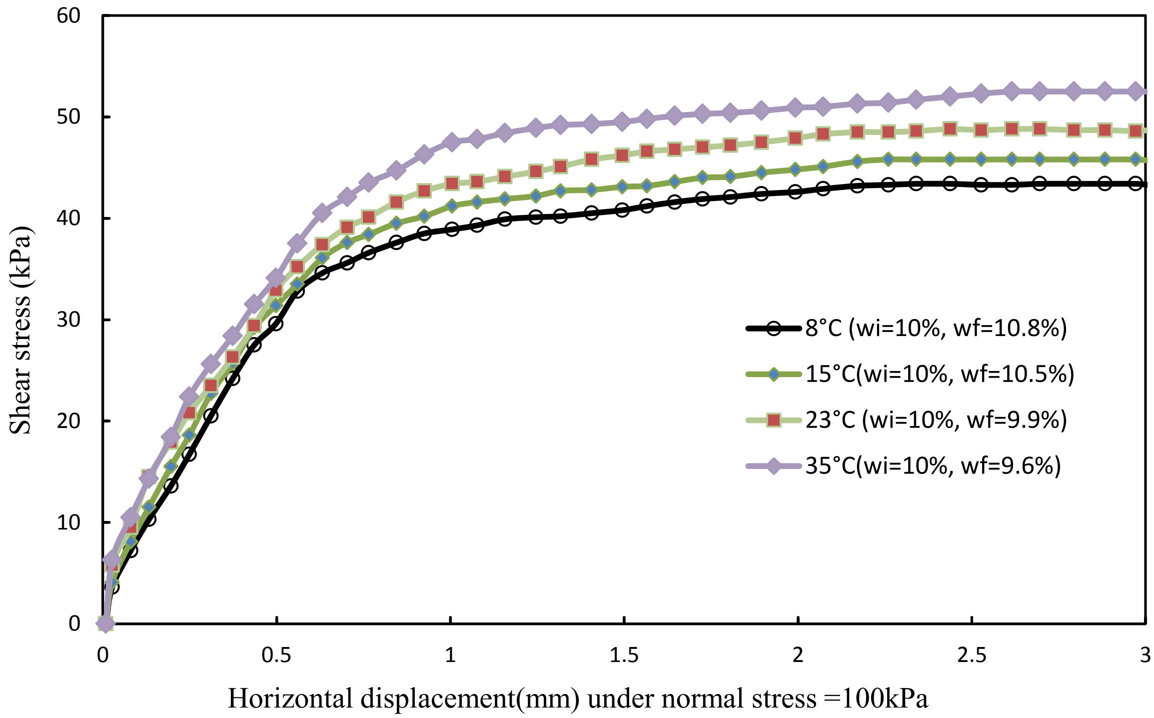

Figure 4.34. Shear stress versus horizontal displacement of soil-steel plate interface with various temperatures (Normal stress = 100 kPa)

4.7.1.2. Shear strength parameters at various temperatures

The failure envelopes can be obtained by plotting the normal stress vs peak shear stress. Figure 4.35 shows the failure envelopes for the interfaces between kaolin-sand mixture and the steel plate at temperatures of 8^{o}C, 15^{o}C, 23^{o}C and 35^{o}C and the corresponding water contents.

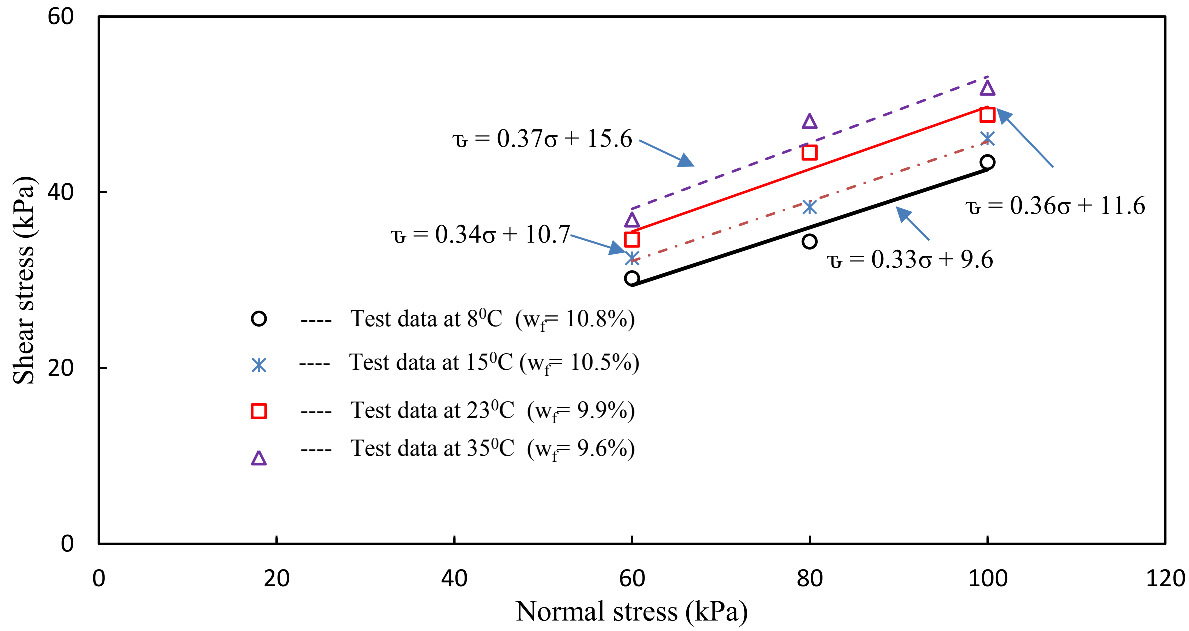

Figure 4.35. Failure envelopes of the interface between kaolin-sand mixture and the steel plate with temperatures at normally- consolidated condition

The shear strength parameters of the interface of soil mixture and steel plate (at various temperatures and matric suctions) are determined from the failure envelopes as shown in Table 4.5.

Table 4.5. Shear strength parameters at various temperatures and matric suction

Temperature	Matric Suction (kPa)	Interface Friction angle (δ)(°)	Apparent Adhesion (f_2) (kPa)
T=8 ^{o}C	58	20.3	9.6
T=15 ^{o}C	63	20.9	10.7
T=23^{o}C	66	21.7	11.6
T=35 ^{o}C	72	23.1	15.6

From this table, it can be seen that the apparent adhesion increase due to the combined effects of increasing temperatures and decreasing water contents (i.e. increasing suction). The interface friction angles change slightly with variation of temperature and matric suction. The reason of the increase in the apparent adhesion with increasing temperature may be explained by using the information provided in Table 4.4 and Figure 4.36. It can be noted that first, the elevated temperature reduces the void ratio of soil, the height of soil decreases, thermally induced the soil contraction; second, the degree of saturation drops at the interface due to thermally induced water flow away from the interface, the matric suction increases when the degree of saturation decreases. Therefore the trend shown in Table 4.5 is caused by the combined effects of temperature and suction.

4.7.1.3 Thermal effect on the volume of the normally consolidated soil samples

Before interface test is performed, the soil specimen is heated or cooled to the target temperature. During the heating, the height of specimen is measured using LVDT. Figure 4.36 shows the height of the normally consolidated specimen which decreases when the soil is heated from 23^{o}C to 35^{o}C. The soil experiences contraction.

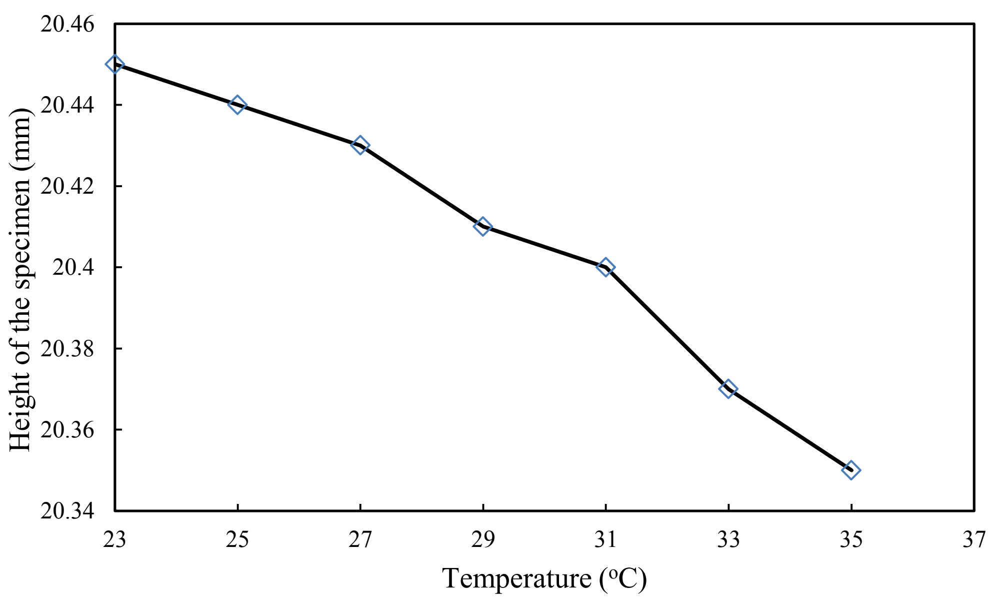

Figure 4.36. Height of the normally consolidated soil sample during heating

4.7.2 Thermal effects on the shear strength parameters of soil-pile interface with high degree of saturation

McCartney (2012) pointed out that unsaturated soil conditions may affect the thermal or mechanical performance of energy piles. In the present study, thermal effects on the shear strength parameters of soil with high degree of saturation, S=85%, are explored.

Interface shear tests were conducted on specimens with controlled interface temperatures of 8°C, 23°C and 35°C. The soil mixtures with initial moisture content of 17.5% were overconsolidated in the shear box under 375 kPa. For every soil-steel plate specimen, three tests were performed by applying normal stresses of 60, 80, and 100 kPa. The overconsolidation ratio ranged between 3 and 6. After each test, the water content of soil near the shearing surface was measured. The measured water contents of soil specimens at the end of experiments ranged from 16.9% for heating test to 18.0% for cooling test as shown in Table 4.6, which may be partially attributed to moisture migration due to temperature gradient.

Table 4.6 Water content, void ratio and degree of saturation at the initial state, as well as after heating, and shearing the overconsolidated soil samples at normal stress 100 kPa. Corresponding peak shear strength values are provided in the last column.

Temperature	w_i (%)	e_i	S_i (%)	e_h	e_f	w_f (%)	S_f (%)	Peak shear strength (kPa)
8	17.5	0.56	85	0.565	0.564	18.0	86.1	57.2
23	17.5	0.56	85	0.566	0.565	17.4	83.2	53.2
35	17.5	0.56	85	0.573	0.578	16.8	79.5	48.5

4.7.2.1 Shear stress versus horizontal displacement relationship for overconsolidated soil samples with high degree of saturation

All shear stress versus displacement curves with various temperatures are presented together in Figure 4.37(corresponding to 60 kPa normal stress) for the purpose of comparison. Similarly, Figures 4.38 and 4.39 show the shear stress versus horizontal displacement curves at various temperatures for 80 kPa and 100 kPa normal stress conditions. The shear stress versus horizontal displacement curves of the interface show that the shear strength of the interface decreases due to the combined effects of change in temperature and soil suction. It should be noted that the water content values are smaller at lower temperatures indicating that the suction is larger at lower temperatures.

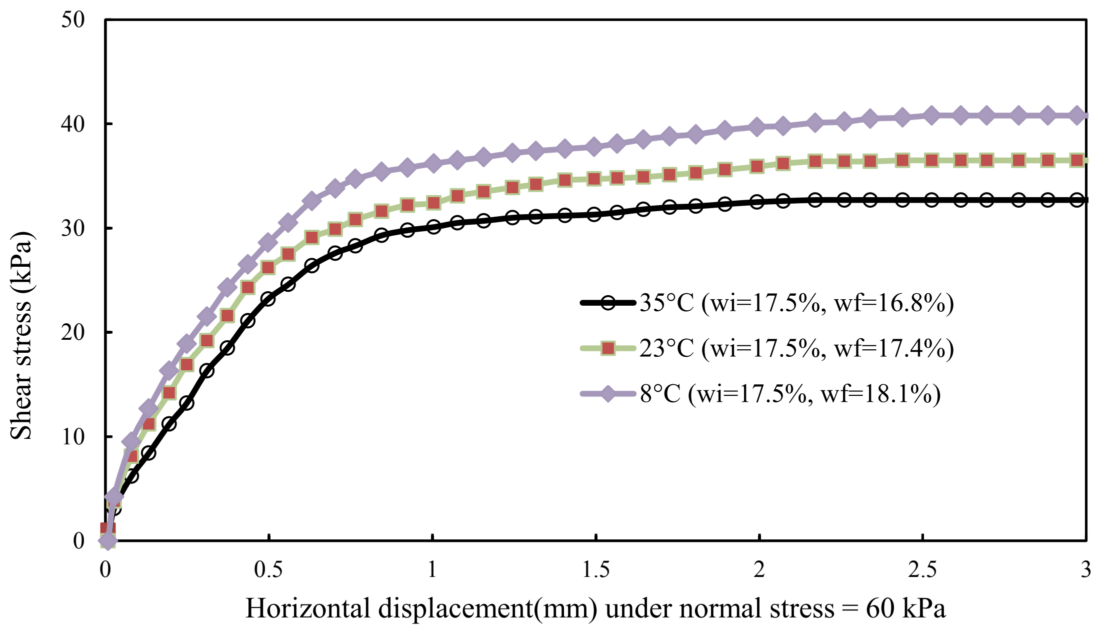

Figure 4.37. Shear stress versus horizontal displacement of soil-steel plate interface with various temperatures (Normal stress = 60 kPa)

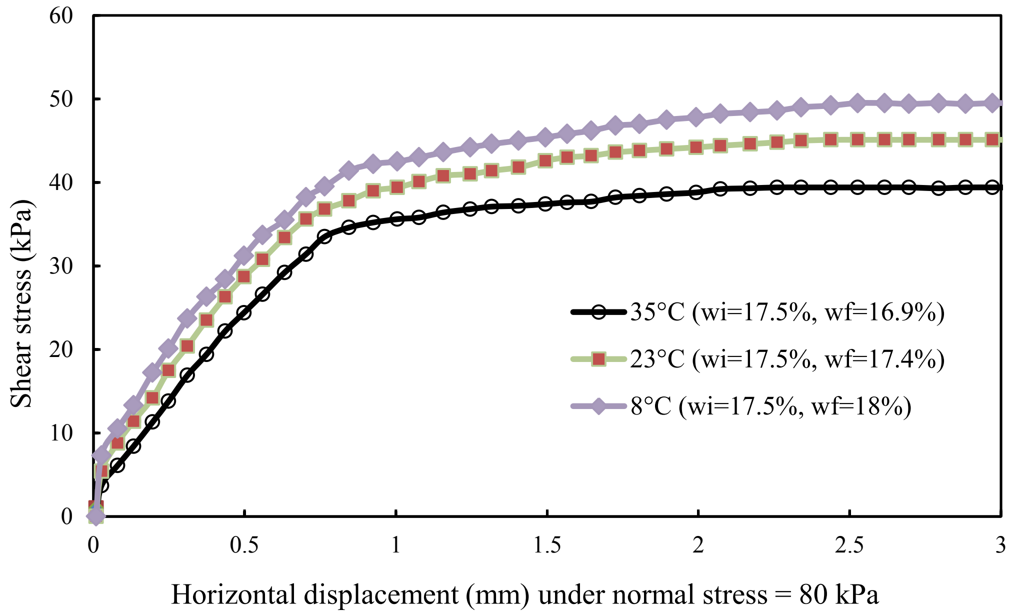

Figure 4.38. Shear stress versus horizontal displacement of soil-steel plate interface with various temperatures (Normal stress = 80 kPa)

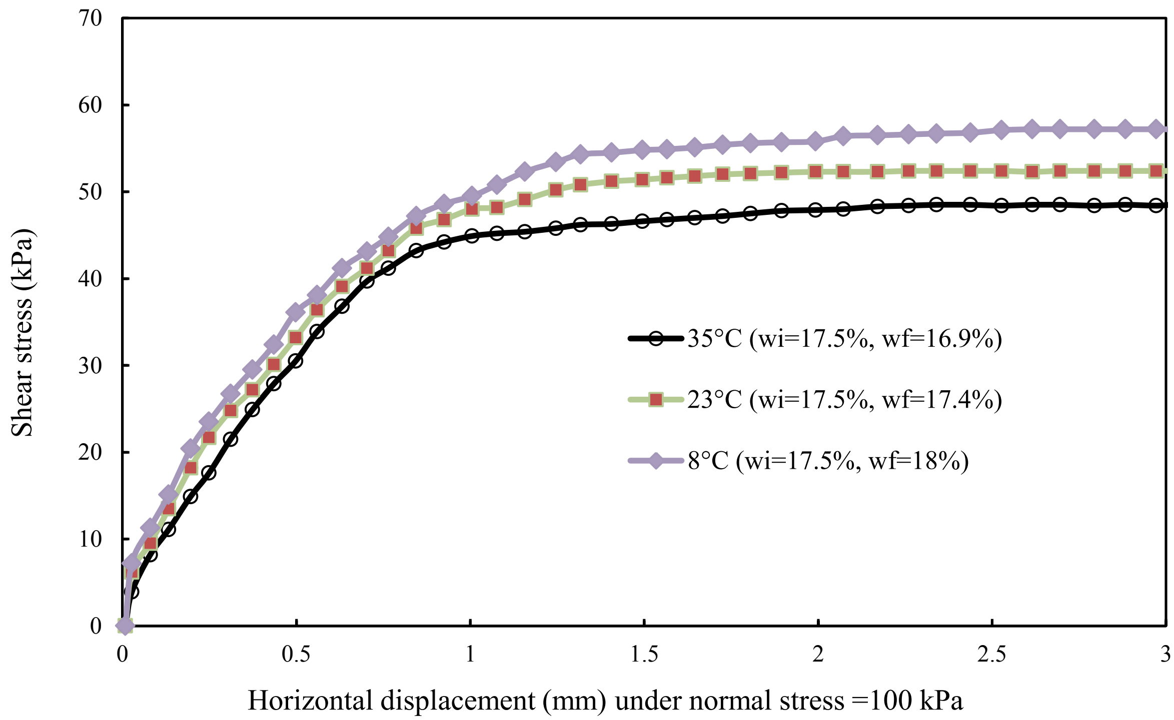

Figure 4.39. Shear stress versus horizontal displacement of soil-steel plate interface with various temperatures (Normal stress = 100 kPa)

4.7.2.2 Shear strength parameters at various temperatures for over consolidated soil samples

The failure envelopes can be obtained by plotting the normal stress vs peak shear stress. Figure 4.40 shows the failure envelopes for the interfaces between kaolin-sand mixture and the steel plate at temperatures of 8^{o}C, 23^{o}C and 35^{o}C.

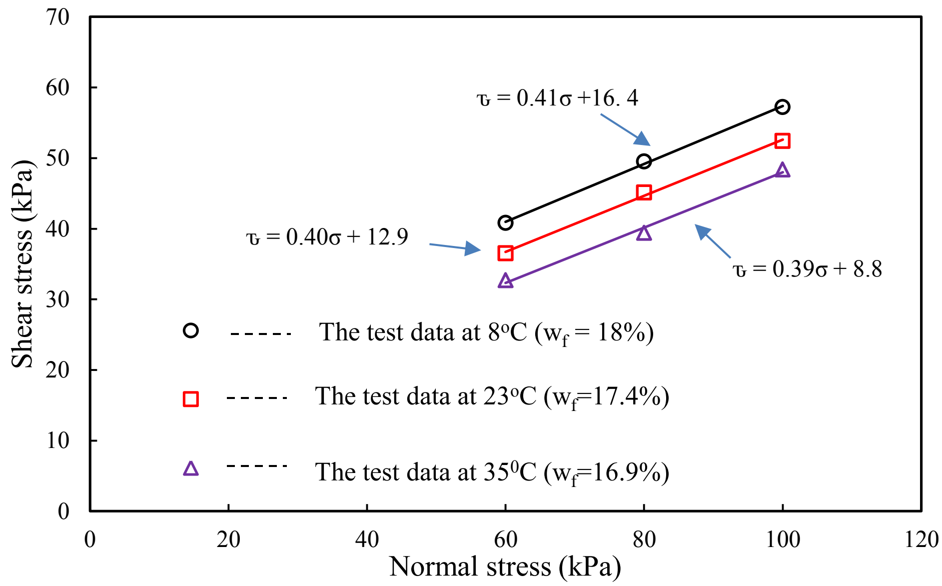

Figure 4.40. Failure envelopes of the interface between kaolin-sand mixture and the steel plate with temperatures at overconsolidated condition

The shear strength parameters of the interface of soil mixture and steel plate at various temperatures and water contents are determined from failure envelopes as shown in Table 4.7.

Table 4.7. Shear strength parameter at various temperatures and matric suction for overconsolidated soil samples

Temperature	Matric Suction (kPa)	Interface Friction angle (δ)(°)	Apparent Adhesion (f_2) (kPa)
T=8 °C	19	24.4	16.4
T=23°C	21	23.5	12.9
T=35 °C	22	22.4	9.8

It can be seen that the apparent adhesion decrease with increasing temperature. The interface friction angles change slightly with temperatures. The reason of the decrease in apparent adhesion with increasing temperatures can be explained by using the information provided in Table 4.6 and Figure 4.41. It can be noted that the void ratio of the soil increases with an increase in temperature. The height of the soil sample increases due to the thermally induced soil expansion. Although the degree of saturation drops at the interface, for highly saturated soil, the change of degree of saturation may not have significant effect on the matric suction.

4.7.2.3 Thermal effects on the volume of the overconsolidated soil sample

Figure 4.41 shows the height of the overconsolidated soil sample increases when the soil is heated from 23^{o}C to 35^{o}C. The soil experienced expansion.

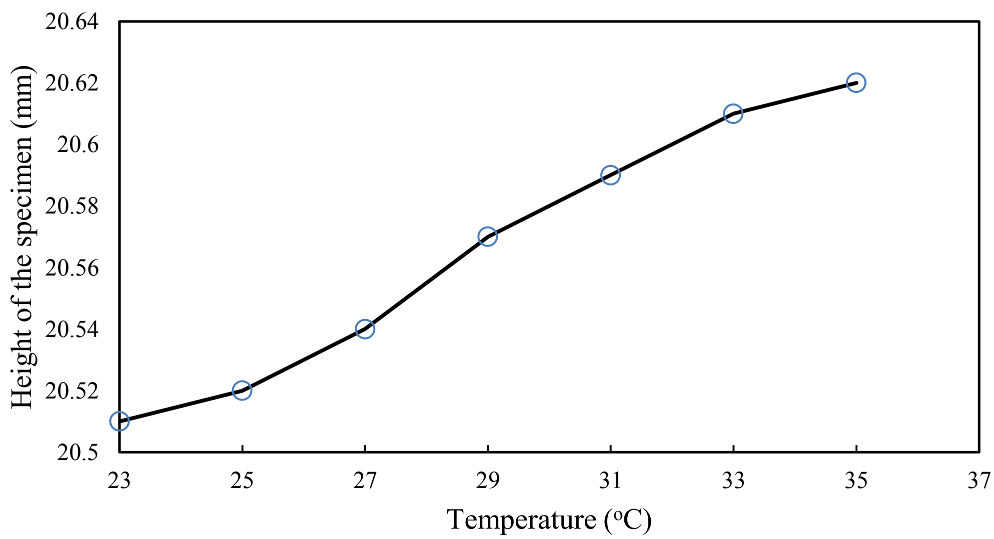

Figure 4.41. Height of the overconsolidated soil sample during heating

4.8 Numerical analysis of interface tests (overconsolidated soil samples)

Fully coupled THM analysis of interface tests using finite element code PLAXIS 2D (More details in section 5.3) is presented in this section. The deformations of the sample, temperature distributions in the soil and the development of shear resistance of interface are calculated. The numerical results are compared with the measured data from laboratory experiments.

4.8.1 Analysis domain

4.8.1.1 Geometry

Several nonlinear thermo-hydro-mechanical plane strain FE analyses are carried out. The geometry of the analysis domain is shown in Figure 4.40. A 40 mm high aluminum loading ram is used to apply mechanical load on the 20 mm high 100 mm long kaolin-sand mixture sample which is supported by the 10 mm high steel plate. An elastic - perfectly plastic model is used to describe the behaviour of the kaolin-sand mixture while the steel plate and aluminum loading ram are assumed to behave elastically.

4.8.1.2 Boundary conditions

(a) Mechanical boundary conditions

The vertical load is applied on top of the aluminum loading ram. Horizontal movement is not allowed on the vertical sides of the aluminum loading ram and the soil sample as shown in Figure 4.42. A total of 3mm horizontal movement is applied on the steel plate to shear the interface.

(b) Thermal boundary conditions

The heat flux occurs through the bottom of the domain. A constant temperature (room temperature 23°C) is applied at the top surface of the aluminum loading ram. The initial soil temperature is also 23°C. In two different tests, a heating or cooling thermal load is applied on the steel plate (8°C, 35°C) before shearing initiated.

(c) Hydraulic boundary conditions

The water flux takes place at the top surface and bottom of the soil sample. Other boundaries are closed to water flow.

The FE domain is discretized using quadrilateral and triangular elements for soil, the steel plate, and the aluminum loading ram. Interface elements are used at the steel plate–soil interface.

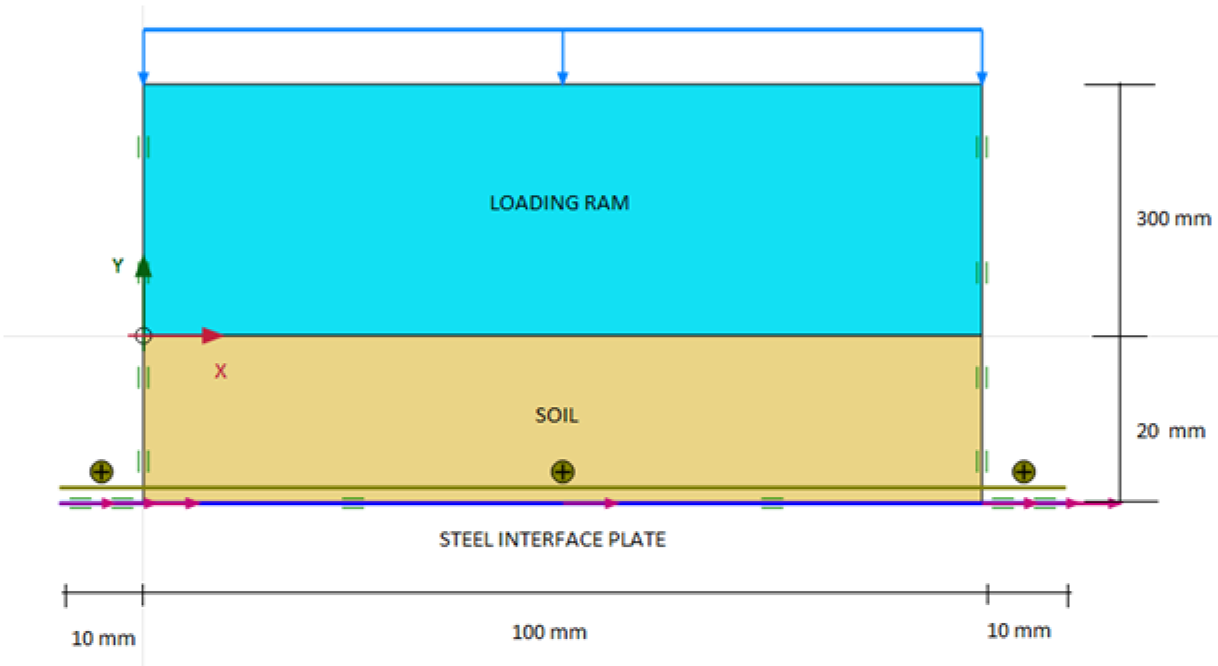

Figure 4.42. Schematics of the geometry used in the FE analysis of interface tests

4.8.2. Types of analysis and results

Numerical analysis of the interface tests on overconsolidated soil samples are conducted with controlled interface temperatures of 8°C, 23°C and 35°C. The 375 kPa normal load is applied on soil mixtures first. Then, for every soil-steel plate specimen, three tests were performed by reducing normal stress to 60, 80, and 100 kPa under different temperatures.

4.8.2.1. Deformation of domain

Figure 4.43 shows the deformation of domain of steel–plate and soil mixture after shearing under the condition of 80 kPa normal stress with 35°C. It is noted that the soil mixture is pushed to the right in horizontal direction.

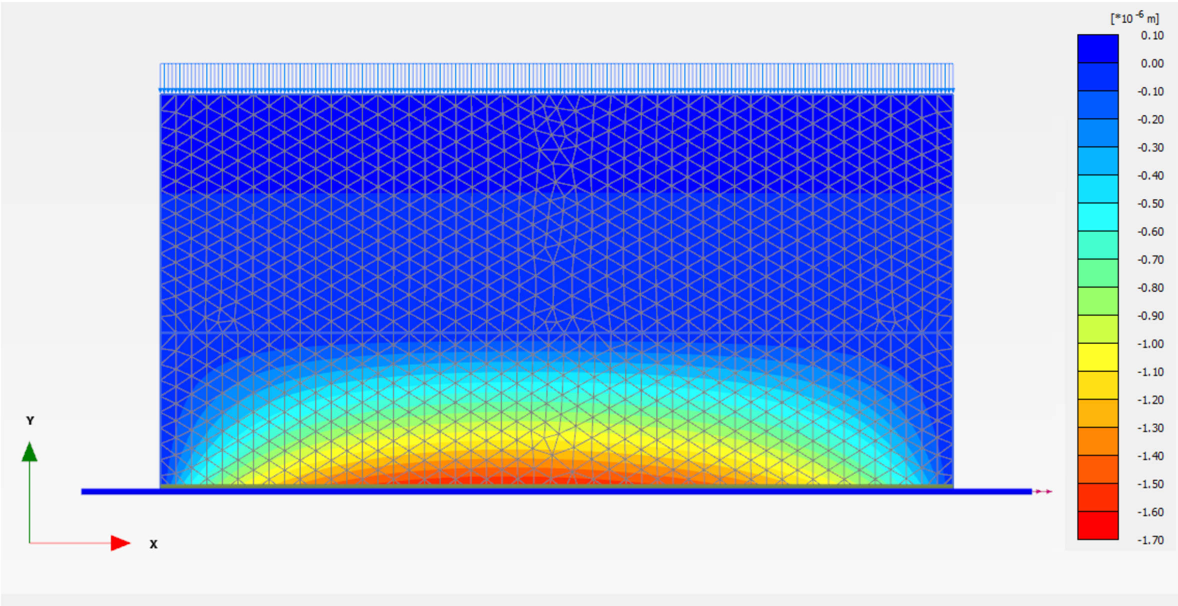

Figure 4.43. Horizontal displacements in soil domain (Normal stress = 80 kPa and T= 35°C)

4.8.2.2. Temperature distributions in soil

Figure 4.44 presents temperature distributions in the soil when the interface plate was heated to 35°C. Although the temperature at the interface is at the target temperature, there is a temperature gradient in the soil sample in the vertical direction.

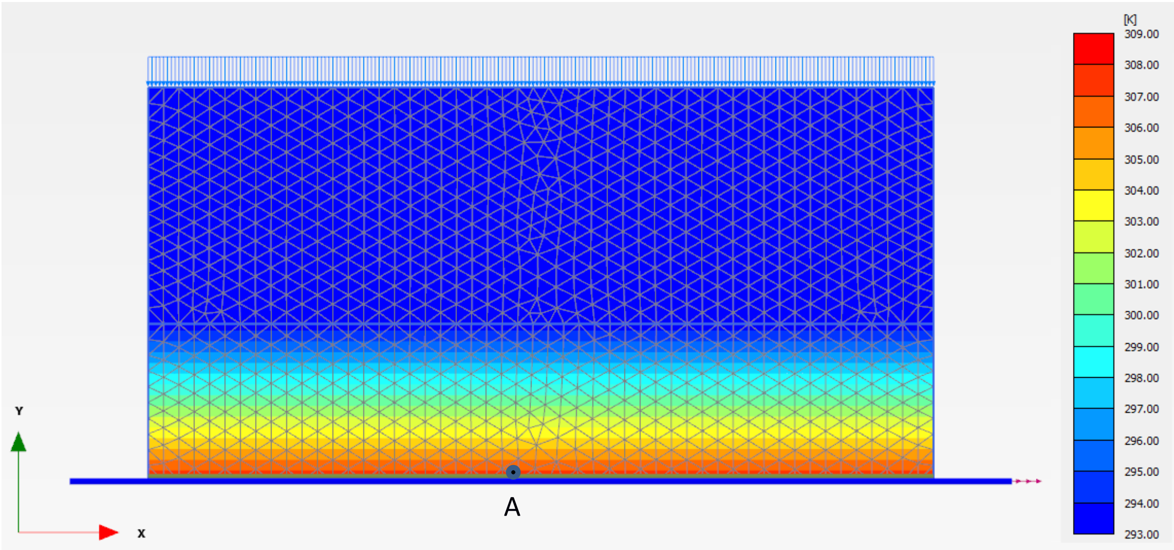

Figure 4.44. Temperature distribution in soil (Normal stress=80 kPa and the interface plate is at 35°C)

The curves of temperature vs. time at point A in the interface are shown in Figure 4.45. It is noted that the temperature changes with time have the same trend in experiments and numerical simulation. After 20-minutes of heating, the target temperature 35^{o}C is reached at the interface.

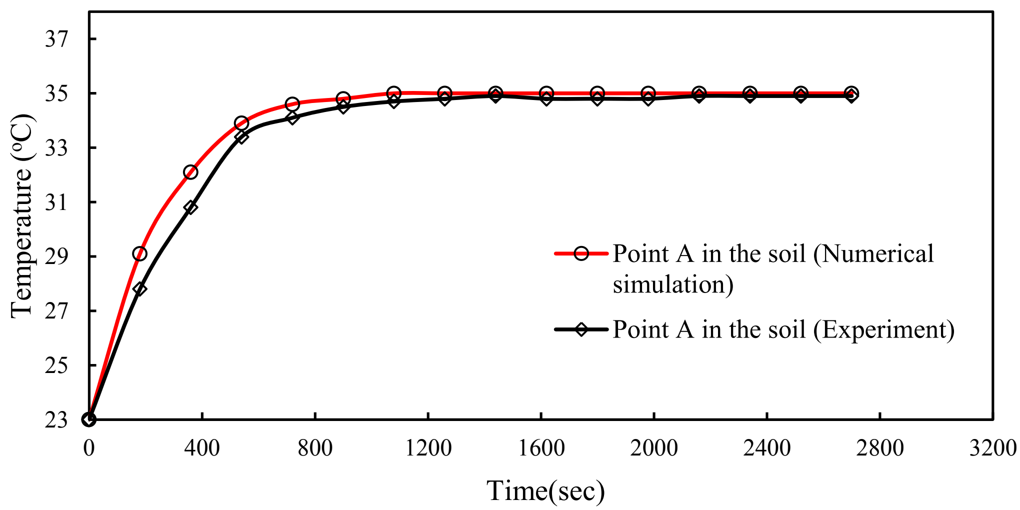

Figure 4.45. Temperature vs. time at point A on the interface plate during the heating to35^{o}C

4.8.2.3. Suction values in overconsolidated soil samples

The suction values in the soil in the interface tests after loading the soil to 375 kPa first, then unloading to 60 or 80 or 100 kPa are used to calculate suction distributions. Figure 4.46 shows the suction distribution in the soil domain when the normal stress was 80 kPa and the temperature of the steel plate was 35^{o}C. The suction values determined by PLAXIS FE code are listed in Table 4.8 for different temperatures and normal stress values. It is noted that the suction slightly decreased with increasing normal stresses due to different degrees of saturation in the soil. For example, the degree of saturation of soil at 8^{o}C is 54.5 % (Normal stress=60 kPa), 54.8 % (Normal stress=80 kPa), 56.2 % (Normal stress=100 kPa).

Table 4.8. Suction values in soil at the interface under different normal load and temperatures

Temperature (°C)		8	23	35
Suction (kPa)	Normal stress 100 kPa	46.3	43.8	38.9
	Normal stress 80 kPa	47.1	43.7	39.0
	Normal stress 60 kPa	47.2	43.7	39.3

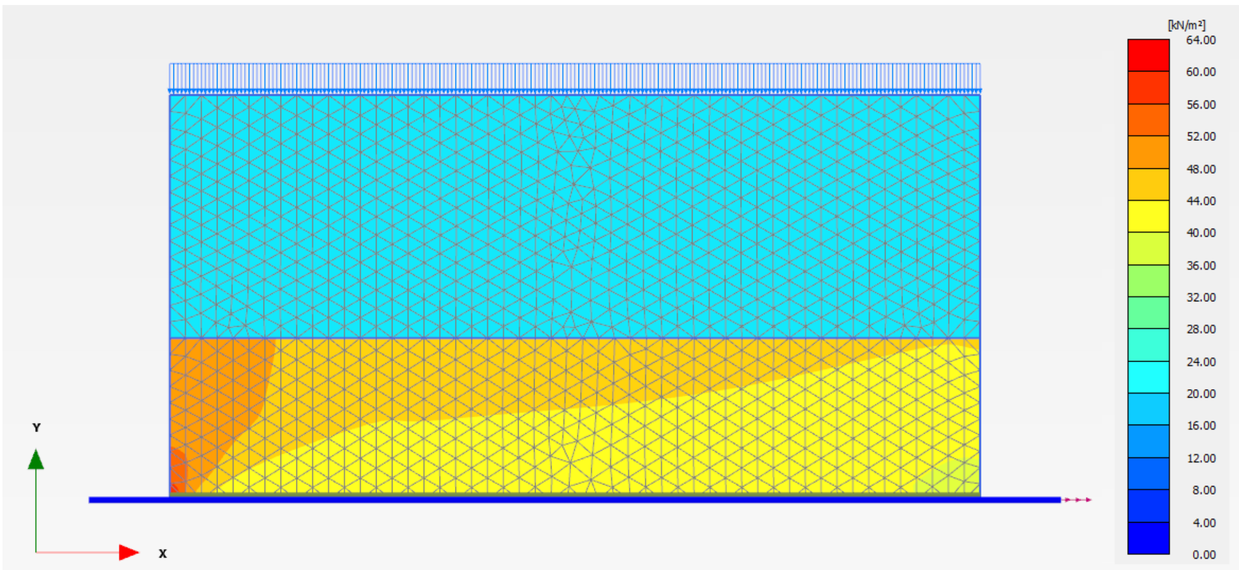

Figure 4.46. Suction distribution in soil domain (Normal stress=80 kPa and T=35°C)

Maximum shear stress distribution in the soil domain is plotted in Figure 4.47.

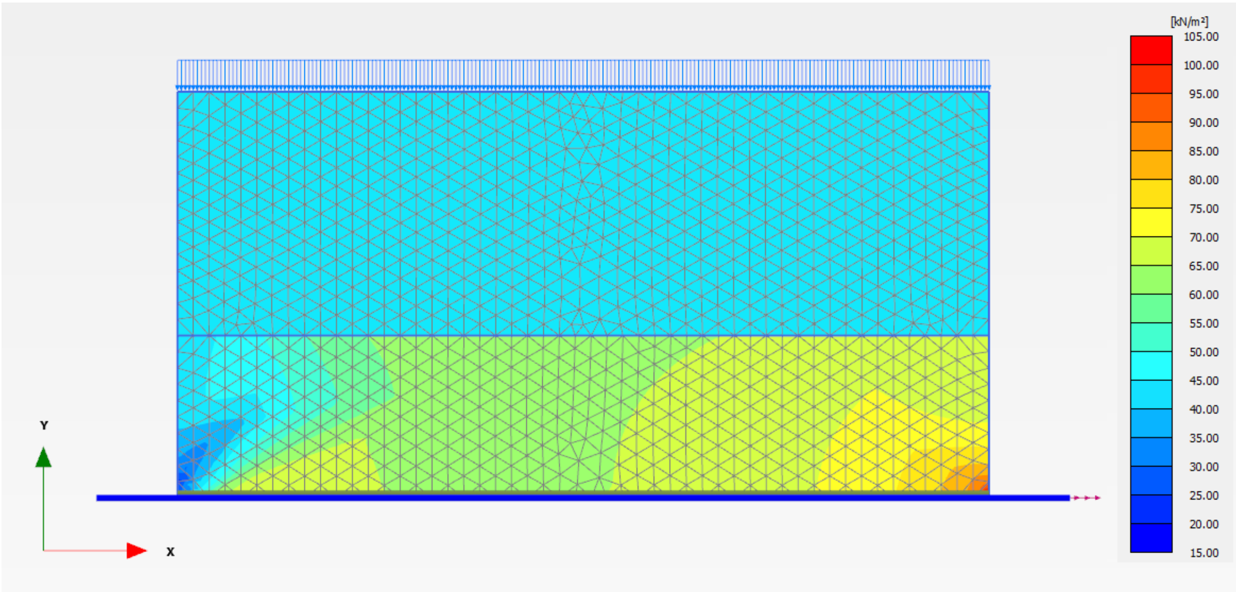

Figure 4.47. Maximum shear stress distribution in soil domain (Normal stress=80 kPa and T= 35°C)

4.8.2.4. Interface shear strength

All shear stress versus displacement curves (data from laboratory experiments and numerical simulations) with various temperatures are presented together in Figure 4.48 (corresponding to 60 kPa normal stress) for the purpose of comparison. Similarly, Figures 4.49 and 4.50 show the shear stress versus horizontal displacement curves at various temperatures for 80 kPa and 100 kPa normal stress conditions. The numerical analysis of shear stress versus horizontal displacement curves of the interface has a good agreement with the laboratory tests results. It is clearly shown that the shear strength of the interface decreases with increasing temperatures in overconsolidated soil samples.

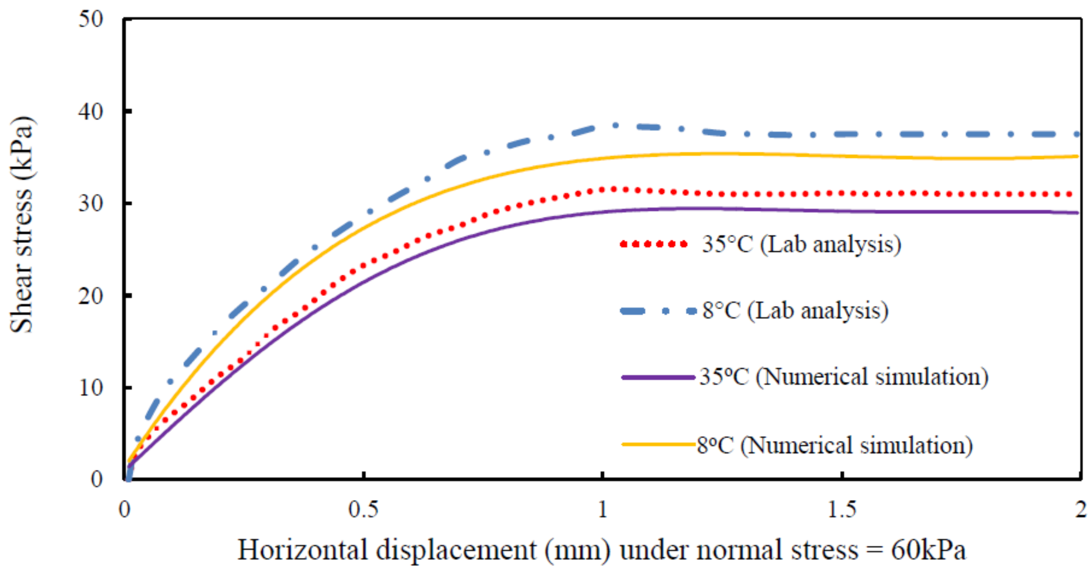

Figure 4.48. Shear stress versus horizontal displacement of soil-steel plate interface with various temperatures (Normal stress = 60 kPa)

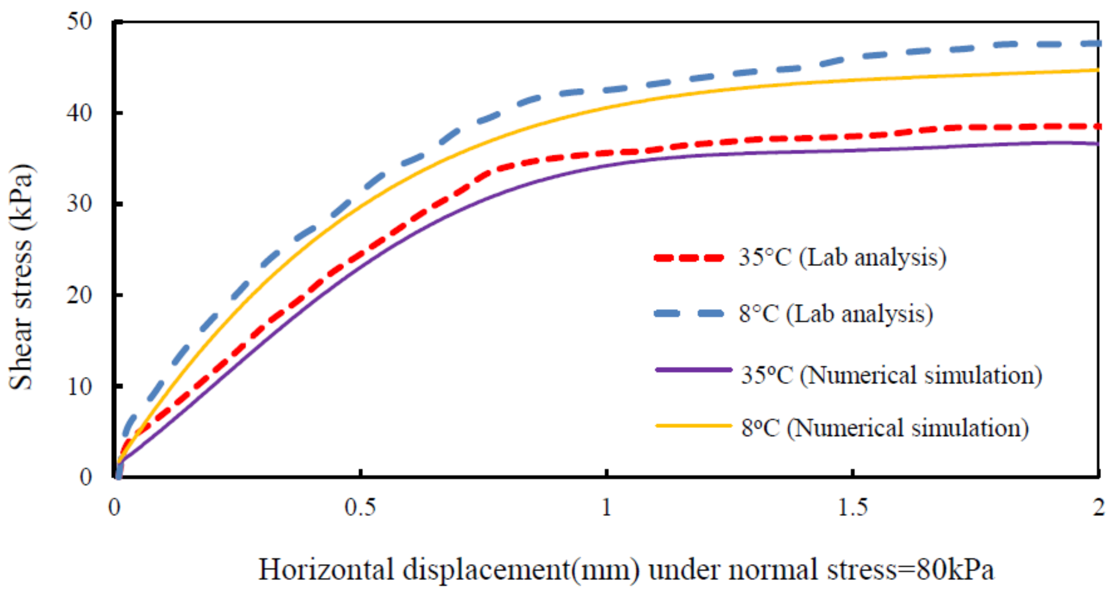

Figure 4.49. Shear stress versus horizontal displacement of soil-steel plate interface with various temperatures (Normal stress = 80 kPa)

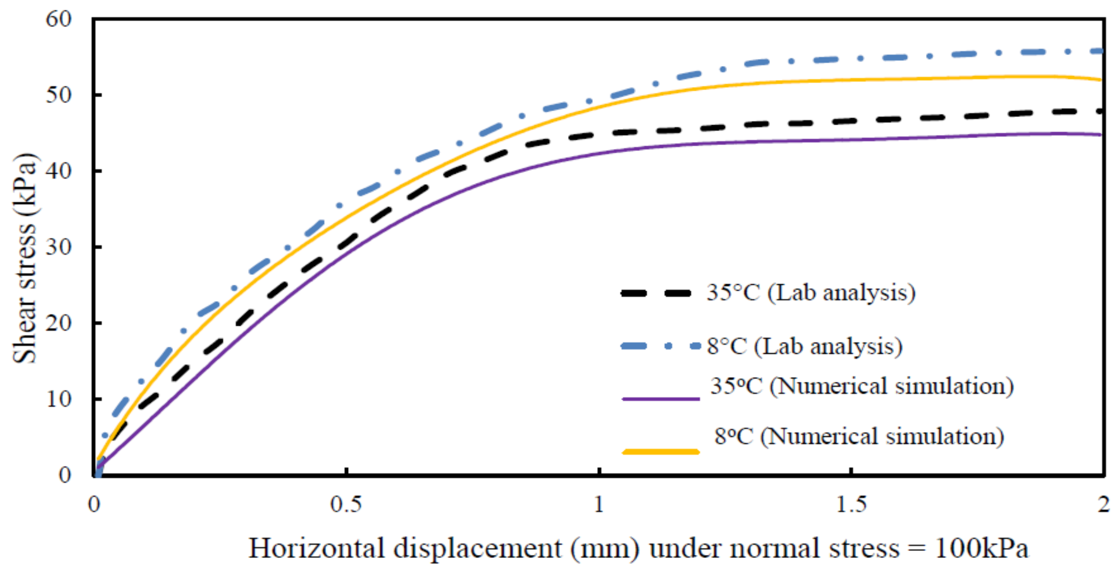

Figure 4.50. Shear stress versus horizontal displacement of soil-steel plate interface with various temperatures (Normal stress = 100 kPa)

4.8.2.5. Calculation of shear strength of unsaturated soil using Vanapalli and Fredlund (2000) method

In order to predict the nonlinear variation in shear strength of unsaturated soil, a semi-empirical model (Equation 4.1) proposed by Vanapalli and Fredlund (2000) is used in this study.

$$\tau_{unsat} = \left[c' + (\sigma - u_a)\tan\phi'\right] + (u_a - u_w)[S^{\kappa}\tan\phi'] \qquad (4.1)$$

where c' is effective cohesion, ϕ' is effective angle of internal friction, σ = normal stress, $(u_a - u_w)$ is matric suction, u_a is pore-air pressure, u_w is pore-water pressure, S is degree of saturation and κ is fitting parameter (for this study, κ = 1 due to 75 % sand in the soil mixture).

The effect of suction on the internal friction angle ϕ' would be not significant (Vanapalli and Fredlund 2000). In Equation 4.1, the contribution of matric suction towards the shear strength can be appended to the apparent cohesion, c which is described by Equation 4.2.

$$c = c' + (u_a - u_w)[S^{\kappa}\tan\phi'] \qquad (4.2)$$

The apparent cohesion is directly obtained from the failure envelope by analyzing lab test dada as listed in Table 4.9 under different thermal conditions.

Table 4.9. Apparent cohesions and internal frictions with different temperatures

Temperature (^oC)	8	23	35
Internal friction φ' (^{o})	24.4	23.5	22.8
Apparent cohesion c (kPa)	18.2	15.2	12.1

The shear strength of unsaturated soil can be calculated using simple form of Equation 4.3.

$$\tau_{unsat} = c + \sigma_n tan\varphi^{'} \quad (4.3)$$

Shear strengths of unsaturated soil under different thermal conditions are listed in Table 4.10.

Table 4.10. Shear strength of unsaturated soil under different thermal conditions

Temperature (^oC)		8	23	35
Normal stress 100 kPa	Shear strength (kPa)	58.5	53.9	49.5
Normal stress 80 kPa		50.5	46.1	42.0
Normal stress 60 kPa		42.4	38.4	34.6

It is noted that the shear strengths of kaolin–sand mixture in unsaturated condition are decreased with the increase in temperature as provided in Table 4.10.

The shear strength of the interface between kaolin–sand mixture and steel plate in unsaturated condition can be estimated using a reduction factor on the shear strength of unsaturated soil mixture. In this study, a reduction factor of 0.9 is used. The shear strength of unsaturated soil-steel plate interface is determined by (a) lab testing, (b) numerical simulations and (c) calculations. A summary of results are listed in Table 4.11.

Table 4.11 Shear strength of unsaturated soil-steel plate interface under different thermal conditions

Temperature (^{o}C)		8			23			35		
		La	Nu	Ca	La	Nu	Ca	La	Nu	Ca
Normal stress 100 kPa	Shear strength (kPa)	54.3	52.7	52.6	51.5	50.2	48.5	46.3	44.2	44.6
Normal stress 80 kPa		46.4	44.5	45.5	45.1	44.2	37.8	38.4	36.5	37.8
Normal stress 60 kPa		38.4	37.1	38.2	38.5	37.2	34.6	31.5	29.2	31.1

Note: La = Laboratory test results, Nu= Numerical results, Ca=Calculation results.

CHAPTER 5

NUMERICAL ANALYSIS OF THERMAL EFFECTS ON THE INTERFACE BEHAVIOUR OF AN ENERGY PILE

The finite element method of analysis is used to find out the thermal effects on the behaviour of interface between an energy pile and soil. The results of the analysis are used (a) to evaluate heat and moisture transfer in the soil as a function of time, (b) to calculate the thermally induced stress and strain changes in the soil surrounding the pile, (c) to find out the amount of expansion and contraction of the pile, (d) to determine how the shaft resistance and the bearing capacity of the pile changes in response to variations in temperature.

These calculations are conducted using the finite element codes SIGMA/W and VADOSE/W of GeoStudio 2012 and PLAXIS 2D. Details of the numerical analysis involving SIGMA/W and VADOSE are given in Sections 5.1 and 5.2. In reporting the outcome of the analysis using SIGMA/W and VADOSE, the figure captions will have the word GeoStudio. Results of PLAXIS analysis are provided in Section 5.3.

5.1. Geometry of a generic energy pile and analysis domain

In this study, a 10 m long energy pile is assumed to be installed in a 20 m deep soil deposit composed of a kaolin-sand mixture. The diameter of the pile is 1 m. A series of thermo-hydro-mechanical FE analyses of the pile are carried out using the mesh shown in Figure 5.1. An elastoplastic model is used to describe the behaviour of the kaolin-sand mixture while the pile is assumed to behave elastically. In some studies, Young's modulus of the energy pile has been reported as 29 GPa (Kramer and Basu 2014), 29.2 GPa (Knellwolf et al. 2011) and 40 GPa (Bourne-Webb et al. 2009). In this study, elastic modulus E = 29.2 GPa is considered. The parameters of material models are listed in Tables 5.1 and 5.2.

The axisymmetric FE domain is discretized using quadrilateral and triangular elements for both soil and the pile. At the pile–soil interface, shear strain localization would occur. In order to simulate the strain localization in the simulations using GeoStudio FE codes, interface elements are placed in the first column of elements next to the pile shaft. The material properties of interface elements are adapted from the laboratory tests. A refined mesh is used for the pile and near the pile–soil interface with the minimum element size of 0.05 m in soil. The maximum size of the elements used is 0.25 m in the rest of the finite element domain. The groundwater table was either at the ground surface or eight meters below the ground surface as indicated by the horizontal dashed line in Figure 5.1.

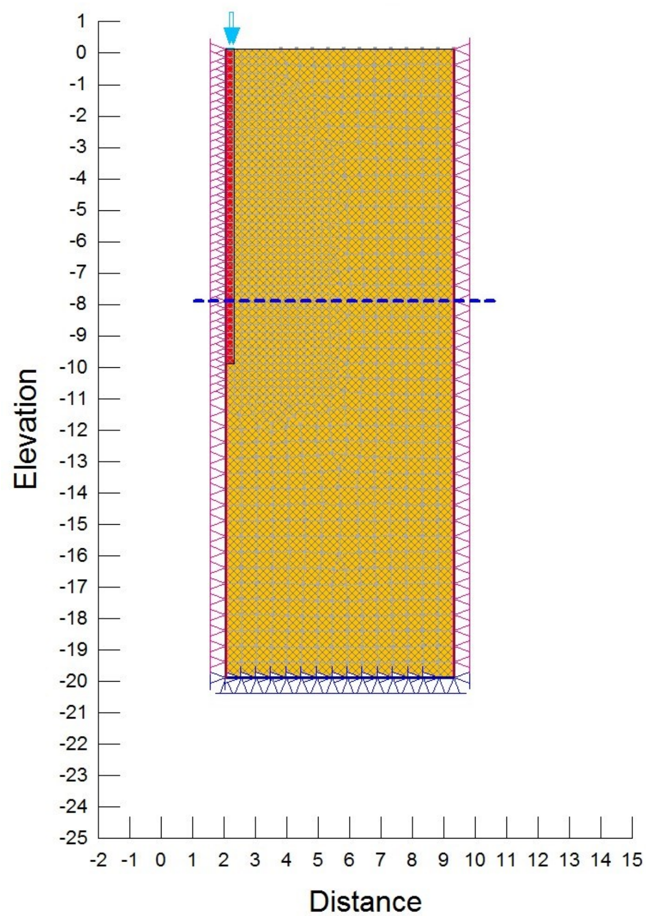

Figure 5.1. Schematics of pile–soil analysis domain (GeoStudio)

Table 5.1. Model parameters of the soil and pile in the mechanical analysis

Material Property	Kaolin-sand mixture	Pile
Young Modulus, E (MPa)	26	2.92 E6
Poisson's Ratio	0.25	0.18
Cohesion *c* (kPa)	5.3	
Friction angle ϕ (°)	29	
Hydraulic conductivity (cm/s)	2.62 E-5	Impervious

Note: The shear strength parameters of soil are obtained from the analysis of drained direct shear tests. The other parameters used in the analysis are suggested by soil lab data in PLAXIS.

Table 5.2. Thermal properties of soil and pile

Soil layer	Heat capacity (J/m^3 $^\circ$C)	Thermal conductivity (W/m / $^\circ$C)	Thermal expansion coefficient (1/K)
Kaolin-sand mixture	2.45	1.5 $\times 10^6$	1.5E-6
Pile	3.47	2.0$\times 10^6$	1.0E-6

5.1.1 Boundary conditions

5.1.1.1 Mechanical boundary conditions

There are no movements in both vertical and horizontal directions at the bottom of the analysis domain. Horizontal movement is prevented on the vertical sides of the analysis domain as shown in Figure 5.2 (a). A vertical movement is applied on the pile head.

5.1.1.2 Thermal boundary conditions

The heat flux occurs through the right-hand side and bottom of the soil mass. There is no heat flux along the axis of symmetry. A constant temperature is applied at the top surface of the domain as shown in Figure 5.2(b). The initial soil temperature is assumed to be 11-15°C. A heating–cooling cycle is assumed to be applied on the pile (12 days of heating then 16 days of cooling) as shown in Figure 5.3. For the whole year-round operation of an energy pile, the number of heating and cooling days would depend on the needs of the structure, geographical location and the climate of the region.

5.1.1.3 Hydraulic boundary conditions

It is assumed that there is no natural groundwater flow in this study. The pile is considered as an impervious material. The water flux can take place at the top and bottom of soil mass and on the right-hand side of the domain. There is no water flux along the axis of symmetry. Two types of analysis were conducted to accommodate two different locations of the groundwater table. For the saturated condition, the water table is located at the top of the soil mass. For the unsaturation condition, the water table is at 2 meter above the toe of the pile as shown in Figure 5.2 (c).

FE analyses of this energy pile in kaolin–sand mixture are performed by using the integration of SIGMA/W and VADOSE/W in two steps: (1) a static step to apply the gravity loading and bring the model in geostatic equilibrium by using SIGMA/W, then continue the analysis, still using SIGMA/W, and apply the mechanical axial load at the pile head; (2) a thermal analysis step to apply temperature variation for heating and cooling cycles by VADOSE/W.

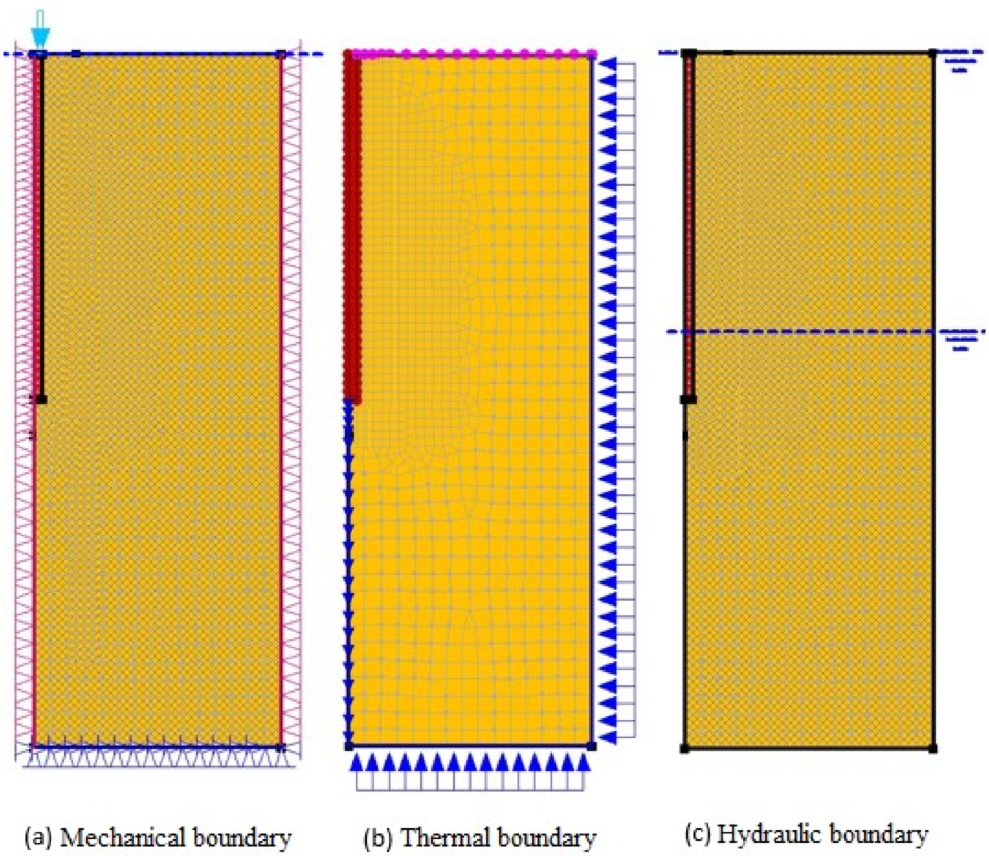

Figure 5.2. Boundary conditions (GeoStudio)

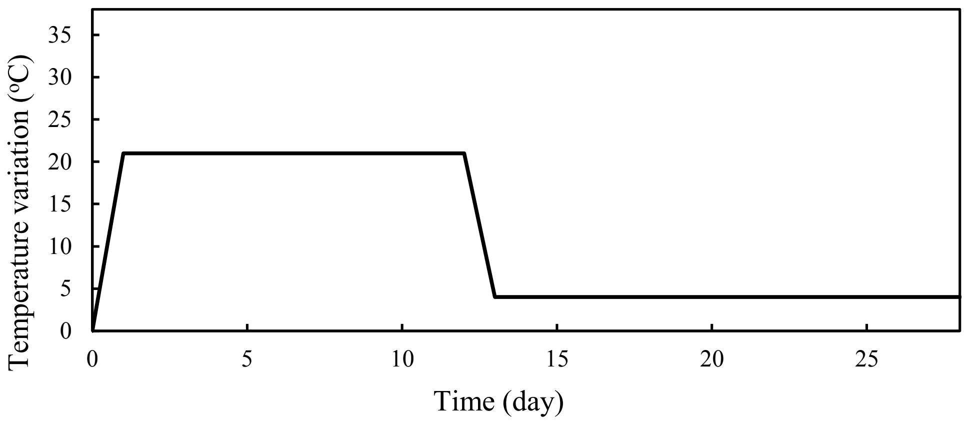

Figure 5.3. A heating–cooling cycle of loading with time

5.2. Analysis results

In this part, the results of coupled thermo-hydro-mechanical analysis under saturated and unsaturated conditions are provided. The model was set up as such that identical thermal boundary conditions were used for two different cases, a uniformly saturated soil mass in one case and an unsaturated soil condition in the second case. These scenarios are computed by placing the groundwater table at the soil surface in the saturated condition, compared with the groundwater table at 8 m depth from the ground surface in the unsaturated condition. The behaviour of the pile is explored first and then that of the soil domain.

5.2.1. Thermo-mechanical behaviour of the pile

5.2.1.1. Axial stress in the pile

When the temperature is increased, the pile would expand in the radial direction and elongate in the vertical direction. In response, the soil would try to counteract the movements of the pile. In the vertical direction, soil would resist, to some extent, the elongation of the pile. As a result, shear stresses would develop along the pile shaft over and above the shear stresses developed during pile installation and mechanical loading imposed on the pile by the building. Shear stresses imposed on the pile shaft are limited by the shear strength of the soil-structure interface.

Some of the important factors that would influence the magnitude of the pile elongation and the resisting forces are: (1) Magnitude of temperature change, (2) Restraints imposed on the pile head by the building, (3) Coefficient of thermal expansion of pile material and soil, (4) Degree of saturation of soil, (5) Strength and deformation properties of soil,(6) Loading history of both pile and soil, (6) Time as a factor that influences the heat transfer and affects the soil behaviour.

In generally, due to the side friction or the restraint conditions on the ends of the pile, part of the pile deformation would be prevented. In this section of the present analysis, no end restraints are imposed on the pile ends. When the free expansion of the pile due to temperature increase is prevented, the existing axial and radial stresses in the pile will change. Figure 5.4 shows a comparison in the axial stress generated in the pile under mechanical and thermo-mechanical loading conditions, respectively. The axial stresses due to thermo-mechanical loading are larger than those due to purely mechanical loading. Meanwhile, higher axial stress developed in the pile as the soil is in the unsaturated condition compared to those in the saturated condition. This behaviour is the result of contribution of matric suction towards the shear strength at the pile-soil interface as reported in Chapter 4 of this study. The shear strength produced in unsaturated conditions is greater than that in saturated conditions. Hence, the side friction in unsaturated states would prevent the development of large amount of thermal strains in the pile than in saturated states. More constrained strains lead to more thermal axial and radial stresses in the pile.

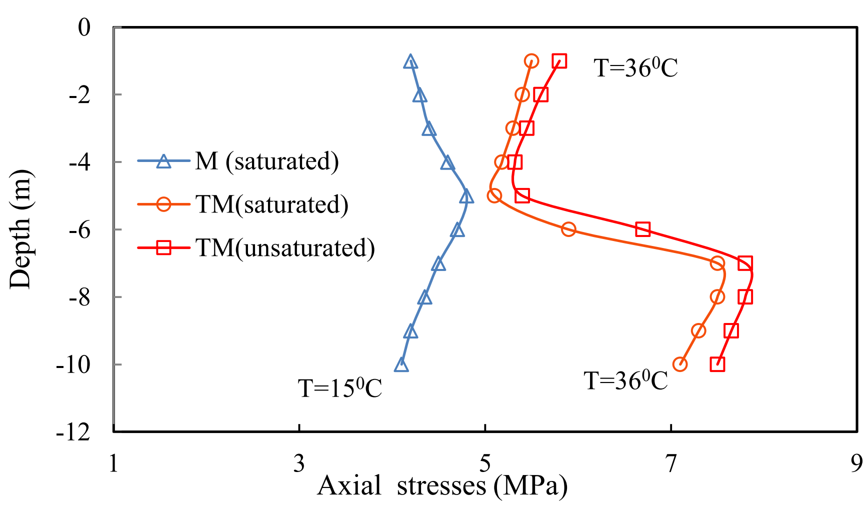

Figure 5.4. Axial stress in the pile under saturated and unsaturated conditions during mechanical and thermo-hydro-mechanical processes at ΔT = 21°C (GeoStudio)

5.2.1.2. Axial strain in the pile

The distribution of axial strains in the pile during the thermos-mechanical process is shown in Figure 5.5. It can be seen that the strain is not uniform and there is a difference in the strain under saturated and unsaturated conditions. The axial strain in the pile is influenced by the friction along the pile shaft. Due to the contribution of matric suction to the shear strength, the axial strain of the pile is smaller in unsaturated conditions.

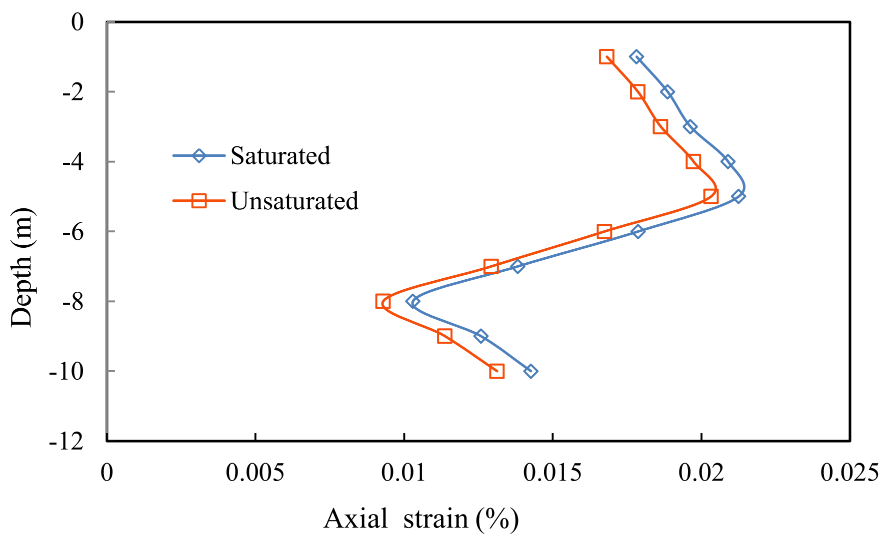

Figure 5.5 Axial strains in the pile at $\Delta T = 21°C$ under saturated and unsaturated conditions (positive for expansion) (GeoStudio)

5.2.1.3. Radial strains in the pile

Radial strains increase in the pile under the influence of thermo-mechanical loading as compared to those under only mechanical loading as shown in Figure 5.6.

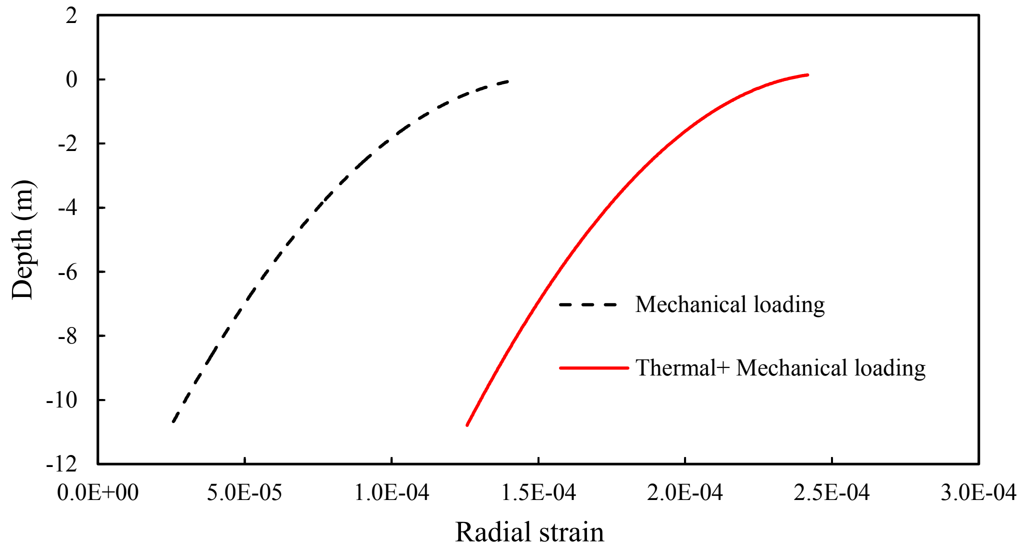

Figure 5.6. Radial strains in the pile under mechanical and thermo mechanical loading ($\Delta T = 21°C$)

5.2.1.4. Thermal effect on the bearing capacity of energy pile

The ultimate capacity of the pile may be achieved as the vertical displacement is equal to about 10% of the average pile diameter (Canadian Foundation Engineering Manual 2006). In the present numerical analysis, the maximum vertical displacement is 15% of the pile with 1 m diameter. The incremental vertical displacement is applied on the pile head, as the pile under the temperature of 15^{o}C, 25^{o}C and 36^{o}C respectively. The shaft resistance is mobilized first; whereas the toe resistance requires larger displacements to fully develop (More details can be found in Section 5.3.2.4).

Figure 5.7 shows the load-displacement (P-δ) behaviour of the energy pile at different temperatures during the heating process. It is noted that the bearing capacity of the energy pile is increased with increased temperature in the pile. This has the same trend as the centrifuge test results by McCartney and Rosenberg (2011) (see Figure 2.6 in section 2.4.2). For example, when the temperature increased from 15°C to 25°C, the bearing capacity of the pile increased from 645 kN/rad to 735 kN/rad. In this study, a temperature increase of 1^{o}C results in an additional temperature-induced vertical force in the order of 9 kN/rad which is about 60 kN change in the total bearing capacity.

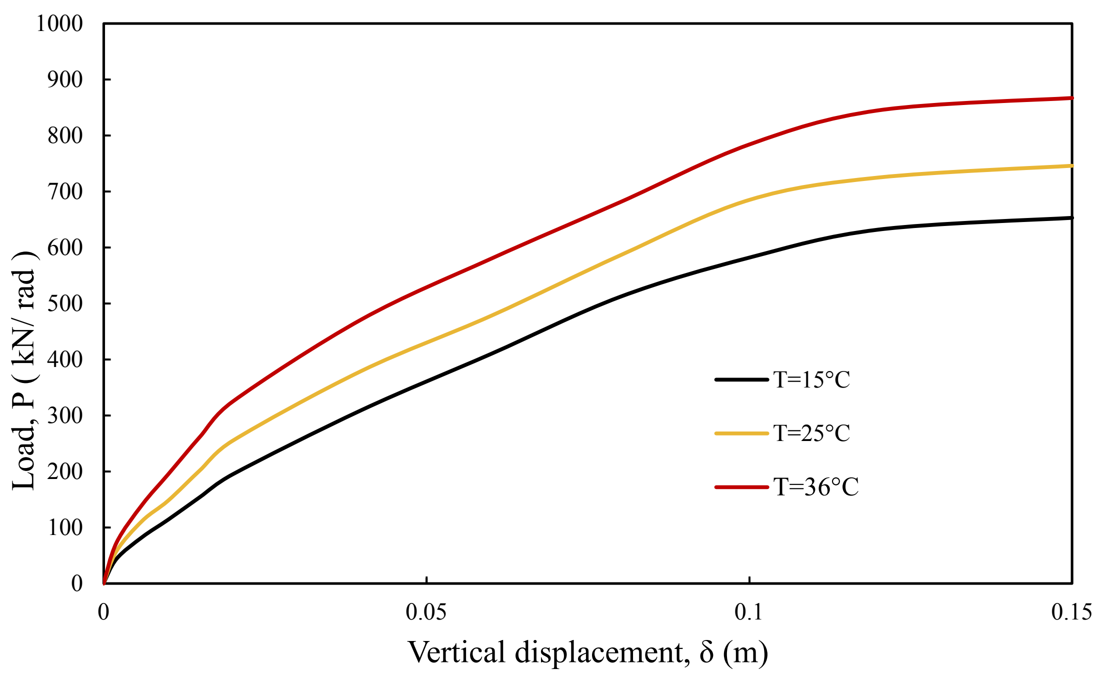

Figure 5.7. Bearing capacity of the pile versus vertical displacement of the pile during the heating process (GeoStudio)

5.2.2. Thermo-mechanical behaviour of the soil

5.2.2.1. Thermal effect on the horizontal stresses acting on the soil – pile interface

Olgun et al. (2014b) conducted an undrained finite-element analysis of an energy pile to assess the horizontal stresses and strains acting on the pile shaft during heating. The soil was fully saturated. Soil suction was not a factor in the analysis. They pointed out that the stiffness of the soil played an important role in preventing the thermal expansion of the pile. Their analysis showed that the pile expansion alone due to temperature changes did not significantly increase the pile capacity. An increase in horizontal normal stress acting on the pile-soil interface corresponded to stiffer soils. In the present study, the development of horizontal normal stress acting on the pile shaft is also investigated under both saturated conditions (groundwater table at the ground surface) and the unsaturated conditions (groundwater table is 8m below the ground surface). It can be seen in Figures 5.8a and 5.8b where the horizontal stresses increase with the increase in the temperature under both cases. However, horizontal stresses under unsaturated conditions are greater than those under saturated conditions due to the added effect of matric suction. From the two curves corresponding to the same temperature in Figures 5.8a and 5.8b, the difference between horizontal stresses is the contribution of matric suction. For example, the horizontal stress at point A in Figure 5.8a is 5kPa. The corresponding point on Figure 5.8b is the point B where the horizontal stress is 30kPa. The difference is 25kPa which is the effect of suction. This indicates that the suction affects the horizontal normal stress acting the soil-pile interface a significant amount. The horizontal normal stresses acting on the pile-soil interface is an important factor in the calculation of the shear strength of the pile-soil interface. Thus, the effects of changes in suction and temperature should be taken into account in the calculation of the shaft resistance of energy piles.

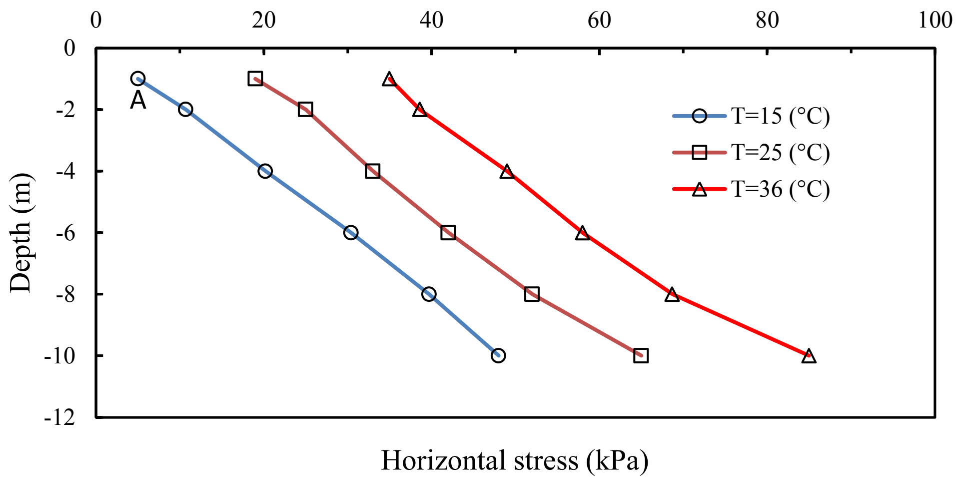

(a) Saturated condition

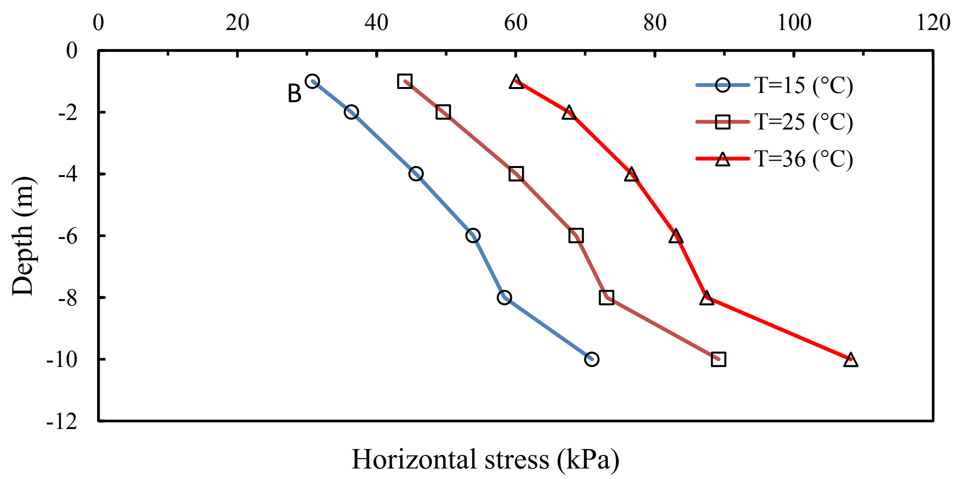

(b) Unsaturated condition

Figure 5.8. Horizontal normal stresses acting on the pile-soil interface along the pile shaft during heating process (PLAXIS) (a) Saturated condition (b) Unsaturated condition

The horizontal stress distribution along the pile calculated by GeoStudio 2012 and PLAXIS can be used to calculate the shaft resistance of a pile by using Equations (2.1), (2.2), (2.3) in Chapter

2. Shaft resistance of a pile under different temperatures is calculated and the results are shown in Tables 5.3, 5.4, 5.5.

Table5.3. Shaft resistance of the pile at 15°C

Sections	Horizontal stresses (kPa) σ'_h		Interface shear strength (kPa) $r_s=\sigma'_h \tan\delta + f_2$	
	GeoStudio 2012	PLAXIS	GeoStudio 2012	PLAXIS
1(0-2m) $\Delta L=2$	5.1	5.3	15.9	16.1
2(2-4m) ΔL=2	15.1	15.7	21.3	21.7
3(4-6m) ΔL=2	26.1	26.3	27.4	27.5
4(6-8m) ΔL=2	36.5	36.7	33.2	33.3
5(8-10m) $\Delta L=2$	47.0	47.3	39.0	39.2
Total shaft resistance (Q_s)(kN) $Q_s=\Sigma\, r_s\, p\, \Delta L$ $(p=2\pi\, r=3.14m)$ $(r=0.5m)$			860.5 kN	864.8 kN

Table 5.4. Shaft resistance of the pile at 25^oC

Sections	Horizontal stress (kPa) σ'_h		Interface shear strength (kPa) $r_s=\sigma'_h \tan\delta+f_2$	
	GeoStudio 2012	PLAXIS	GeoStudio 2012	PLAXIS
1(0-2m) $\Delta L=2$	11.5	12.7	19.4	20.0
2(2-4m) ΔL=2	24.3	25.6	26.5	27.2
3(4-6m) ΔL=2	36.7	37.5	33.3	33.8
4(6-8m) ΔL=2	48.2	49.6	39.7	40.5
5(8-10m) $\Delta L=2$	60.1	61.3	46.3	47.0
Total shaft resistance (Q_s) (kN) $Q_s=\Sigma\, r_s\, p\, \Delta L$ $(p=2\pi\, r=3.14m)$ $(r=0.5m)$			1038.1 kN	1058.7 kN

Table 5.5. Shaft resistance of the pile at 36°C

Sections	Horizontal stress (kPa) σ'_h		Interface shear strength (kPa) $r_s=\sigma'_h \tan\delta + f_2$	
	GeoStudio 2012	PLAXIS	GeoStudio 2012	PLAXIS
1(0-2m) $\Delta L=2$	19.4	21.4	23.8	24.9
2(2-4m) $\Delta L=2$	35.1	38.1	32.5	34.1
3(4-6m) $\Delta L=2$	49.4	52.4	40.4	42.0
4(6-8m) $\Delta L=2$	62.2	65.4	47.5	49.3
5(8-10m) $\Delta L=2$	73.9	77.1	54.0	55.7
Total shaft resistance (Q_s) $Q_s=\Sigma\, r_s\, p\, \Delta L$ ($p=2\pi r=3.14m$)			1244.3 kN	1294 kN

5.2.2.2. Volumetric water content

Figure 5.9 presents the volumetric water content distribution in the soil located at 4 m above the water table along the radial direction after 12 days of thermal loading increment of ΔT= 21°C. It can be seen that a significant change in the moisture contents takes place within a distance of 2 meters from the energy pile. The volumetric water content of the soil near the energy pile decreases sharply from the initial value of 0.23 to 0.1 after heating. Most of the drop in moisture content occurs in the soil between r = 0 m and r = 1 m (here, the letter r is used for the horizontal distance measured from the soil-pile interface.). The moisture content increases slightly in the region of 1 m < r < 1.5 m due to condensation happening when the warmer water vapor migrates to the region of lower temperature, and hence leads to a rise in volumetric water content. However, no significant variation of moisture content is observed beyond r = 2 m. The change of volumetric water content has great effect on the soil suction near the soil-pile interface.

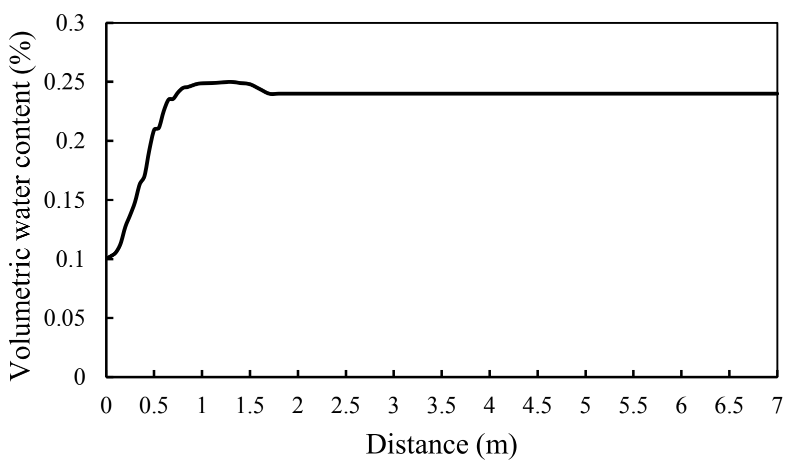

Figure 5.9. Variation of volumetric water content in the soil at points along the radial direction after thermal loading of 21°C (GeoStudio)

5.2.2.3. Matric suction

Moisture transfers in the soil during the heating also cause changes in matric suction in the soil. Figure 5.10 indicates the suction distribution in the soil at 4 m above the groundwater table along the radial direction after 12 days of temperature increase of 21°C. It is noted that suction increases from an initial value of 40 kPa to 46 kPa near the interface (r = 0 m). However, the increase in suction in soil ceases at about r = 1m. Thereafter, the suction drops slightly in the region of 1m < r < 1.5 m. There is a slight increase in suction in the region of 1.5m < r < 2 m. Beyond r = 2 m there is no change in the suction values.

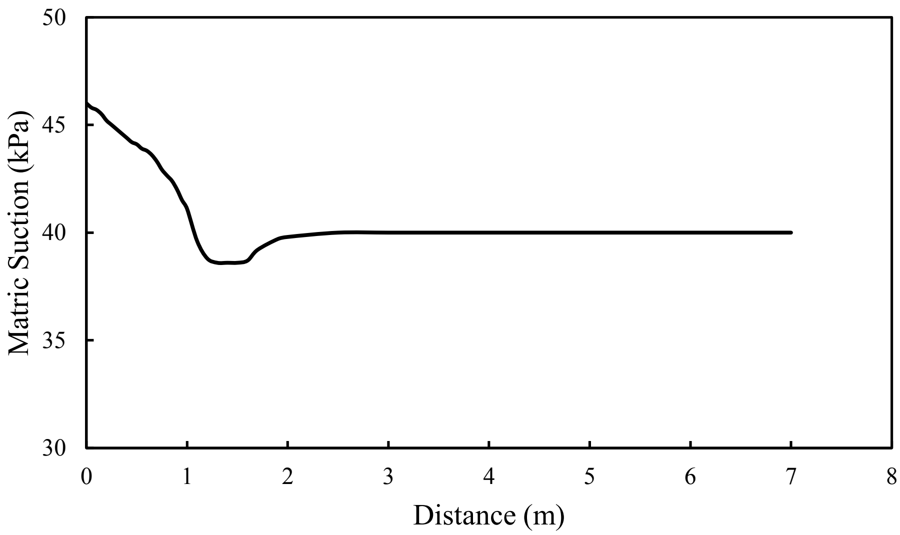

Figure 5.10. Variation of matric suction in the soil along the radial direction after 12 days of thermal loading increment of 21°C (GeoStudio)

5.2.2.4. Temperature distributions in the soil

Temperature distributions in the soil after 12 days of heating indicate that the energy transferred into the soil mainly takes place within a zone extending 2 meters away from the energy pile during a heating period as shown in Figure 5.11. It is noted that although the pile reaches a temperature of T=32^{o}C after 12 days of heating, the soil is not necessarily at the same temperature everywhere. Soil temperature changes as a function of location and time as illustrated in Figure 5.12 for points along Section A-A between r = 0 to r = 2 m. However, the temperature in the soil remains at the initial value T_0 = 11^{o}C at all points approximately more than 2 m away from the pile shaft. It can be seen that temperature in the soil is increasing with time and higher temperatures more than initial value is obtained inside the soil near the pile.

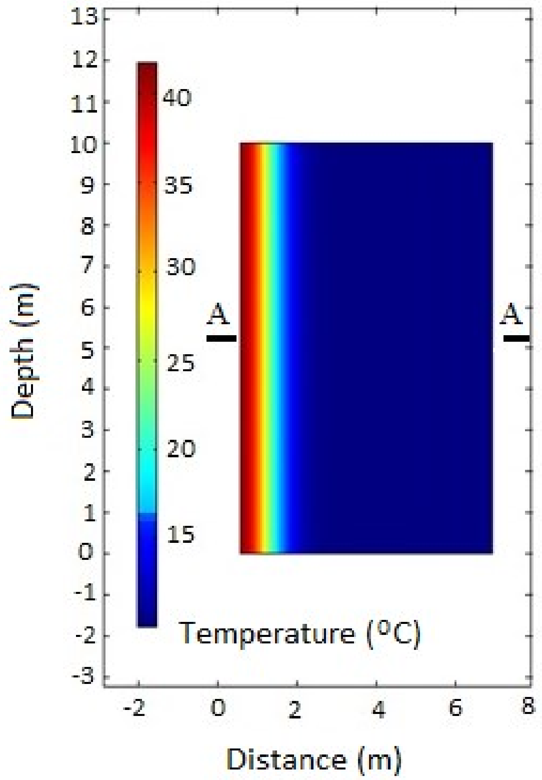

Figure 5.11. Temperature distributions in the soil after 12 days of heating (GeoStudio)

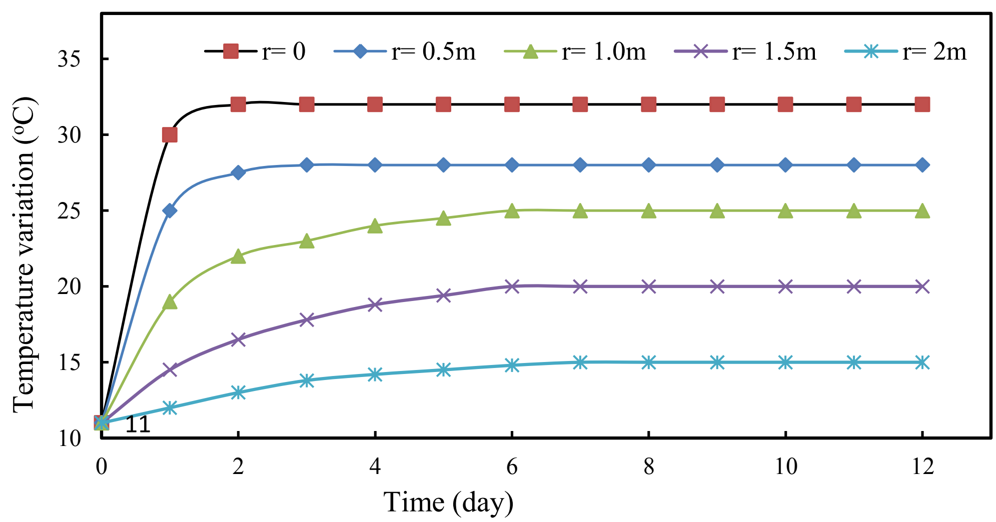

Figure 5.12. Temperature distributions in the soil (A-A section) as a function of time (r = horizontal distance from soil-pile interface) (GeoStudio)

5.2.2.5. Heat flux in the soil

In order to explore the energy transferred to the soil, heat fluxes are calculated during the thermo-hydro-mechanical processes. Figure 5.13 shows the heat flux in the horizontal direction with time along the section A-A. It can be seen that the energy transferred into the soil mainly takes place within a zone extending 2 meters away from the energy pile during a period of 12 days of heating. Meanwhile, the rate of energy transferred into the soil is 25% higher in saturated conditions than that in unsaturated conditions as shown in Table 5.6. This is because the moisture of soil decreases with increasing temperature; the reduction of moisture in the soil leads the thermal conductivity and heat capacity of the soil to drop.

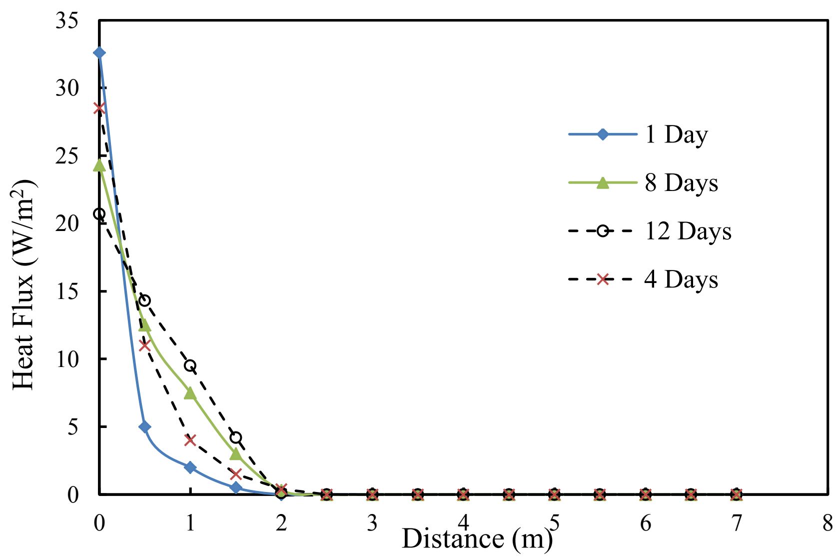

Figure 5.13. Heat flux distributions in the horizontal direction as a function of time along section A-A (GeoStudio)

Table 5.6. Heat flux in saturated and unsaturated conditions (GeoStudio)

Heat Flux (W/m^2)	1day	4 days	8 days	12 days
Unsaturated Condition	32.6	28.5	24.3	20.7
Saturated Condition	40.5	35.6	32.1	26.8

The design of energy piles cannot be completed simply by deciding on the length and diameter of the pile on the basis of bearing capacity and settlement consideration. Heating and cooling needs of the building as well as the ability of energy piles to meet these requirements must be taken into consideration. The type of information provided in Figure 5.16 and the data given in Table 5.6 will help the designers of energy piles.

5.3 Fully coupled THM analysis of energy piles using finite element code PLAXIS 2D

In order to calculate the settlement and bearing capacity of energy piles, it is necessary to take into consideration the effect of temperature changes on the mechanical response of the pile and the hydro-mechanical properties of the soil. As indicated in the literature survey, the best way of studying the behaviour of energy piles is to carry out a coupled analysis. The finite element code PLAXIS 2D is well known for its capability for a fully coupled analysis. It should be noted that the numerical analysis results presented in Section 5.2 were obtained from a sequential analysis using SIGMA/W and VADOSE codes.

Important features of PLAXIS 2D software relevant to the analysis of thermo-hydro-mechanical processes are listed below.

- Coupled THM analysis in unsaturated soils
- Vapour flux
- Anisotropic thermal expansion
- Effect of temperature on permeability
- Convective boundary conditions
- Ground freezing

One of the limitations of THM analysis in PLAXIS is that the temperature has no effect on SWCC and mechanical properties of soil.

During the operation of an energy pile system, the soil-pile interface is subjected to coupled thermo-hydro-mechanical processes as listed in the followings.

- Temperature changes cause expansion or contraction of pile and soil.
- Temperature changes cause moisture flow in the soil.
- Moisture flow results in a change in the degree of saturation.
- A change in the degree of saturation causes a change in the matric suction.
- Matric suction affects the stress-strain-strength behaviour of unsaturated soils.
- A change in the degree of saturation changes the thermal conductivity of soil.

It can be seen that one process affects the initiation and progress of the others. In PLAXIS, non-isothermal unsaturated water flow, water mass balance and balance of momentum (equilibrium) equations are the governing equations to consider the coupled thermo-hydro-mechanical process. The independent variables are displacement, pore water pressure, and temperature. More details are given in Appendix A.

5.3.1. Validation of procedures used in the present study in utilizing PLAXIS

In order to validate the procedures followed in the simulation of energy piles, the following approach is adapted. Three simulations by PLAXIS 2D were conducted from the simplest to more complicated cases so that comparisons were possible between measured and calculated quantities relevant to energy piles. In this section, numerical analysis is presented in three subsections: (1) Mechanical analysis alone, (2) Thermo-Mechanical analysis, and (3) Thermo-hydro-mechanical analysis.

5.3.1.1. First validation (Mechanical loading)

The load versus axial displacement of a pile head was reported by Al-Khazaali et al. (2016). No temperature change was involved in this case. A 200 mm long model pile with 38 mm diameters were installed in the Unimin 7030 sand. A 4 kPa suction was applied on the pile tip. The model pile was subjected to a 20 mm vertical displacement.

A numerical model is set up by PLAXIS to simulate the load versus axial displacement of the model pile in a 2-D axisymmetric analysis as shown in Figure 5.14. The material properties for the pile and the soil are taken from Al-Khazaali et al. (2016) and presented in Table 5.7. The soil stress–strain response is simulated by the elastoplastic Mohr-Coulomb model. The pile stress–strain response is considered as a linear elastic model. The Figure 5.15 shows a comparison in the vertical load generated in the pile due to 20 mm vertical displacement. The calculated results are very close to the test results.

Table 5.7. Mechanical parameters of soil and pile (from Al-Khazaali et al.2016)

Soil layer	Saturated Unit weight Υ_{sat} (kN/m^3)	Friction angle ϕ (°)	Cohesion c (kPa)	Poisson's ratio μ	Young's modulus E (MPa)
Sand	20.4	35.3	2.27	0.33	5.2
Pile	25	-	-	0.15	$20*10^3$

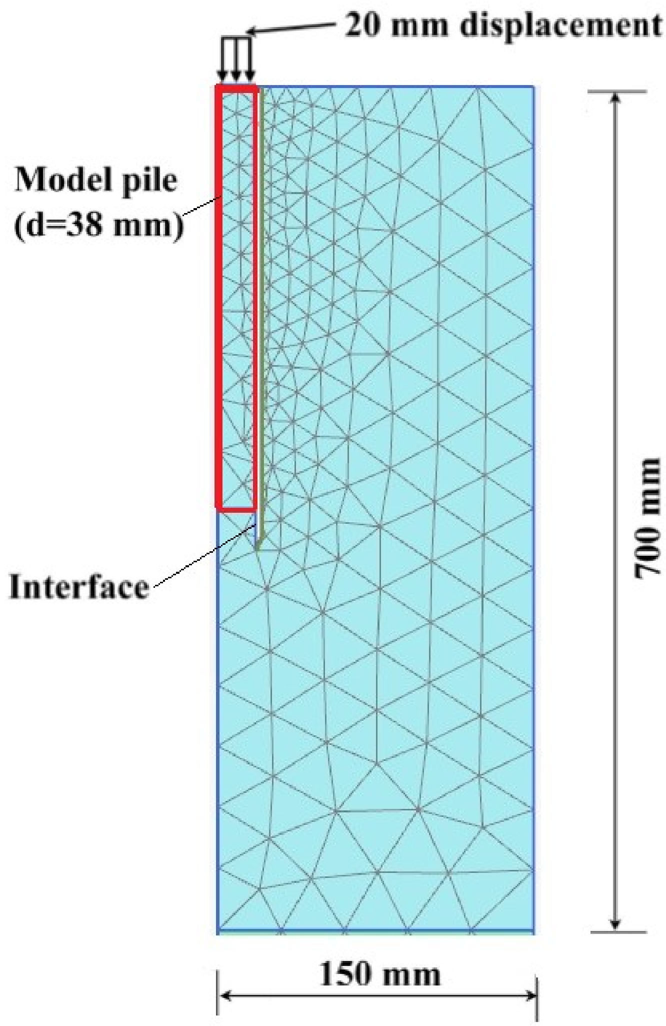

Figure 5.14. Numerical model setup (PLAXIS)

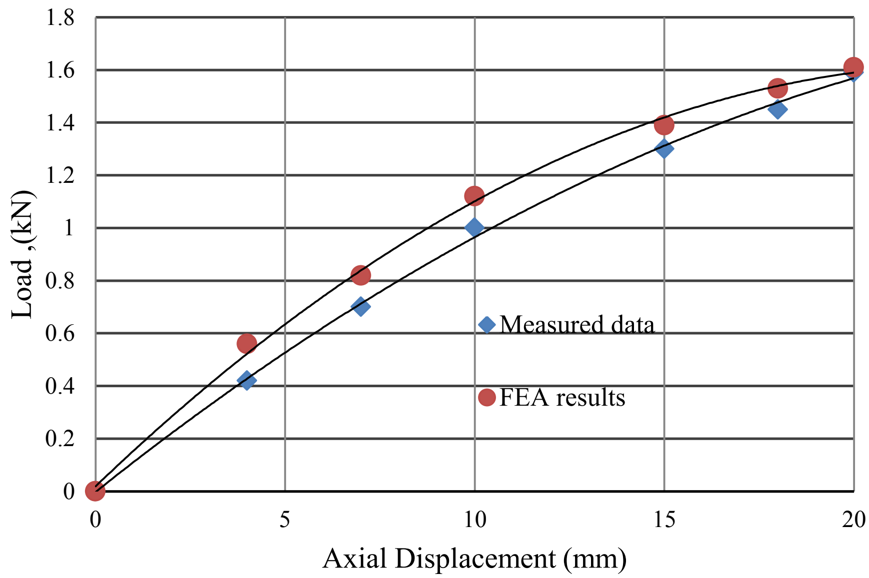

Figure 5.15. Measured and calculated results of load versus axial displacement of the model pile (PLAXIS)

5.3.1.2. Second validation (Thermo-Mechanical)

Tang et al. (2014) reported the effect of temperature change on the behaviour of a model scale pile in dry sand. The experimental setup is presented in Figure 5.16. The pile head was subjected to axial loads by dead weights. After the application of mechanical load, the pile was heated from 25°C to 50°C. Subsequently, the pile was cooled to 25°C. A numerical model is built by PLAXIS to simulate the behaviour of model pile subjected to a 200 N axial load with a heating–cooling cycle of (25°C → 50°C → 25°C) as shown in Figure 5.17. Simulations were made for the thermal effect on the pile head displacement and the results were compared with the measured values as shown in Figure 5.18.

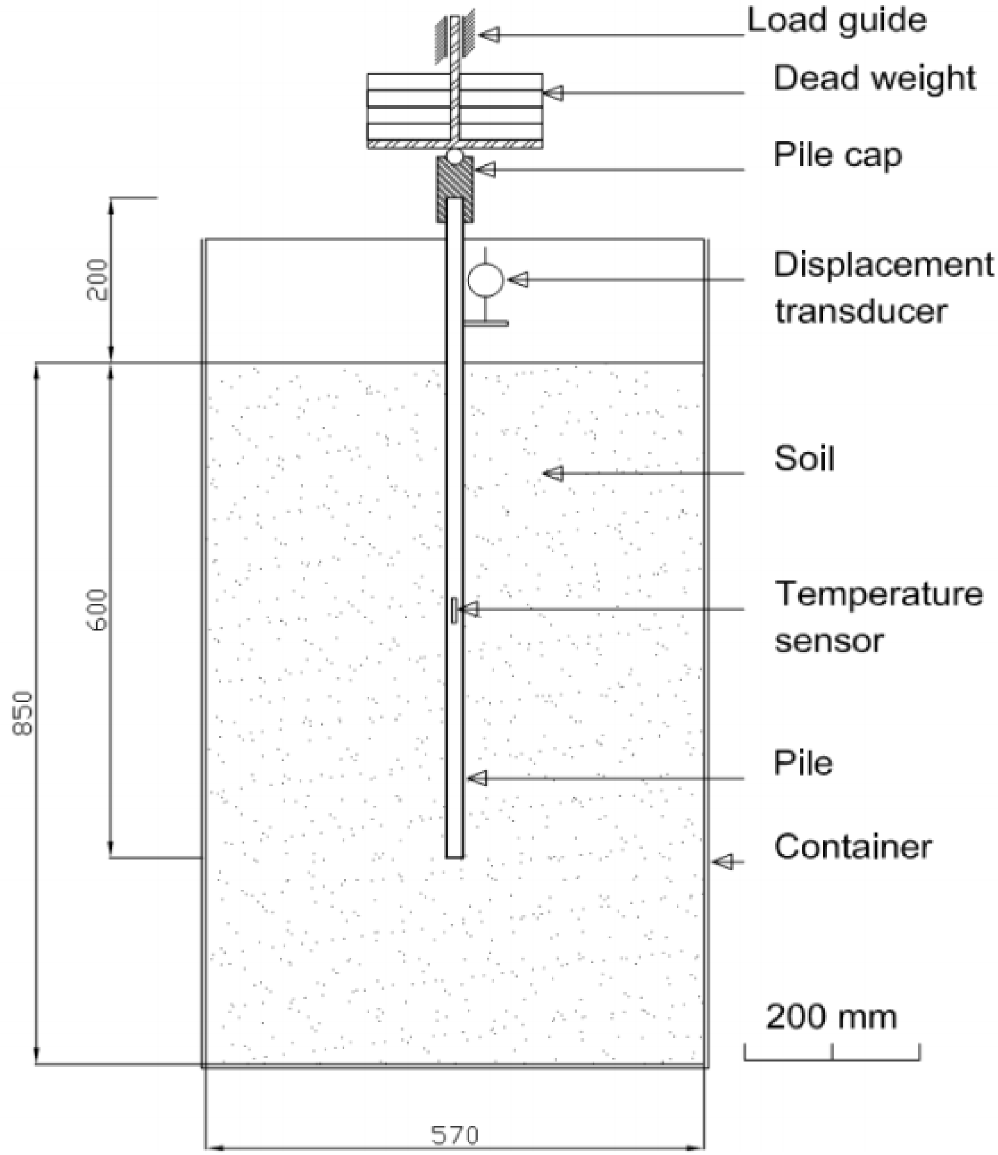

Figure 5.16. Experimental setup (After Tang et al. 2014)

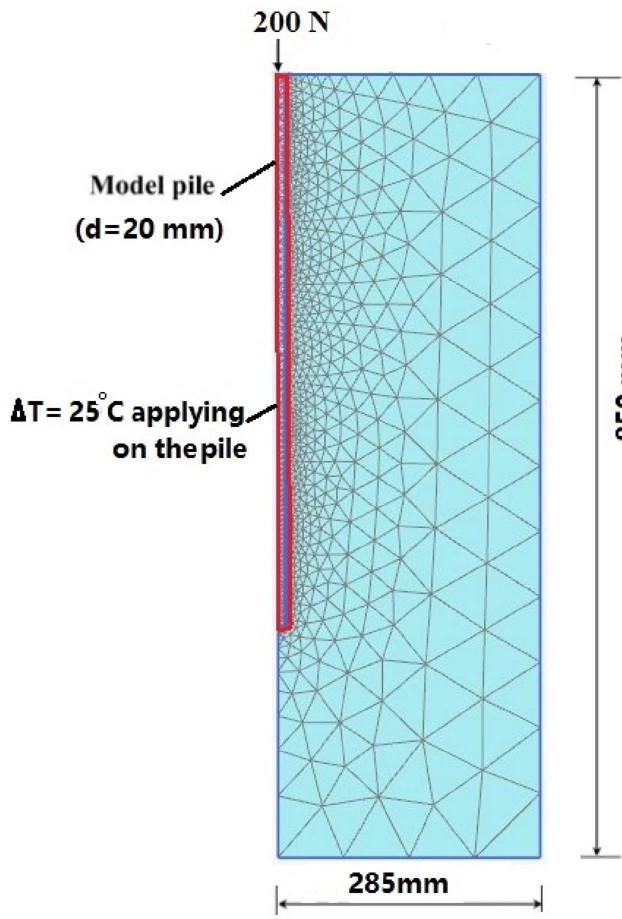

Figure 5.17. Schematics of pile–soil analysis domain (PLAXIS)

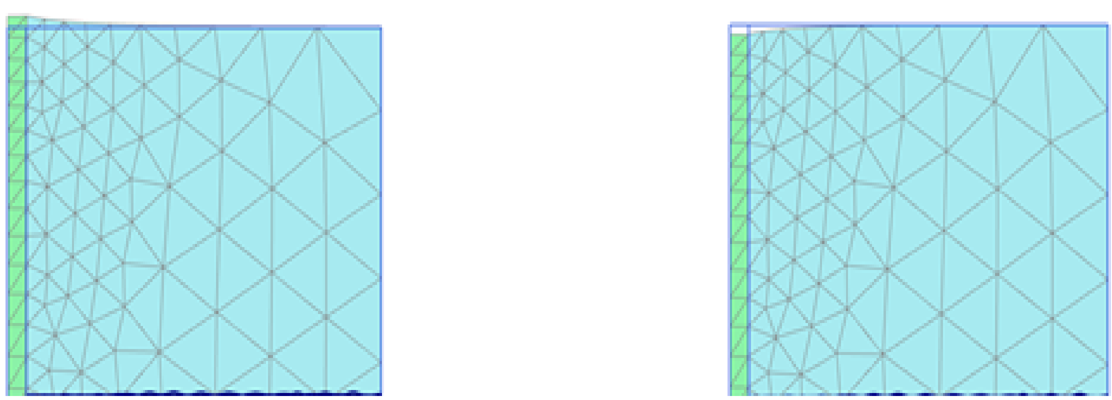

a) Pile expansion after heating

(Calculated uplift is 0.3 mm)
(Test is 0.33 mm (Tang et al. 2014))

b) Pile contraction after cooling

(Calculated settlement is 0.29mm)
(Test is 0.31mm (Tang et al.2014))

Figure 5.18. Deformation of pile during heating and cooling processes (PLAXIS)

5.3.1.3. Third validation (Thermo–Hydro-Mechanical coupling)

Laloui et al. (2006) published a paper entitled "Experimental and numerical investigations of the behaviour of a heat exchanger pile". The soil was fully saturated in this full scale field test. Laloui et al. (2006) carried out the thermal pile load tests in Lausanne, Switzerland for a 28 day duration of heating–cooling cycle (12 days of heating and then 16 days of cooling). The variation of the thermal load was in the order of $\Delta T = 15°C$ imposed in the pile. An axial load of 1300 kN was applied on the pile head. The test pile was drilled vertically in a layered soil deposit consisting of alluvial soils, sandy gravelly moraine and molasses.

A numerical model is set up by using PLAXIS to simulate the behaviour of the energy pile in thermal–hydro-mechanical processes in a 2-D analysis. An axisymmetric geometry is considered in the numerical analysis as shown in Figure 5.19. The length and radius of the pile were 25.2 m and 0.5 m, respectively. The elastic modulus of the pile is 29200 MPa. The density of the pile is 2500 kg/m^3.The elastic and thermal material properties for the pile and the soil layers have been taken from Laloui et al. (2006) and presented in Tables 5.8 and 5.9. The soil stress–strain response is simulated by the elastoplastic Mohr-Coulomb model. The pile stress–strain response is considered as a linear elastic model. The Figure 5.20 shows a comparison in the vertical stress generated in the pile due to thermo-mechanical loading when subjected to an axial load of 1300 kN and $\Delta T = 15°C$. The uplift of the pile head due to heating is calculated and the results are shown in Figure 5.21. The results of present calculations using PLAXIS are in close agreement with the field test data and the numerical simulation results from Laloui et al. (2006).

Table 5.8. Mechanical parameters of soil (from Laloui et al. 2006)

Soil layer	ρ (kg/m^3)	w (%)	n	k (m/s)	K (MPa)	G (MPa)	ϕ (°)	*c* (kPa)
Alluvial soils (A1)	2000	30	0.1	$2*10^{-6}$	122	113	30	5
Alluvial soils (A2)	1950	30	0.1	$7*10^{-7}$	122	113	27	3
Sandy gravelly moraine (B)	2000	30	0.35	$1*10^{-6}$	59	1000	23	6
Bottom moraine (C)	2200	17	0.3	$1*10^{-6}$	83	1400	27	20
Molasses (D)	2550				1900	1650		

Note: ρ - Density, w - Water content, n - Porosity, k - Permeability, K - Bulk Mod., G - Shear Mod., ϕ - Friction angle and *c*- Cohesion.

Table 5.9. Thermal parameters of soil and pile (from Laloui et al. 2006)

Soil layer	Heat capacity (J/m^3 °C)	Thermal conductivity (W/m / °C)
A1	1.8	2.4×10^6
A2	1.8	2.4×10^6
B	1.8	2.4×10^6
C	1.8	2.4×10^6
D	1.1	2.0×10^6
Pile	2.1	2.0×10^6

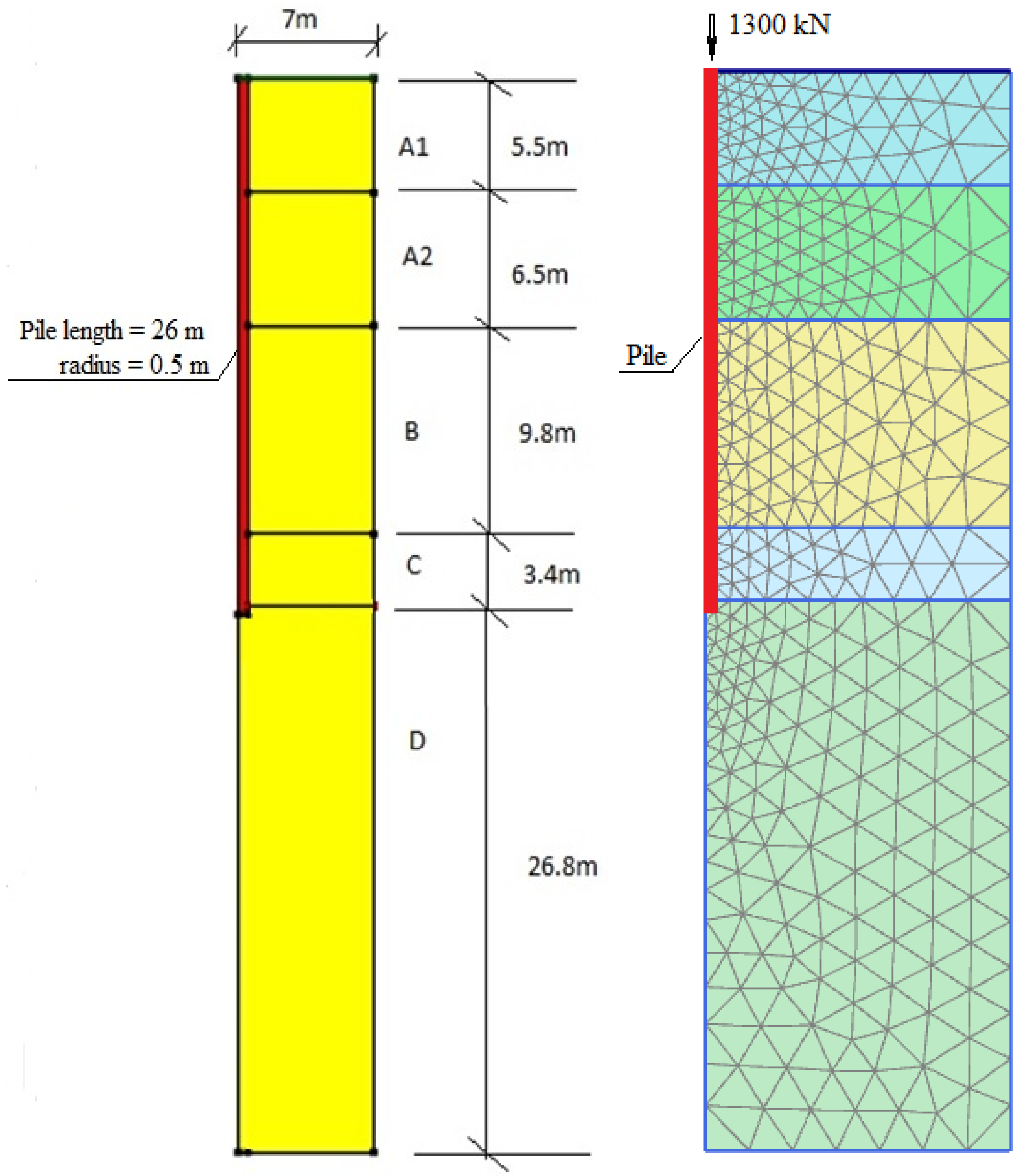

A1--------Alluvial Soil   A2-------- Alluvial Soil   B---------Sandy gravelly moraine

C---------Bottom moraine D---------Molasses

Figure 5.19. Schematics of solution region for validation (Dimensions are from Laloui et al. 2006)

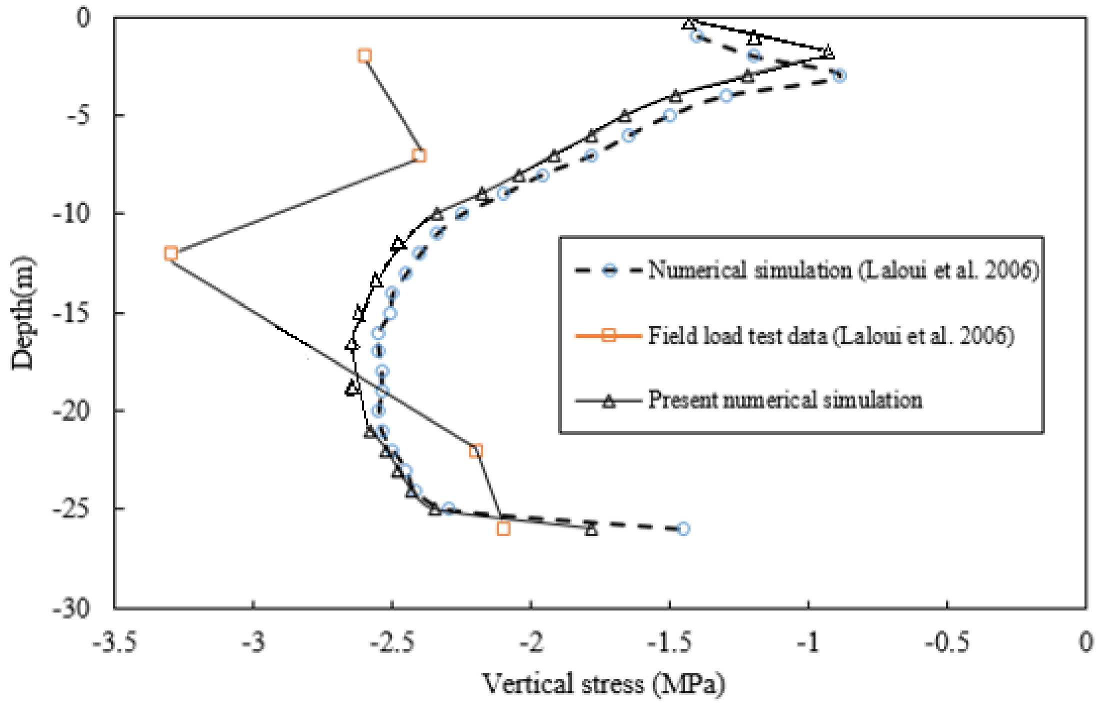

Figure 5.20. Vertical stresses in the pile at ΔT = 15°C (PLAXIS)

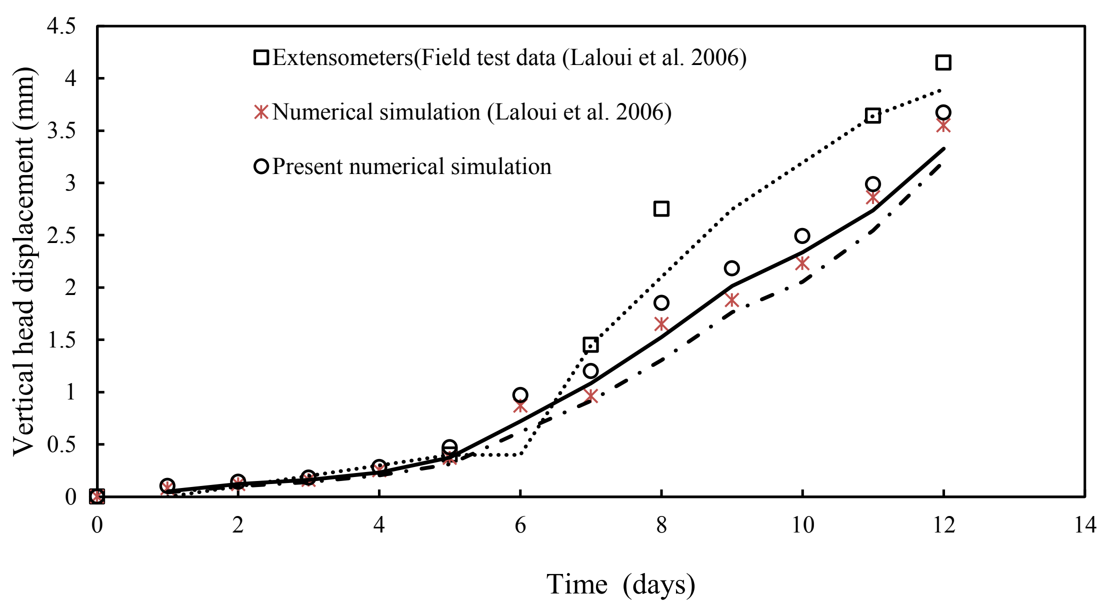

Figure 5.21. Thermal pile head uplift during the heating process (PLAXIS)

5.3.2. Analysis of an energy pile

The behaviour of a generic energy pile installed in the kaolin-sand mixture during thermal–hydro-mechanical processing is explored using PLAXIS 2D. The geometry of the pile and material parameters are same as those in section 5.1. Mechanical, hydraulic and thermal boundary conditions are followed the boundary conditions mentioned in section 5.1. The coupled thermo-hydro-mechanical analysis under saturated and unsaturated-conditions are conducted.

The distributions of temperature, degree of saturation, suction and heat flux in the analysis domain are mainly discussed in this section. Meanwhile, more numerical results by the fully-coupled method would be presented and compared with previous sequential analysis.

5.3.2.1. Saturation of soil

Figure 5.22 presents the distribution of the degree saturation in the soil mass after heating the pile to 21^{o}C. It can be seen that a significant change in the degree saturation takes place within a distance of 2.5 meters from the energy pile. Due to the increase in temperature, the degree of saturation in the soil near the pile shaft decreases sharply. For example, degree of saturation near the pile on the A-A section is reduced from its initial value 21.4% to 17.8% after heating. Most of the reduction in degree saturation occurs in the soil between r = 0 m and r = 2.5 m (here, the letter r is used for the horizontal distance measured from the soil - pile interface.). However, no significant variation of moisture content is observed beyond r = 2.5 m.

Figure 5.23 shows distribution of the degree saturation in the soil mass after the pile is cooled down to 21^{o}C. It can be noted that the degree of saturation increases near the pile due to moisture movement from high to low temperature in the soil. The change in degree of saturation has a major effect on the soil suction near the soil - pile interface.

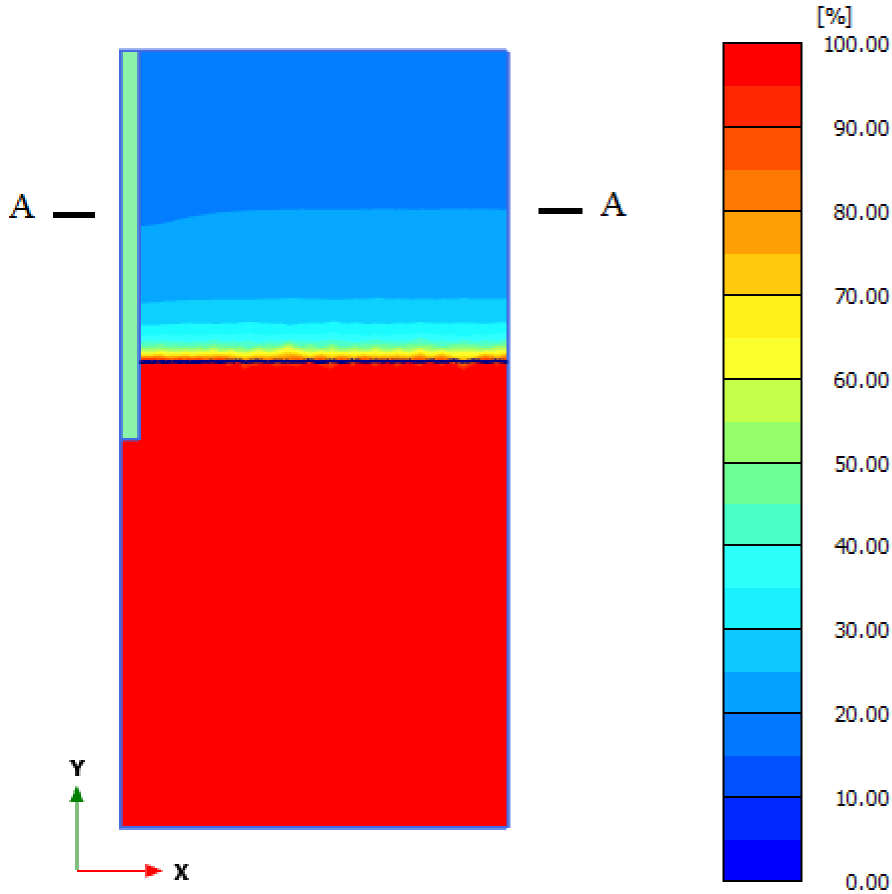

Figure 5.22. Distribution of degree of saturation in soil after heating the pile to 32^{o}C for 12 days (PLAXIS)

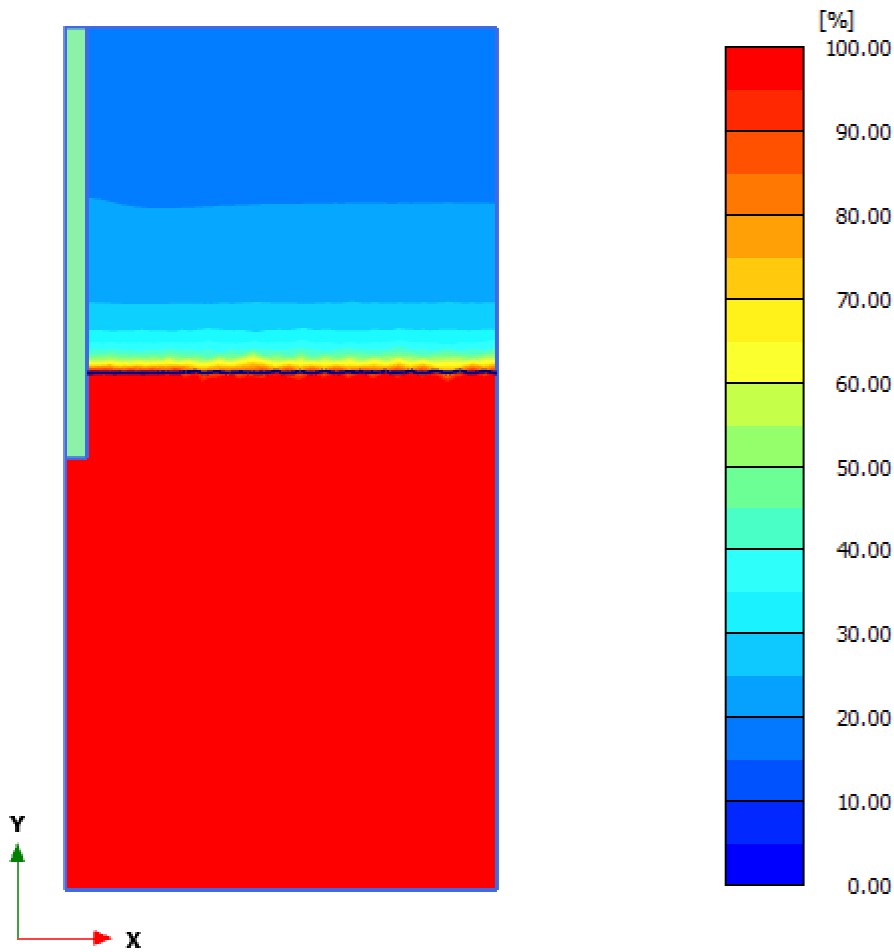

Figure 5.23. Distribution of degree of saturation in soil after cooling the pile to 11^{o}C for 16 days (PLAXIS)

5.3.2.2. Matric suction

Figures 5.24 and 5.25 indicate that suction distributions in the soil during the heating and cooling of the pile. During the heating process, the suction near the interface (r = 0 m) on section A-A in Figure 5.24 increases from an initial value of 50 kPa to 55 kPa, and smaller rise takes place in the soil at r = 2.5 m. Beyond r = 2.5 m there is no change in the suction. The developments of suction near the pile are reversed during the cooling process as shown in Figure 5.25.

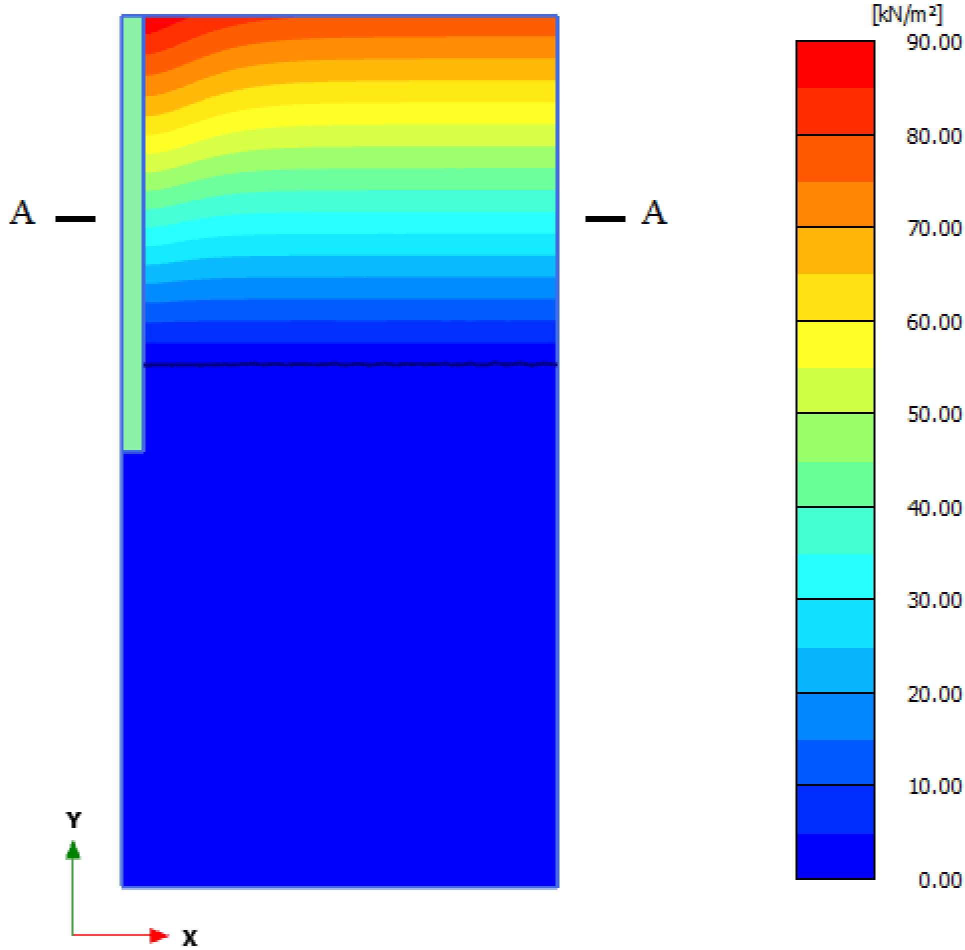

Figures 5.24. Suction distributions in soil after heating the pile to 32°C for 12 days (PLAXIS)

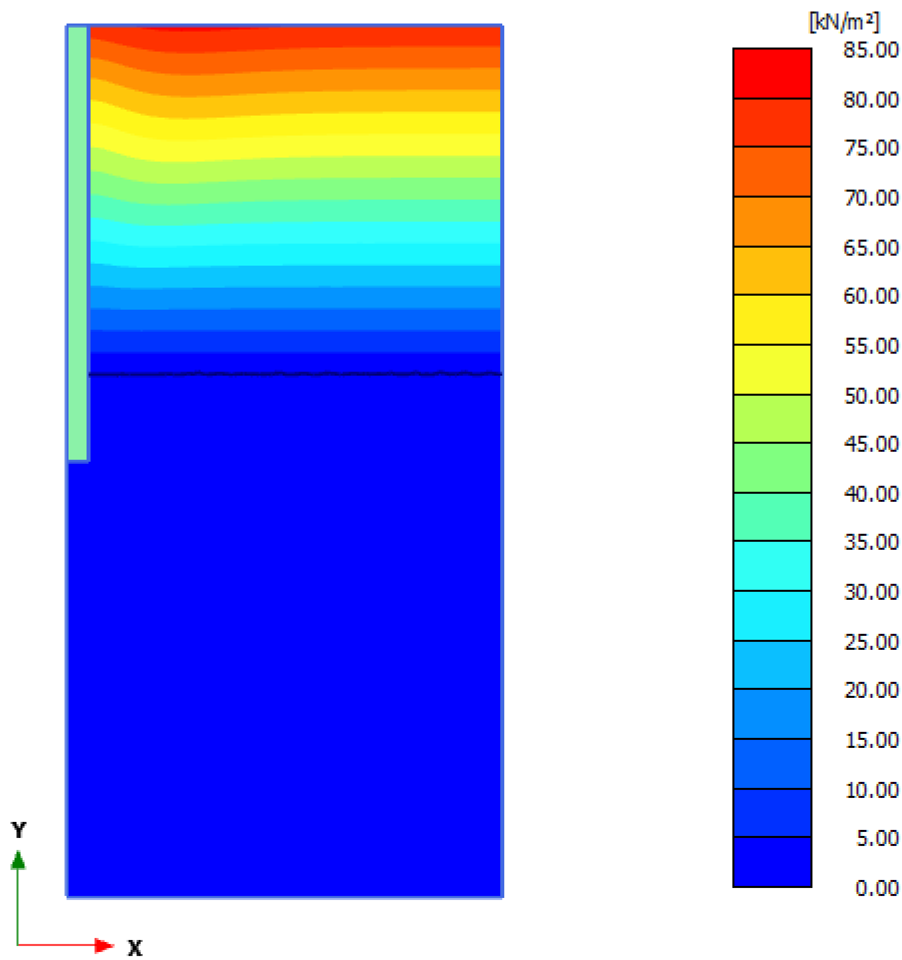

Figures 5.25. Suction distributions in soil after cooling the pile to 11°C for 16 days (PLAXIS)

The development of matric suction in the soil-pile interface along the pile shaft during a heating - cooling cycle is plotted in Figure 5. 26.

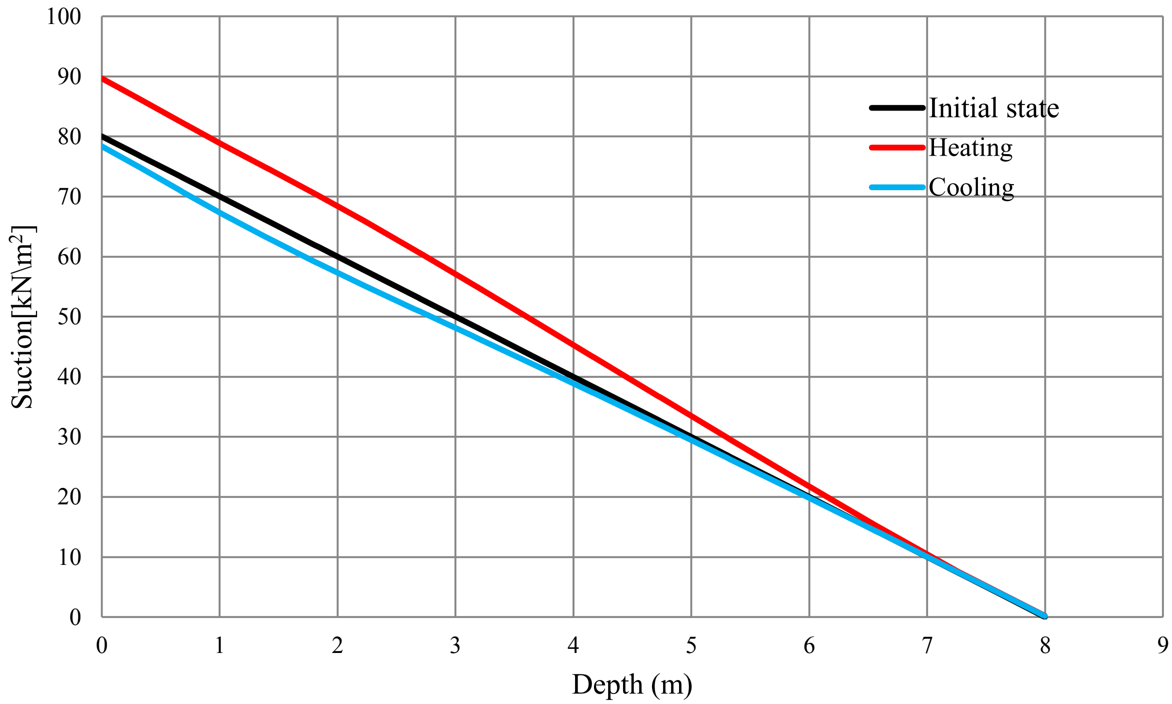

Figure 5.26. Matric suction in the soil along pile shaft during a heating-cooling cycle (PLAXIS)

5.3.2.3. Temperature distribution in the soil

Temperature distribution in the soil after 12 day heating indicates that the energy transferred into the soil mainly takes place within a zone extending 3 meters away from the energy pile during the heating period as shown in Figure 5.27.

Temperature distribution in the soil after 16 days of cooling indicates that pile extracts energy from the soil. This process mainly takes place within a zone 3 times the pile diameter away from the energy pile during a cooling period as shown in Figure 5.28.

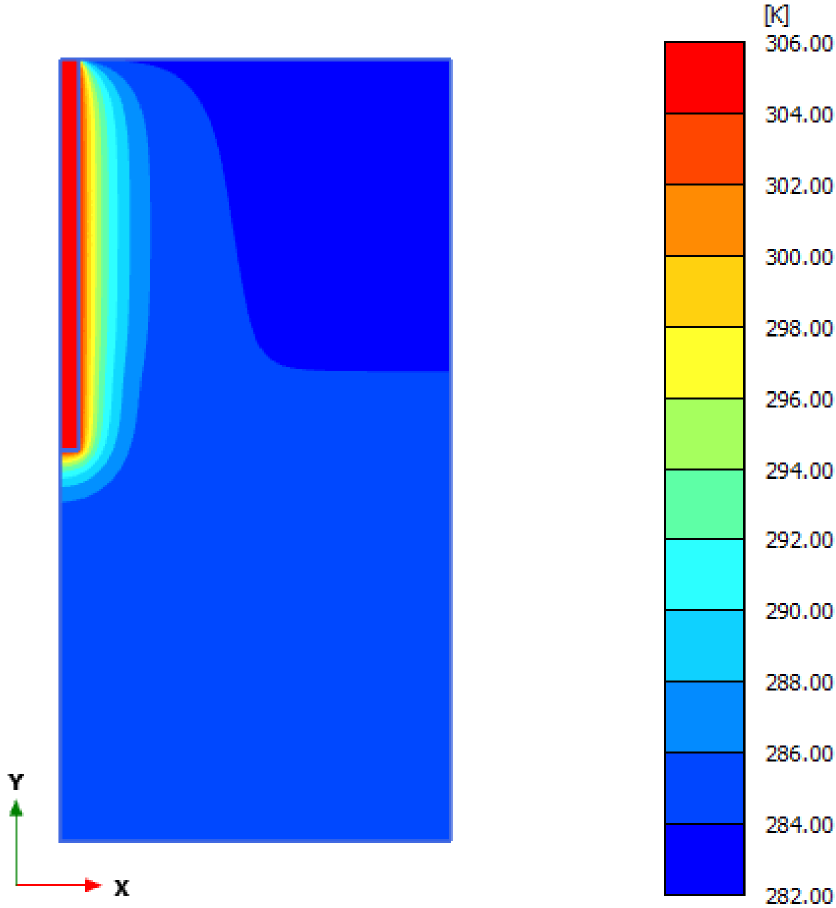

Figure 5.27. Temperature distributions in the soil after 12 days of heating (PLAXIS)

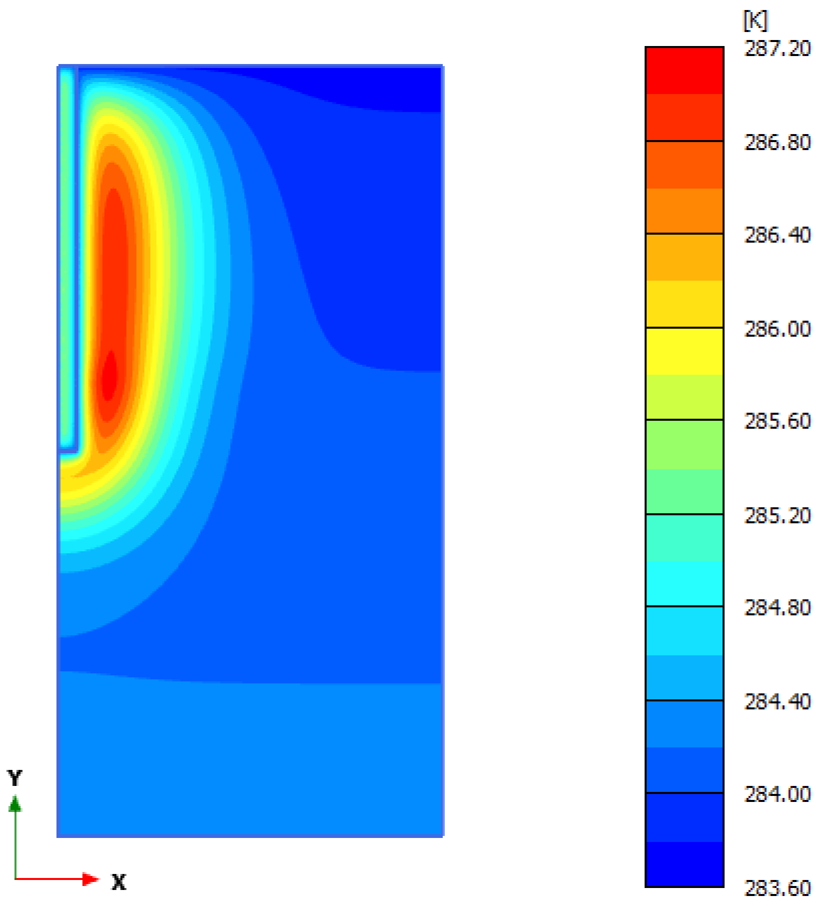

Figure 5.28. Temperature distributions in the soil after 16 days of cooling (PLAXIS)

5.3.2.4. Thermal effects on the bearing capacity of the energy pile

5.3.2.4.1. Saturated soil condition

Figures 5.29 to 5.31 show the load-displacement (p-δ) behaviour of the generic energy pile in fully saturated soil under different temperatures. In this section, the results of PLAXIS analysis are compared with the results of GeoStudio. It is noted that the predictions made by GeoStudio and PLAXIS for the bearing capacity of the generic energy pile were very close to each other. Although the results of PLAXIS were obtained from fully coupled analyses, they were not much different than the results obtained from the sequential analysis using GeoStudio software as can be seen in Figures 5.29, 5.30, and 5.31.

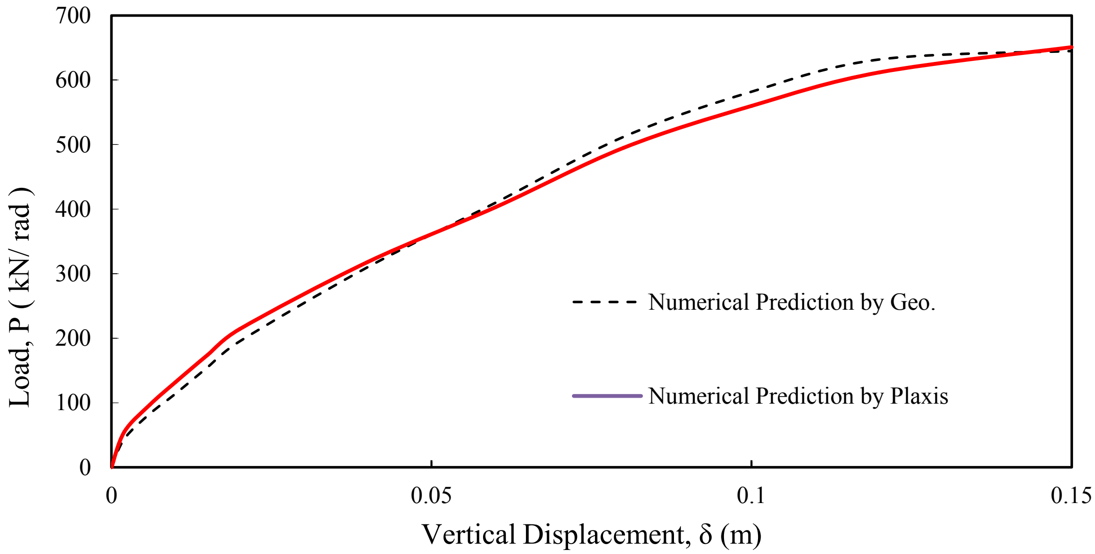

Figure 5.29. Bearing capacity of the pile versus vertical displacement of the pile head at 15^{o}C (GeoStudio and PLAXIS)

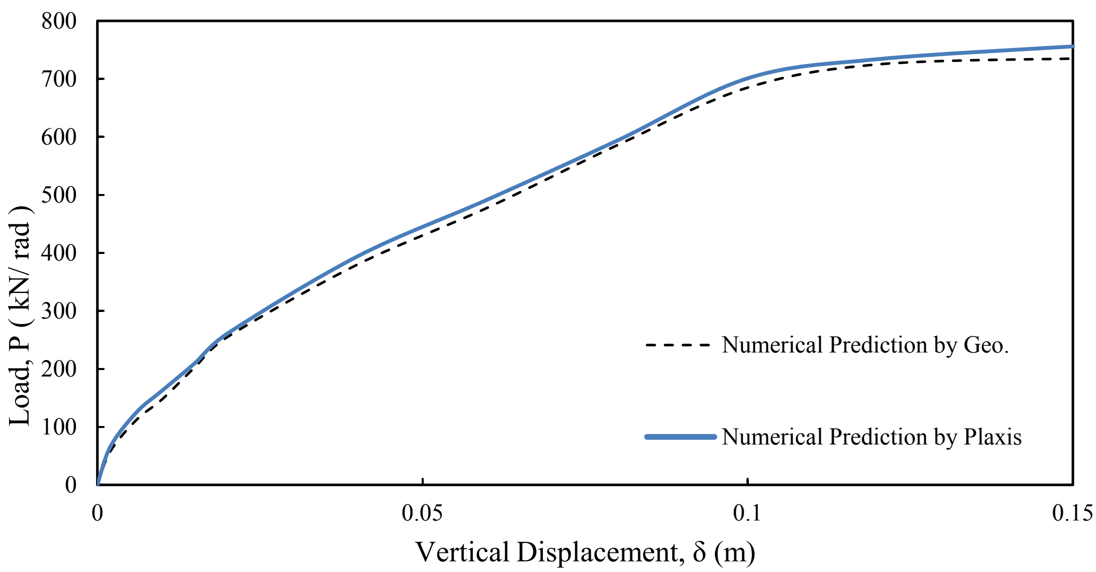

Figure 5.30. Bearing capacity of the pile versus vertical displacement of the pile head at 25^{o}C (GeoStudio and PLAXIS)

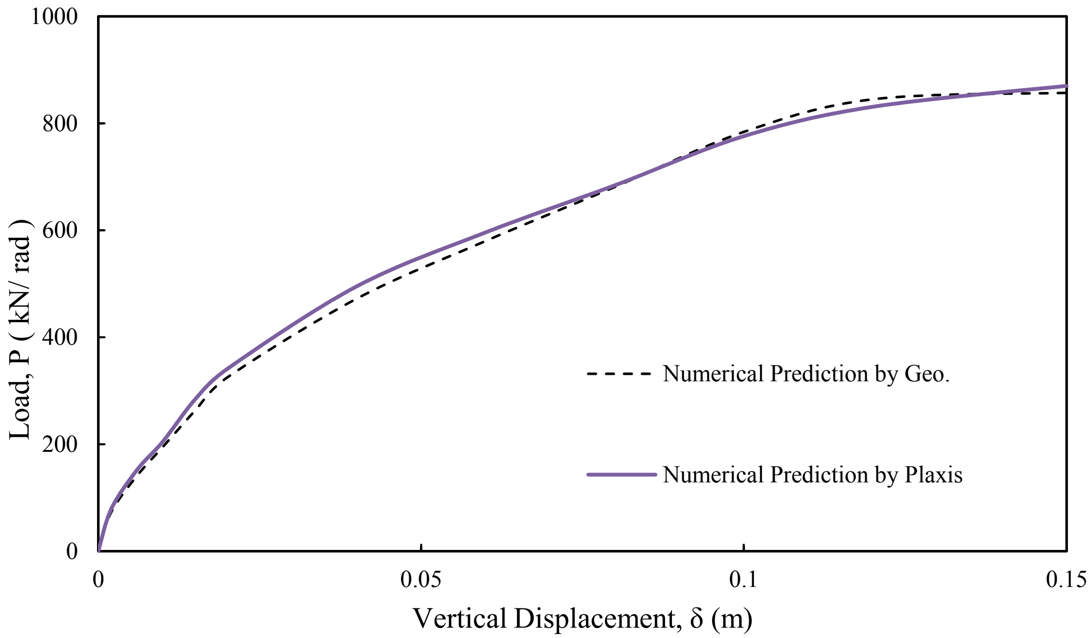

Figure 5.31. Bearing capacity of the pile versus vertical displacement of the pile head at 36^{o}C (GeoStudio and PLAXIS)

Figure 5.32 shows where the soil begins to fail at different points around the pile shaft and pile toe with increasing amount of vertical displacements at the pile head. These results were obtained when the pile temperature was 15^{o}C. It is noted that when the vertical displacement is 0.008 m, the soil-structure interface already failed near the upper part of the pile shaft. As the applied vertical displacement at the pile head is increased, failed points along the pile shaft spread downward. At about 0.036 m pile head displacement, the shaft resistance is fully developed. Toe resistance does not reach its maximum value until the pile head displacement is about 0.1 m. Although Figure 5.32 illustrates the gradual development of the bearing capacity of an energy pile, the magnitude of the shaft resistance and toe resistance of a pile would depend on many other factors such as the method of pile installation, short term and long term response of the soil and soil-structure interface, time dependent temperature variations, etc.

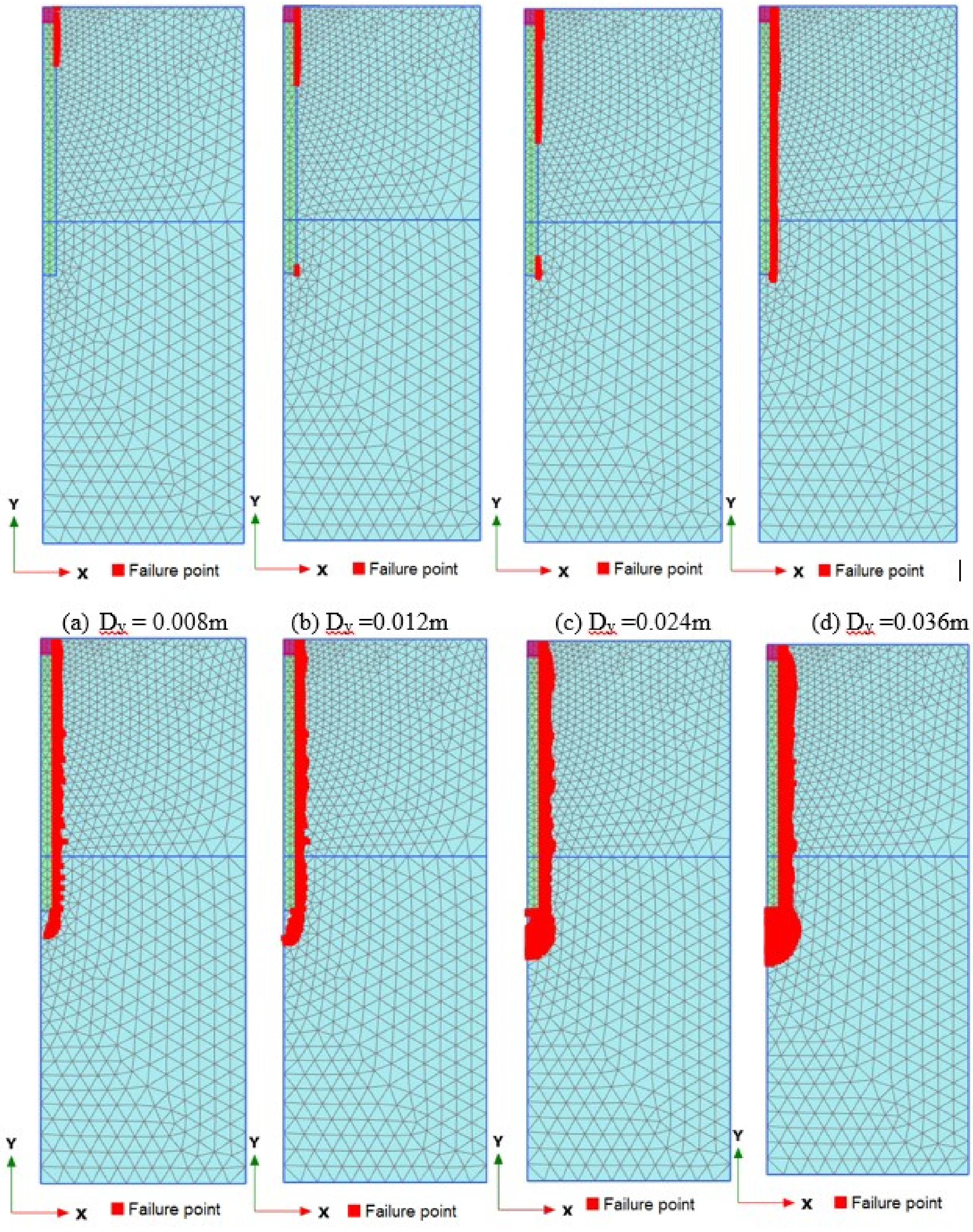

(a) $D_y = 0.008m$ (b) $D_y = 0.012m$ (c) $D_y = 0.024m$ (d) $D_y = 0.036m$

(e) $D_y = 0.05m$ (f) $D_y = 0.08m$ (g) $D_y = 0.10m$ (h) $D_y = 0.15m$

Figure 5.32. Developments of failure points in the soil around the pile with increments of vertical displacements (D_y) applied on pile head at 15°C (PLAXIS)

5.3.2.4.2. Unsaturated soil conditions

Figures 5.33 to 5.35 show the load-displacement (p-δ) behaviour of an energy pile installed partly in an unsaturated soil layer (groundwater level is 8 m below the ground surface, similar to the geometry shown in Figure 5.1) and the pile is at different temperatures in three separate analyses. These figures suggest that the bearing capacity of the pile increases with increasing temperature. Same trend is observed when the pile was in a fully saturated soil mass. However, the bearing capacity of the pile in a partly unsaturated soil mass has a greater value than that in fully saturated soil mass as shown in these figures. The increase in matric suction due to heating contributes to the increase in bearing capacity of the pile as discussed in Section 5.3.2.2.

The difference between the load-displacements curves is caused by the difference in the shaft resistance related to saturated and unsaturated soil conditions. As shown in Figure 5.32, maximum shaft resistance develops much before the mobilization of maximum toe resistance of the pile. Matric suction increases the shaft resistance. In addition, the modulus of elasticity of the soil in unsaturated conditions becomes larger than that of saturated soils. As a result of increase in elastic modulus, the slope of the load-displacement curve of the pile in unsaturated soils becomes steeper than that of pile in fully saturated soils. The differences between the response curves become smaller at large vertical displacements of the pile head. However, at working load conditions, the difference would be significant.

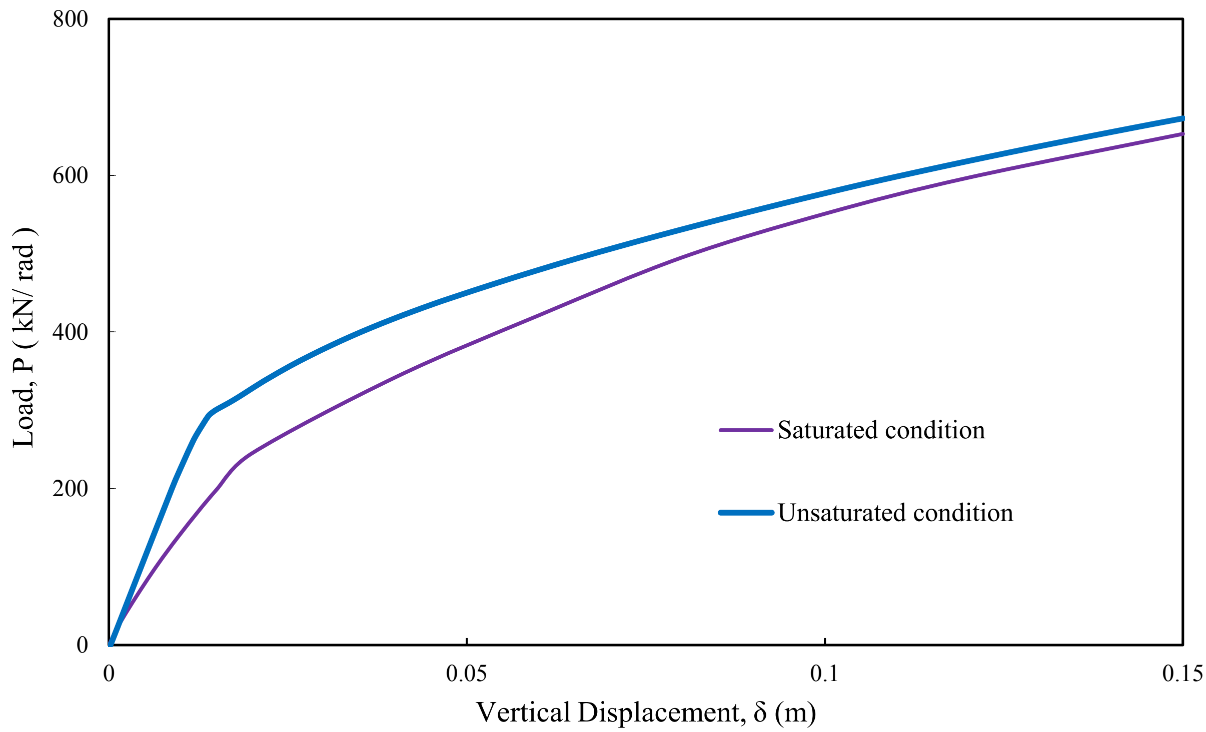

Figure 5.33. Bearing capacity of the pile versus vertical displacements of the pile head at 15^{o}C (PLAXIS)

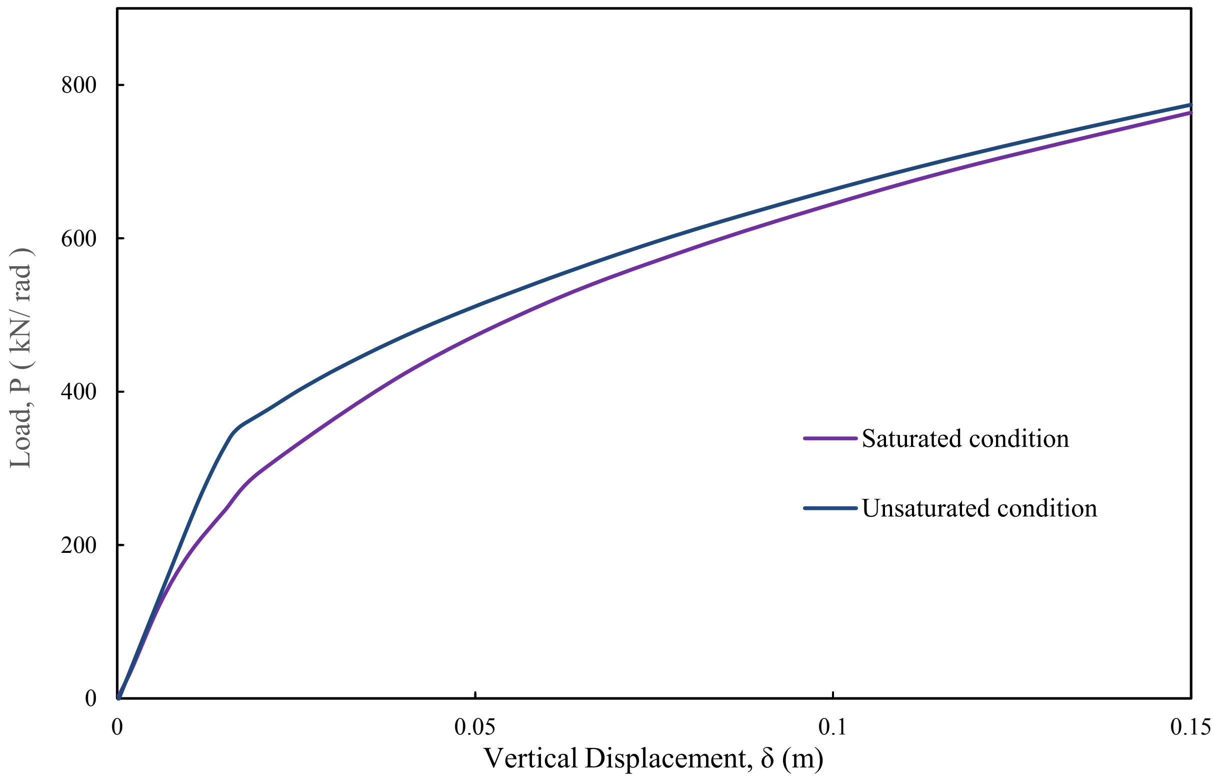

Figure 5.34. Bearing capacity of the pile versus vertical displacements of the pile head at 25°C (PLAXIS)

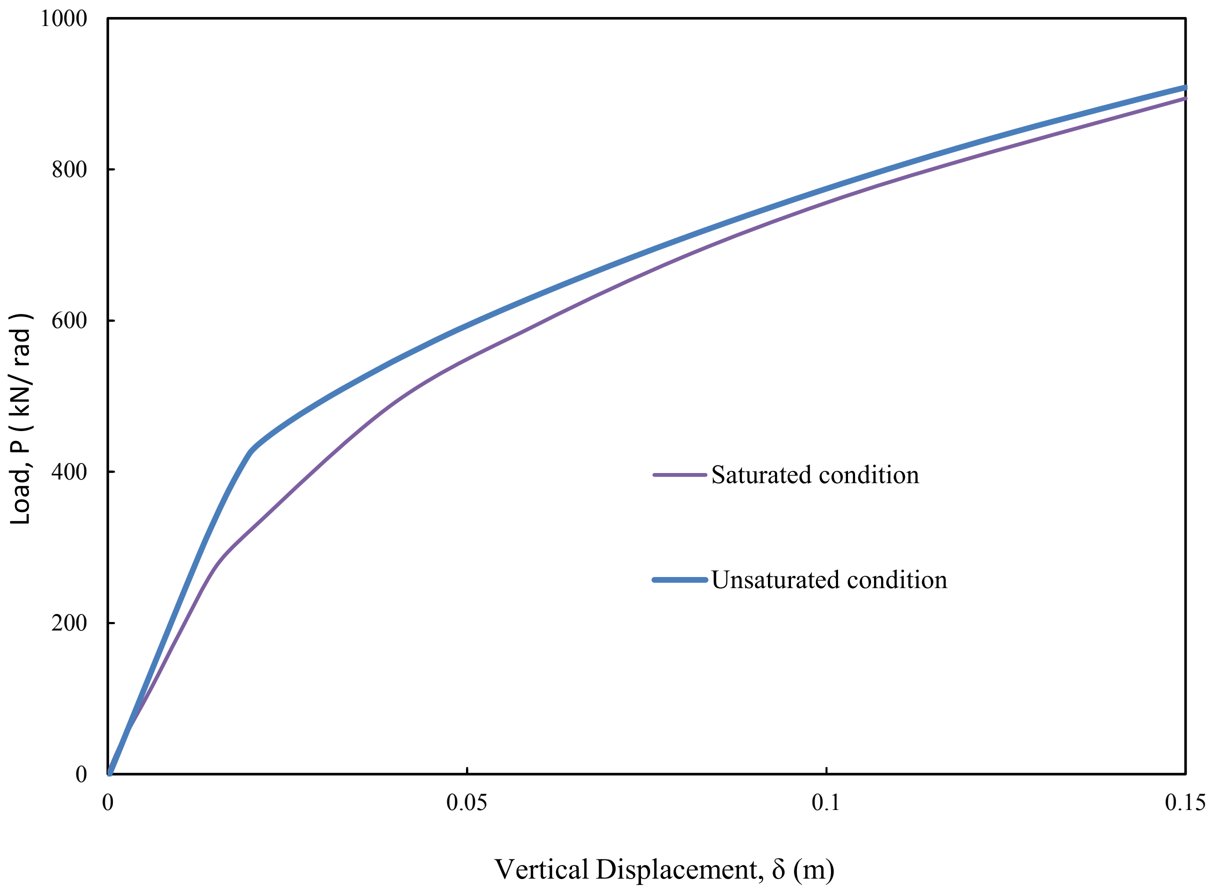

Figure 5.35. Bearing capacity of the pile versus vertical displacements of the pile head at 36^{o}C (PLAXIS)

5.3.2.5. Heat flux in the soil

One of the essential information required in the design of a group of energy piles is the heat flux that can take place in the soil around a single pile. The number of energy piles required for a building can be estimated by dividing the heating and cooling demands of the building with the amount of heat that can be transferred by a single pile. Of course, this number has to satisfy the settlement restrictions and mechanical load transfer ability of the building foundation. Figure 5.36 shows the heat flux in the horizontal direction along the section A-A (shown in Figure 5.24) after first day of heating. It can be seen that the energy transferred into the soil mainly takes place within a zone extending 3 meters away from the energy pile during heating for this short period of time. Meanwhile, the rate of energy transferred into the soil is higher in saturated condition than that in unsaturated condition as shown in the figure.

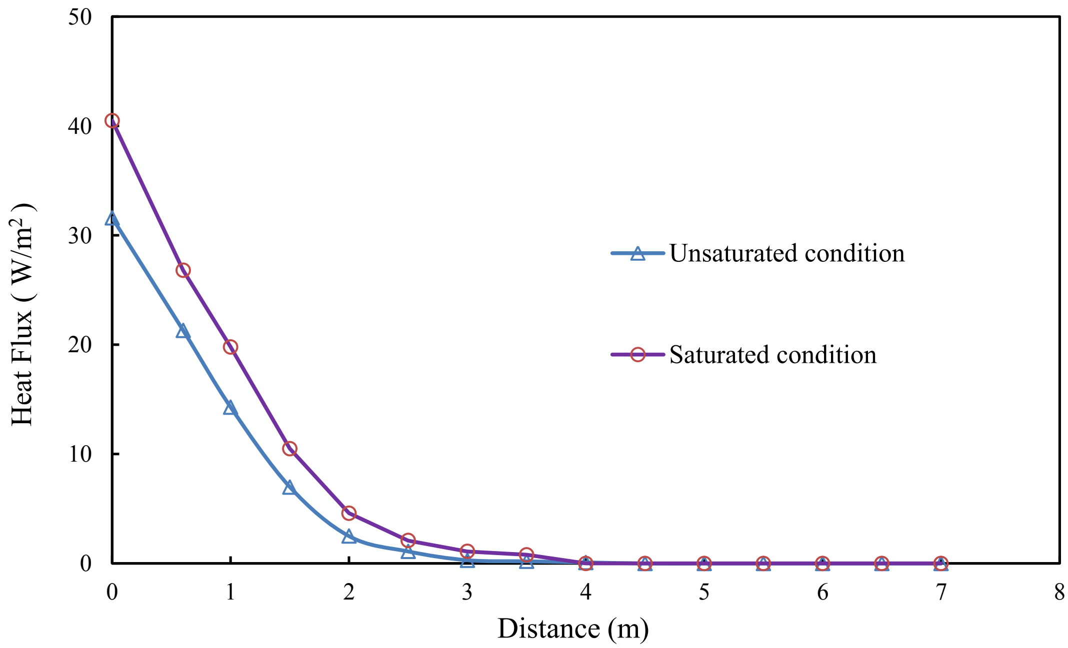

Figure 5.36. Heat flux distributions in the horizontal direction along section A-A (PLAXIS)

CHAPTER 6

SUMMARY AND CONCLUSIONS OF THE PRESENT STUDY

6.1 Summary and conclusions

In the following, a summary and the conclusions drawn from this investigation are provided.

1. The C3DSSI interface apparatus has been modified to investigate the behaviour of soil-pile interfaces under coupled thermo-hydro-mechanical loading conditions.

2. In the interface tests with normally consolidated soil samples with low degree saturation, the adhesion and the friction angle increased with the combined effects of changes in temperatures and matric suction. These results are in agreement with the test results published in the literature.

3. In the interface tests with overconsolidated soil samples at high degree saturation, both the adhesion and the friction angle decreased with the combined effects of changes in temperatures and matric suction.

4. The magnitude of the initial temperature, amount of temperature change, initial soil moisture content (i.e. soil suction), and the loading history (both mechanical and thermal) has a significant influence on the behaviour of an interface between a steel plate and unsaturated/saturated soils.

5. SIGMA/W and VADOSE finite element codes were used sequentially to analyze the effects of temperature, matric suction, and mechanical loading on the behaviour of soil-structure interfaces and the behaviour of energy piles.

6. A multi-physics finite element code (PLAXIS) is also used to simulate the coupled thermo-hydro-mechanical (THM) processes related to interface experiments and the energy piles.

7. A finite element model is developed for the simulation of a full-scale energy pile (Mimouni et al. 2013). The results of the numerical analysis of the present study were nearly identical to the results obtained in their analysis. However, the pile was installed in a fully saturated soil. Therefore, it was not possible to find out the influence of unsaturated soil conditions on the behaviour of an energy pile from this field test.

8. In order to investigate the effects of various influential factors (including the unsaturated soil conditions) on the behaviour of an energy pile, a series of finite element analyses were conducted using a 10 m long generic pile. The parameters required to describe the soil behaviour were taken from the experimental program (lab testing) of the present study.

9. The results of fully coupled and sequential FE analyses of the generic pile are compared. The fully coupled analysis was conducted by using PLAXIS. Sequential analysis used SIGMA/W and VADOSE codes. For the cases investigated, the results of the sequential analysis and the coupled analysis were very close.

10. PLAXIS is a well-known finite element code for the coupled hydro-mechanical analysis of geotechnical engineering problems. The extension of the capabilities of PLAXIS to the analysis of THM problems is relatively new. In order to investigate further the suitability of PLAXIS finite element code in simulating the behaviour of piles in unsaturated soils with and without the effect of temperature changes, two numerical simulations were conducted. One of these experiments was reported by Al-Khazaali et al. (2016) and the other one, where the model scale pile was subjected to heating, was reported by Tang et al (2014). The results of the numerical simulations conducted for these model scale piles in unsaturated soils were very close to the experimental data.

11. In unsaturated conditions, matric suction had a significant effect on the behaviour of the generic energy pile.

12. Axial strains and stresses in the generic energy pile are modified during THM processes. It would be necessary to look into the integrity of the pile itself when the changes in stresses are large.

13. Both the sequential and coupled finite element analyses provided heat flux values needed for the design of an energy pile system.

6.2 Major contributions

Concerning the thermal-hydro-mechanical effects on the unsaturated soil-structure interface, very few results exist in the literature. In the present investigation, laboratory studies and numerical analyses are carried out to evaluate the THM effect on the behaviour of interfaces between an energy pile material and an unsaturated soil. The major contributions of this research work are listed as follows:

A) In this study, the existing interface apparatus has been modified to investigate the behaviour of soil-pile interfaces under coupled thermo-mechanical testing conditions.

B) The thermal effects on shear strength parameters of unsaturated soil-structure interface were investigated. The experiments were conducted on soil samples with low degree of saturation and high degree of saturation. It was found that in interface tests using soil samples with low degree of saturation, the adhesion increased due to a positive effect of suction on strength than the negative effect of increasing temperatures. However, in interface tests on soil samples with high degree of saturation, the adhesion decreased with increasing temperatures while the effect of suction was not large enough to overcome the negative effect of temperature increase. This is a new finding that has not been reported anywhere in the literature. The friction angle for both soil samples (with different degrees of saturation) changed slightly with temperature change.

C) A fully-coupled thermo-hydro-mechanical finite element analyses conducted in the present study provided the following geotechnical information that would be useful for the design of energy piles: (a) Bearing capacity of the pile with and without the effect of temperature, (b) The effect of degree of saturation (or suction) on the strength and deformation characteristics of both the soil and the soil-structure interface, (c) Temperature effects on the amount of pile head movements (up or down), (d) Temperature induced stresses in the pile, (f) Amount of heat that can be stored or extracted from the ground as a function of time.

REFERENCES

Abdelaziz, S. L., Olgun, C. G., and Martin, J.R. 2011. Design and Operational Considerations of Geothermal Energy Piles. *Geo-Frontiers 2011 © ASCE 2011*. P450 - 460.

Abuel-Naga, H., Raouf, M. I.N., Raouf, A.M.I. and Nasser, A.G. 2015. Energy piles: current state of knowledge and design challenges. *Environmental Geotechnics*, August 2015 Issue EG4 Pages 195 – 210.

Al-Khazaali, M., Han, Z., and Vanapalli, S. K. 2016. Modelling the Load-Settlement Behavior of Model Piles in Unsaturated Sand and Glacial Till. *Geotechnical and Structural Engineering Congress*. P2075-2087.

Amatya, B. L., Soga, K., Bourne-Webb, P.J., Amis, T., and Laloui, L. 2012. Thermo-mechanical behaviour of energy piles. *Geotechnique* 62, No. 6, P503–519.

Amis, T., and Loveridge, F. 2014. Energy piles installed in the UK and Resultant annual CO_2 savings. *REHVA Journal*, January, P32-35.

Arson, C., Berns, E., Akrouch, G., Sanchez, M., and Briaud, J.L.2013. Heat propagation around geothermal piles and implications on energy balance, energy book series—volume # 1: materials and processes for energy: communicating current research and technological developments. In: Mendez-Vilas A (ed) Formatex Research Center, ISBN (13): 978-84-939843-7-3, P628–635 Bose, J.E.1991. Design and installations standards. International Ground Source Heat Pump Association, Stillwater. Pages 177.

Boënnec, O. 2009. Piling on the energy. Geodrilling Int 150 (2009): P25–28.

Bourne-Webb, P.J., Amatya, B.L., Soga, K., Amis, T., Davidson, C., and Payne, P. 2009. Energy pile test at Lambeth College, London: geotechnical and thermodynamic aspects of pile response to heat cycles. *Geotechnique* ,59(3): P237–248.

Bourne-Webb, P.J, Burlon, S., Javed, S., Kürten, S., and Loveridge, F. 2016. Analysis and design methods for energy Geostructures. *Renewable and Sustainable Energy Reviews,* 65, P402-419.

Brandl, H. 1998. Energy piles and diaphragm walls for heat transfer from and into the ground. *Deep Foundations on Bored and Auger Piles,* Van Impe & Haegeman, Eds. P37-60.

Brandl, H. 2006. Energy foundations and other thermo-active ground structures. *Geotechnique*, 56(2): P81-122.

Brooks, R., and Corey, A. 1964. Hydraulic properties of porous media. Hydrology Paper No. 3, Colorado State University, Fort Collins, CO., U.S.A.

Buckingham, E. 1907. Studies on the movement of soil moisture. U.S. Department of Agriculture Bureau of Soils, Bulletin 38.

Caulk, R., Ghazanfari, E., and McCartney, J.S.2016. Parameterization of a calibrated geothermal energy pile model. *Geomechanics for Energy and the Environment*, 5 (3): 1–15.

Cekerevac, C. and Laloui, L. 2004. Experimental study of thermal effects on the mechanical behaviour of clay. Int. J. *Numer.Analyt. Methods Geomech*.28, No. 3, P 209–228.

Chen, D., and McCartney, J.S. 2016. Calibration parameters for load transfer analysis of energy piles in uniform soils. ASCE International Journal of Geomechanics. 04016159-1-17. 10.1061/ (ASCE) GM.P1943-562

Chen, W.F., and Zhang, H. 1991. Structural plasticity: theory, problems and CAE software. Springer-Verlag.

Claesson, H., and Eskilson, P. 1988. Conductive heat extraction by a deep borehole: thermal analysis and dimensioning rules. *Energy,* 1988; 13:P509–27.

Côté, J., and Konrad, J. M. 2005. Thermal conductivity of base-course materials. *Canadian Geotechnical Journal*, 42(1), P61-78.

Curtis, R., Lund, J., Rybach, L., and Hellström, G.2005. Ground source heat pumps – geothermal energy for anyone, anywhere: current worldwide activity. *Proceedings World Geothermal Congress, Antalya, Turkey,* April 2005. P24-29.

DeJong, J.T., Randolph, M.F., and White, D.J. 2003. Interface load transfer degradation during cyclic loading: a mircoscale investigation. *Soils and Foundations*, Vol.43, No.4, P81-93.

Desai, C.S., Drumm, E.C., and Zaman, M.M.1985. Cyclic testing and modeling of interfaces. *Journal of geotechnical engineering*, Vol.111, No.6, P793-815.

Di Donna, A., Ferrari, A., and Laloui, L. 2016. Experimental investigations of the soil–concrete interface: physical mechanisms, cyclic mobilization, and behaviour at different temperatures. *Canadian Geotechnical Journal*, 53:P659-672.

Dupray, F., Laloui, L., and Kazangba, A. 2014.Numerical analysis of seasonal heat storage in an energy pile foundation. *Computers and Geotechnics,* 55(1), P67-77.

Energy Star. 2013. Overview of Geothermal Heat Pumps. Energy Star: A Joint Pro- gram of the U.S. Environmental Protection Agency and the U.S. Department of Energy. http://www.energystar.gov/index.cfm?c=geo heat.pr geo heat pumps.

Evgin, E., and Svec, O.J. 1988. Heat and moisture transfer characteristic of compacted Mackenzie silt. *Geotechnical Testing Journal*, 11: 92-99.

Fabrice, D., Bertrand, F., and Lyesse, L. 2013. Analysis of the FEBEX multi-barrier system including thermoplasticity of unsaturated bentonite. *International journal for numerical and analytical methods in geomechanics*, (2013); 37:P399–422.

Fabrice, D., Lyesse, L. and Albin, K. 2014. Numerical analysis of seasonal heat storage in an energy pile foundation. *Computers and Geotechnics*, 55 (2014) P67–77.

Fakharian, K., and Evgin, E. 1996. An automated apparatus for three-dimensional monotonic and cyclic testing of interfaces. *Geotechnical Testing Journal*, ASTM, Vol.19, P22-31.

Farouki, O. T. 1986. Thermal Properties of Soils. *Series on Rock and Soil Mechanics* Volume 11, Trans Tech Publications, Germany.

Francois, B., and Laloui, L. 2008. A constitutive model for unsaturated soils under non-isothermal conditions. *Int. J. Numer. Anal. Meth. Geomech*. 2008(32):P1955–1988

Fredlund, D. G., and Xing, A. 1994. Equations for the soil-water characteristic curve. *Canadian Geotechnical Journal*, 31(4): P521-532.

Fu, Z., Infante Sedano, J.A., and Evgin, E. 2013. Thermal loading applied on the interface testing apparatus. *GeoMontreal 2013*.

Ghasemi-Fare, O., and Basu, P. 2013. A practical heat transfer model for geothermal piles. *Energy Build*, 66:P470–479

GEO-SLOPE International, Ltd. 2012. Vadose-Zone Modeling with VADOSE/W 2012: An Engineering Methodology, 4th Edition.

Goode, J. C. III., and McCartney, J.S. 2015.Centrifuge Modeling of End-Restraint Effects in Energy Foundations. *ASCE Journal of Geotechnical and Geoenvironmental Engineering,* 141(8), 04015034-1-13.

Goode, J. C. III., Zhang, M., and McCartney, J.S. 2014. Centrifuge Modeling of Energy Foundations in sand. *Proc. 8th International Conference on Physical Modelling in Geotechnic,* P729-736.

Grant, S. A., and Salehzadeh, A. 1996. Calculations of temperature effects on wetting coefficients of porous solids and their capillary pressure functions. *Water Resources Res.* 32, (2), P261–279.

GSHP Association 2012 Thermal pile design, installation and materials standards. Ground Source Heat Pump Association, National Energy Centre, Davy Avenue, Knowlhill, Milton Keynes, MK5 8NG

Hamidi, A., Tourchi S., and Khazaei, C. 2014. Thermomechanical constitutive model for saturated clays based on critical state theory. *International Journal of Geomechanics,* 15(1), 04014038.

Hamdhan, I.N., and Clarke, B. G. 2010. Determination of Thermal Conductivity of Coarse and Fine Sand Soils. *Proceedings World Geothermal Congress 2010*

Houston, S. L., Dye, H. B., Lingnau, B., and Houston, W. N. 2015.Thermally-Induced Settlements for Heat Generating Structures on Unsaturated Soils. *Geotech Geol Eng* (2015) 33:P307–319

Jing, L. 2003. A review of techniques, advances and outstanding issues in numerical modeling for rock mechanics and rock engineering. *International Journal of Rock Mechanics & Mining Sciences* 40 (2003) P 283–353.

Johansen, O. 1975. Thermal conductivity of soils. Ph.D. thesis. CRREL Draft Translation 637, 1977, ADA 044002.

Kalantidou, A., Tang, M., Pereira, J., and Hassen, G. 2013. Preliminary study on the mechanical behavior of heat exchanger pile in physical model. *Geotechnique* 62(11):P1047–1051

Katzenbach, R., Clauss, F., and Waberseck, T. 2008. Coupled numerical simulation of geothermal energy systems. *In 12th International Conference of the International Association for Computer Methods and Advances in Geomechanics (IACMAG).* Curran Associates, Inc., Goa, India, 2008, P 1170–1179.

Knellwolf, C., Peron, H., and Laloui, L. 2011. Geotechnical analysis of heat exchanger piles. *Journal of Geotechnical and Geoenvironmental Engineering,* 137 (10):P890–902

Kramer, C.A., and Basu, P. 2014. Performance of a model geothermal pile in sand. *Proc. 8th International Conference on Physical Modelling in Geotechnics*.P771-777.

Kusuda, T., and Achenbach, P.R. 1965. Earth temperature and thermal diffusivity at selected stations in the United States. *ASHRAE Transactions*, 71 (1), P 61-75.

Laloui, L., Moreni M., and Vulliet, L. 2003. Comportement d'un pieu bi-fonction, fondation et e´changeur de chaleur. *Can Geotech J* 40(2):P388–402.

Laloui, L., Nuth M., and Vulliet, L. 2006. Experimental and numerical investigations of the behavior of a heat exchanger pile. *Int. J. Numer. Anal. Meth. Geomech,* 2006; 30:P763–781.

Laloui, L., and Di Donna, A. 2011. Understanding the thermo-mechanical behaviour of energy piles. *Civil Engineering,* 164, P184-191.

Leong, E. C., and Rahardjo, H. 1997. Review of soil-water characteristic curve equations. *Journal of Geotechnical and Geoenvironmental Engineering,* 123(12):1106-1117.

Lund, J.W., Freeston, D.H., and Boyd, T.L. 2011. Direct utilization of geothermal energy 2010 worldwide review. *Geothermic* 40, P159–180.

McCartney, J.S, Rosenberg, J.E., and Sultanova, A. 2010. Engineering performance of thermo-active foundation systems. In:Goss C.M., Kerrigan J.B., Malamo J., McCarron M.O., Wiltshire R.L. (eds) GeoTrends: *the Progress of Geological and Geotechnical Engineering* in Colorado at the Cusp of a New Decade (GPP 6), P27–42.

McCartney, J.S., and Rosenberg, J.E. 2011.Impact of Heat Exchange on Side Shear in Thermo-Active Foundations. *Geo-Frontiers 2011*(GSP 211), P488-498.

McCartney, J.S. 2011. Engineering performance of energy foundations. *2011 Pan-Am CGS Geotechnical Conference.*

McCartney, J.S., and Murphy, D.K. 2012. Strain distribution in full scale energy foundations. *DFI Journal - The Journal of the Deep Foundations Institute* 6(2):P26–38.

McCartney, J.S. 2012. Issues involved in using temperature to improve the mechanical behaviour of unsaturated soils. *5th Asia-Pacific Unsaturated Soils Conf.* Pattaya, Thailand.P509-514.

Mimouni, T. and Laloui, L. 2013. Full-scale in situ testing of energy piles. In: Laloui L., Di Donna A (eds) Energy Geostructures: *Innovations in underground engineering*. Wiley-ISTE P23–42.

Milly, P.C. 1982. Moisture and heat transport in hysteretic, inhomogeneous porous media: A matric head based formulation and a numerical model. *Water Resources Research*, 18(3).

Murphy, K. D., and McCartney, J.S. 2015. Seasonal response of energy foundations during building operation. *Geotechnical and Geological Engineering.* 33(2), P343–356.

Murphy, K. D., McCartney, J.S. and Henry, K.S. 2015. Thermo-mechanical response tests on energy foundations with different heat exchanger configurations. *Acta Geotechnical*.10 (2), P179-195.

Murphy, K. D., McCartney, J.S., and Henry, K.S. 2014. Impact of horizontal run-out length on the thermal response of full-scale energy foundations. 2014. *Geo-Congress 2014 GSP 234.*

Murphy, K. D., and McCartney, J.S. 2014. Thermal borehole shear device. *Geotechnical Testing Journal.* 37 (6), P1040-1055.

Ng, C.W.W., Shi C., Gunawan, A., Laloui, L., and Liu, H.L. 2015.Centrifuge modelling of heating effects on energy pile performance in saturated sand. *Canadian. Geotechnical Journal.* 52, P1045–1057.

Olgun, C.G., Ozudogru, T.Y., Abdelaziz, S. L., and Senol, A. 2014a. Long-term performance of heat exchanger piles. *Acta Geotechnica.* (10), P553–569.

Olgun, C.G., Ozudogru, T.Y. and Arson, C.F. 2014b.Thermo-mechanical radial expansion of heat exchanger piles and possible effects on contact pressures at pile–soil interface. *Geotechnique Letters* 4, P170–178.

Olgun, C.G. and McCartney, J. S. 2014. Outcomes from international workshop on thermoactive geotechnical systems for near-surface geothermal energy: from research to practice, *DFI Journal - The Journal of the Deep Foundations Institute*. 8(2), P59-73.

Omer, A.M. 2008. Ground-source heat pumps systems and applications. *Renewable and Sustainable Energy Reviews.* 12, P344–371.

Ouyang, Y., Soga, K. and Leung, Y.F. 2011. Numerical back-analysis of energy pile test at Lambeth College, London. *Geo-Frontiers 2011*.P440-449.

Rees, S. W., Adjali M. H., Zhou, Z., Davies M., and Thomas, H. R. 2000. Ground heat transfer effects on thermal performance of earth contact structures, *Renewable and Sustainable Energy Reviews.* 4, P213-265.

Romero, E., Gens, A., and Lloret, A. 2003. Suction effects on a compacted clay under non-isothermal conditions. *Geotechnique.* 53 (1), P65–81.

Romero, E., Gens, A., and Lloret, A. 2001. Temperature effects on the hydraulic behaviour of an unsaturated clay. *Geotechnical and Geological Engineering* .19(3), P311-332.

Roshani, P., and Sedano, J.I. 2016. Incorporating temperature effects in soil-water characteristic curves. *Indian Geotechnical Journal*. 46 (3), P309-318.

Rotta, Loria A.F., Gunawan, A., Shi, C., Laloui, L., and Ng, C.W.W. 2015. Numerical modelling of energy piles in saturated sand subjected to thermo-mechanical loads. *Geomechanics for Energy and the Environment.* Vol.1, P1–15.

Reuss, M., Beck M., and Muller J.P.1997. Design of seasonal thermal energy storage in the ground. *Solar Energy 1997*, Vol. 59, No. 4-6, P 247-257.

Rutqvist, J., Börgesson, L., Chijimatsu, M., Kobayashi, A., Nguyen, TS., Jing, L., Noorishad, J., and Tsang, CF. 2001. Thermo-hydro-mechanics of partially saturated geological media – Governing equations and formulation of four finite element models. *Int J Rock Mech Min Sci* 38:P105-127.

Saggu, R., and Chakraborty, T. 2015. Cyclic thermo-mechanical analysis of energy piles in sand. *Geotech Geol Eng (2015)* 33:P321–342.

Salager, S., El Youssoufi, M. S., and Saix, C. 2007. Influence of temperature on the water retention curve of soils. *In Experimental unsaturated soil mechanics (ed.T.Schanz).* vol.112, P251–258.

Salager, S., Francois, B., El Youssoufi, M.S., Laloui, L., and Saix, C. 2008. Experimental investigations of temperature and suction effects on compressibility and pre-consolidation pressure of a sandy silt. *Soils and Foundations*. Vol.48, No. 4,453-466.

She, H. Y., and Sleep, B. E. 1998. The effect of temperature on capillary pressure-saturation relationships for air-water and perchloroethylene-water systems. *Water Resources Res*. 34(10), P2587–2597.

Sillers, W. S., Fredlund, D. G., and Zakerzadeh, N. 2001. Mathematical attributes of some soil-water characteristic curve models. *In Proceeding of Unsaturated Soil Concepts and Their Application in Geotechnical Practice Conference,* Springer Netherlands, P243-283.

Singh, R.M., Bouazza, A., Wang, B., Haberfield, C.H., Baycan, S., and Carden, Y. 2015. Thermal and thermo-mechanical response of a geothermal energy pile, Proceedings World Geothermal Congress 2015, Melbourne, Australia, 19-25 April 2015.

Stewart, M.A., and McCartney, J.S. 2012. Strain distributions in centrifuge model energy foundations. *Proc., GeoCongress 2012*, P4376-4385.

Stewart, M.A., and McCartney, J.S. 2014. Centrifuge modeling of soil-structure interaction in energy foundations. ASCE *Journal of Geotechnical and Geoenvironmental Engineering.* 140(4), 04013044-1-11.

Suryatriyastuti, M.E., Mroueh, H., and Burlon, S. 2012.Understanding the temperature-induced mechanical behaviour of energy pile foundations. *Renewable and Sustainable Energy Reviews* 16, P3344–3354.

Tang, A.M., Kalantidou, A., Pereira, J.M., Hassen, G., and Yavari, N. 2014. Mechanical behaviour of energy piles in dry sand .*Geotechnical Engineering Journal of the SEAGS & AGSSEA* Vol. 45 No.3 September 2014 ISSN 0046-5828.

Tolooiyan, A., and Hemmingway, P. 2012. A preliminary study of the effect of groundwater flow on the thermal front created by borehole heat exchangers. *International Journal of Low-Carbon Technologies*. 2012, 0, P1–12.

Tsubakihara, Y., Kishida, H., and Nishiyama, T. 1993. Friction between cohesive soils and steel. *Soils and Foundations* Vol.33, No.2, P145–156

Uesugi, M., Kishida, H., and Tsubakihar, Y. 1989. Friction between sand and steel under repeated loading. *Soils and Foundations*. Vol.29, No.3, P127-137.

Uchaipichat, A., and Khalili, N. 2009. Experimental investigation of thermo-hydro-mechanical behaviour of an unsaturated silt. *Geotechnique*. 59(4), P339–353.

van Genuchten, M. T. 1980. A closed-form equation for predicting the hydraulic conductivity of unsaturated soils. *Soil Science Society of America Journal*. 44(5): 892898.

Vanapalli S.K., Fredlund D.G. 2000. Comparison of different procedures to predict unsaturated soil shear strength. *Proc. the Conf. on Advances in Unsaturated Geotechnics Geo-Denver*, P195-209.

Vanapalli S.K., and Taylan Z. 2012. Design of single piles using the mechanics of unsaturated soils. *International Journal of GEOMATE* Vol. 2, No.1, P 197-204

Villar, M.V., and Gómez-Espina, R. 2009. Report on thermo-hydro-mechanical laboratory tests performed by CIEMAT on Febex Bentonite 2004-2008. ENRESA, 2009. Wang, B., Bouazza, A., Singh, R., Haberfield, C., Barry-Macaulay, D., and Baycan, S. 2014. Post temperature effects on shaft capacity of a full-scale geothermal energy pile. *Journal of Geotechnical and Geoenvironmental Engineering*. ISSN 1090-0241/04014125

Wang, B., Bouazza, A., Barry-Macaulay, D., Singh, R., Webster, M., Haberfield, C., Chapman, G., and Baycan, S. 2012. Field and laboratory investigation of a heat exchanger pile. *GeoCongress 2012*. P4396-4405.

Wang, B., Bouazza, A., and Haberfield, C. 2011. Preliminary observations from laboratory scale model geothermal pile subjected to thermo-mechanical loading. *Geo-Frontiers 2011*. P430-439.

Wang, W., Regueiro, R.A., and McCartney, J.S. 2014.Coupled thermo-poro-mechanical finite element analysis of an energy foundation centrifuge experiment in partially saturated silt. *Geo-Congress 2014*, GSP 234: P 2675-2684.

Williams, P.J. 1982. The surface of the Earth, an introduction to geotechnical science. Longman Inc., New York.

Wilson, G.W. 1980. Soil evaporative fluxes for geotechnical engineering problems. Ph.D. Thesis, University of Saskatchewan, Saskatoon, Canada.

Wu, W., Li, X., Charlier, R., and Collin, F. 2004. A thermo-hydro-mechanical constitutive model and its numerical modelling for unsaturated soils. *Computers and Geotechnics.* 31(2), P155-167.

Xiao, S., Suleiman, M.T. and McCartney, J. S. 2014. Shear behavior of silty soil and soil-structure interface under temperature effects. *Geo-Congress 2014*, P4105-4114.

Yavari, N., Tang, A.M., Pereira, J-M., and Hassen, G. 2016. Effect of temperature on the shear strength of soils and the soil-structure interface. *Canadian Geotechnical Journal.* **53**, P1-9.

Yavari, N., Tang, A.M., Pereira, J-M., and Hassen, G. 2014. Experimental study on the mechanical behaviour of a heat exchanger pile using physical modelling. *Acta Geotechnica*. 9, P385–398.

APPENDIX A

FORMULATION OF THM PROCESSES IN PLAXIS

All information provided below is taken from PLAXIS Manual. The independent variables are displacements (v), pore water pressure (p_w) and temperature (T).

Non isothermal unsaturated water flow

An extended Richards' equation is used to describe non isothermal unsaturated water flow. The mass flux of water J_w is defined as:

$$J_w = \rho_w \left(\frac{k_{rel}}{\mu} \kappa_{int} (\nabla p_w + \rho_w g) \right) \qquad A.1$$

where μ is the dynamic viscosity of the fluid and κ_{int} is the intrinsic permeability of the porous medium. The relative permeability k_{rel} is defined as the ratio of the permeability at a given saturation to the permeability in saturated state.

The mass flux of vapour is formulated similar to Rutqvist et al. (2001) as shown below.

$$J_v = -D_v \nabla \rho_v = D_{\rho v} \nabla p_w - D_{Tv} \nabla T \qquad A.2$$

where T is temperature in Kelvin. D_v is the vapour diffusion coefficient in a porous media. Its value depends on temperature, tortuosity of the medium and gas pressure. $D_{\rho v}$ and D_{Tv} are hydraulic and thermal diffusion coefficients.

$$D_{\rho v} = D_v \left(\frac{\partial \rho_v}{\partial p_v} \right) = \frac{D_v \, \rho_v}{\rho_w \, RT}$$

$$D_{Tv} = f_{Tv} D_v \left(\frac{\partial \rho_{vS}}{\partial T} \right) = f_{Tv} \, D_v \left(\theta \frac{\partial \rho_{vS}}{\partial T} + \frac{\rho_v p_w}{\rho_w \, RT^2} \right)$$

f_{Tv} is the thermal diffusion enhancement factor. ρ_w is the vapour density and ρ_{vS} is the saturated vapour density. θ is the relative humidity which is defined as:

$$\theta = \exp\left(\frac{-p_w}{\rho_w RT}\right)$$

where R is the specific gas constant for water vapour. The vapour density is related to the temperature dependent saturated vapour density (Rutqvist et al. 2001) as shown below.

$$\rho_v = \theta\rho_{vS}$$

The saturated vapour density is a function of temperature only. PLAXIS uses the following relation developed by Wang et al. (2009).

$$\rho_{vS} = 10^{-3}\exp\left(19.891 - \frac{4974}{T}\right)$$

The unit of ρ_{vS} is kg/m^3 and T is in Kelvin.

Mass Balance Equation

The water mass balance equation is the same as in the publication by Rutqvist et al. (2001).

$$n\frac{\partial}{\partial t}(S\rho_w + (1-S)\rho_v) + (S\rho_w + (1-S)\rho_v)\left[\frac{\partial \varepsilon_v}{\partial t} + \frac{1-n}{\rho_s}\frac{\partial \rho_s}{\partial t}\right] = -\nabla.(J_w + J_v) \qquad \text{A.3}$$

The first term in the above equation is expended as follows:

$$n\frac{\partial}{\partial t}(S\rho_w + (1-S)\rho_v) = n\frac{\partial S}{\partial t}\rho_w + nS\frac{\partial \rho_w}{\partial t} - n\frac{\partial S}{\partial t}\rho_v + n(1-S)\frac{\partial \rho_v}{\partial t}$$

$$= n\left(\frac{\partial S}{\partial p_w}\frac{\partial p_w}{\partial t} + \frac{\partial S}{\partial T}\frac{\partial T}{\partial t}\right)\rho_w + nS\left(-\rho_w\beta_{wP}\frac{\partial p_w}{\partial t} - \rho_w\beta_{wT}\frac{\partial T}{\partial t}\right)$$
$$- n\left(\frac{\partial S}{\partial p_w}\frac{\partial p_w}{\partial t} + \frac{\partial S}{\partial T}\frac{\partial T}{\partial t}\right)\rho_v$$

$$+n(1-S)\rho_w\left[\frac{\rho_v}{\rho_w^2 R_v T}\frac{\partial p_w}{\partial t} + \left(\frac{\theta}{\rho_w}\frac{\partial \rho_{vS}}{\partial T} + \frac{\rho_v p_w}{\rho_w^2 R_v T^2}\right)\frac{\partial T}{\partial t}\right] \qquad \text{A.4}$$

In the equation above, β_{wP} and β_{wT} are the compressibility and volumetric thermal expansion of water. The volumetric thermal expansion of water at 293.15 K is 2.1x10^{-4}. The water density is calculated by using the following equation where water pressure and temperature are used as influencing factors.

$$\frac{\rho_w}{\rho_{w0}} = 1 - \beta_{wP}(p_w - p_{w0}) - \beta_{wT}(T - T_0)$$

The second term of the left-hand side of Eq.A.3 is expanded as:

$$(S\rho_w + (1-S)\rho_v)\left[\frac{\partial \varepsilon_v}{\partial t} + \frac{1-n}{\rho_s}\frac{\partial \rho_s}{\partial t}\right] = (S\rho_w + (1-S)\rho_v)\left[\frac{\partial \varepsilon_v}{\partial t} - (1-n)\beta_{sT}\frac{\partial T}{\partial t}\right]$$

$$(S\rho_w + (1-S)\rho_v)\frac{\partial \varepsilon_v}{\partial t} - (S\rho_w + (1-S)\rho_v)(1-n)\beta_{sT}\frac{\partial T}{\partial t} \qquad \text{A.5}$$

where β_{sT} is the volumetric thermal expansion of soil grains. By substituting Eq. A.5 and Eq. A.4 into Eq. A.3, the water mass balance can be written as:

$$\left[n(\rho_w - \rho_v)\frac{\partial S}{\partial p_w} - nS\rho_w\beta_{wp0} - n(1-S)\frac{\rho_v}{\rho_w R_v T}\right]\frac{\partial p_w}{\partial t}$$

$$+\left[n(\rho_w - \rho_v)\frac{\partial S}{\partial T} - nS\rho_w\beta_{wT0} - n(1-S)\left(\theta\frac{\partial \rho_{vs}}{\partial T} + \frac{\rho_v p_w}{\rho_w R_v T^2}\right) - (S\rho_w + (1-S)\rho_v)(1-n)\beta_{sT}\right]\frac{\partial T}{\partial t}$$

$$+ (S\rho_w + (1-S)\rho_v)\frac{\partial \varepsilon_v}{\partial t} + \nabla.(J_w + J_v) = 0 \qquad \text{A.6}$$

The term $(1-S)\rho_v$ is neglected for saturated states of soils.

Non-isothermal deformation

For representative volumetric element of soil, the linear momentum balance equation is

$$\nabla . \sigma + \rho g = 0$$

where σ is the total stress and g is the vector of acceleration of gravity.

The density of the multiphase medium is calculated from:

$$\rho = (1 - n) \rho_s + nS \rho_w + n(1 - S) \rho_g$$

ρ_s, ρ_w and ρ_g are the densities of solids, water and gas.

For unsaturated soils, the total stress is written in the following form:

$$\boldsymbol{\sigma} = \boldsymbol{\sigma}' + Pm$$

where m is the identity tensor, σ' is the effective stress and P is the average pore pressure. P is a function of pore water pressure, pore gas pressure, the degree of saturation of water and the degree of saturation of gas as given by the following equation.

$$P = S_w P_w + S_g P_g = S p_w + (1 - S) p_g$$

The temperature dependence of the mechanical behavior is limited to linear elastic thermal expansion in the current PLAXIS THM-model. Modeling the development of thermal plastic strains, temperature dependent stiffness and temperature dependent apparent preconsolidation pressure are not available in PLAXIS so far.